FLUTTER ANALYSIS AND
SIMULATED FLUTTER TEST OF WINGS

A THESIS SUBMITTED TO
THE GRADUATE SCHOOL OF NATURAL AND APPLIED SCIENCES
OF
MIDDLE EAST TECHNICAL UNIVERSITY

BY

TANER BİRTAN BALEVİ

IN PARTIAL FULFILLMENT OF THE REQUIREMENTS
FOR
THE DEGREE OF MASTER OF SCIENCE
IN
AEROSPACE ENGINEERING

SEPTEMBER 2012

Approval of the thesis:

FLUTTER ANALYSIS AND
SIMULATED FLUTTER TEST OF WINGS

submitted by TANER BİRTAN BALEVİ in partial fulfillment of the requirements for the degree of Master of Science in Aerospace Engineering Department, Middle East Technical University by,

Prof. Dr. Canan Özgen   _____
Dean, Graduate School of Natural and Applied Sciences

Prof. Dr. Ozan Tekinalp   _____
Head of Department, Aerospace Engineering

Prof. Dr. Altan Kayran   _____
Supervisor, Aerospace Engineering Dept., METU

Examining Committee Members:

Prof. Dr. Nafiz Alemdaroğlu   _____
Aerospace Engineering Dept., METU

Prof. Dr. Altan Kayran   _____
Aerospace Engineering Dept., METU

Assoc. Prof. Dr. D. Funda Kurtuluş   _____
Aerospace Engineering Dept., METU

Asst. Prof. Dr. Melin Şahin   _____
Aerospace Engineering Dept., METU

Dr. Evren Özşahin   _____
Aerospace Engineering Department Manager, 1st ASMC

Date: 21.09.2012

I hereby declare that all information in this document has been obtained and presented in accordance with academic rules and ethical conduct. I also declare that, as required by these rules and conduct, I have fully cited and referenced all material and results that are not original to this work.

Name, Last name: Taner Birtan Balevi

Signature :

ABSTRACT

FLUTTER ANALYSIS AND
SIMULATED FLUTTER TEST OF WINGS

Balevi, Taner Birtan

M.S., Department of Aerospace Engineering

Supervisor : Prof. Dr. Altan Kayran

September 2012, 109 pages

Flutter is a dynamic instability which can result in catastrophic failures of an air vehicle. Preventing flutter can be an important factor in the aircraft design, affecting the structural design. Thus, the weight and performance of the aircraft is also being affected. Understanding the role of each design factor of a wing on the onset of flutter can help designers on the flutter clearance of the aircraft. Analysis to predict flutter, ground vibration tests and flight flutter tests, which are performed to verify that the dedicated flight envelope is clear from flutter, are the most important certification processes in modern aviation.

Flight flutter testing is a very expensive process. In flight flutter tests the air vehicle is instrumentated with exciters, accelerometers and transmitters to send the test data simultaneously to the ground station to be analyzed. Since flutter is a very severe instability, which develops suddenly, the data should be followed carefully by the engineers at the ground station and feedback should be provided to the pilot urgently when needed. Low test step numbers per flight, increases the cost of flutter testing. Increasing efforts in pre-flight test processes in flutter prediction may narrow the flight flutter test steps and decrease the costs.

In this study, flutter prediction methods are investigated to aid the flutter test process. For incompressible flight conditions, some sample problems are solved using typical section model. Flutter solutions of a simple 3D wing are also performed via a coupled finite element linear aerodynamics approach using the commercial tool Nastran. 3D flutter solutions of the wing are compared with the typical section solutions to see how close can the typical section method predict flutter compared to the flutter analyis using the three dimensional wing model. A simulated flutter test method is introduced utilizing the two dimensional typical section method. It is shown that with a simple two dimensional typical section method, flutter test simulation can be performed successfully as long as the typical section model approximates the dynamic properties of the wing closely.

Keywords: Aeroelasticity, Flutter, Flutter Test, Simulated Flutter Test, Typical Section Model.

ÖZ

ÇIRPINTI ANALİZİ VE
KANATLARIN SİMULE ÇIRPINTI TESTLERİ

Balevi, Taner Birtan
Yüksek Lisans, Havacılık ve Uzay Mühendisliği Bölümü
Tez Yöneticisi : Prof. Dr. Altan Kayran

Eylül 2012, 109 sayfa

Çırpıntı, hava aracında ölümcül sonuçlara yol açabilecek dinamik bir kararsızlıktır. Çırpıntıyı önlemek, hava aracının yapısal tasarımını da etkileyen önemli bir tasarım girdisidir. Hava aracının ağırlığı ve performansı da bu girdiden etkilenir. Kanat tasarım faktörlerinin çırpıntı oluşumundaki rolünün anlaşılması tasarımcılara çırpıntı açısından güvenli bir tasarım yapmaları için yardımcı olacaktır. Çırpıntı kestirme analizleri, yer titreşim testleri ve bir uçuş zarfının çırpıntı açısından güvenli olduğunu değerlendirmek için yapılan uçuş çırpıntı testleri modern havacılıkta sertifikasyon sürecinin önemli parçalarıdır.

Uçuş çırpıntı testleri oldukça pahalı bir süreçtir. Bu testlerde hava aracı, tahrik sistemleri, ivmeölçerler, ve alınan uçuş test verilerini eş zamanlı olarak analiz edilmek üzere yer istasyonuna gönderilmesini sağlayan veri aktarım sistemleri ile ölçümlendirilir. Çırpıntı, ani olarak gelişen yıkıcı bir kararsızlık olduğundan yere aktarılan uçuş test verisi mühendisler tarafından dikkatli bir şekilde takip edilip gerektiğinde pilota hızlı olarak geri besleme yapılmalıdır. Uçuş başına düşen test adımlarının azlığı çırpıntı testlerinin maliyetini artırmaktadır. Test Uçuşları öncesi çırpıntı kestirimi çalışmalarına ağırlık verilmesi ilgilenilecek test adımlarını azaltarak çırpıntı uçuş test maliyetlerini düşürebilir.

Bu çalışmada çırpıntı kestirim yöntemleri çırpıntı testleri sürecine yardımcı olmak üzere araştırılmıştır. Sıkıştırılamaz akışlar için örnek problemler tipik kesit modeli kullanılarak çözülmüştür. Basit bir üç boyutlu kanat için çırpıntı çözümleri doğrusal aerodinamik yaklaşımı ve sonlu elemanlar yöntemi ile NASTRAN ticari yazılımı kullanılarak gerçekleştirilmiştir. Elde edilen çözümler tipik kesit modeli çözümleri ile karşılaştırılarak tipik kesit yöntemi çözümlerinin üç boyutlu kanat çözümlerine ne ölçüde yaklaştığı gözlemlenmiştir. Simule çırpıntı testleri yöntemi iki boyutlu tipik kesit yöntemi kullanılarak sunulmuştur. İki boyutlu kesit yöntemi kullanılarak simule çırpıntı testlerinin, kullanılan basit kesitin, kanadın dinamik özelliklerini etkin olarak temsil ettiği taktirde başarı ile icra edilebildiği gösterilmiştir.

Anahtar Kelimeler: Aeroelastisite Çırpıntı, Çırpıntı Testi, Simule Çırpıntı Testi, Tipik Kesit Modeli

To my father Fahri Balevi.

ACKNOWLEDGEMENTS

TABLE OF CONTENTS

LIST OF TABLES

LIST OF FIGURES

xiv

xv

LIST OF SYMBOLS AND ABBREVIATIONS

1st ASMC : 1st Air Supply and Maintenance Command

a : Nondimensional distance of the elastic axis from the midchord.

A(k) : Aerodynamic influence coefficient matrix.

A_I : Area of the crossection of the stiffener I profile.

AR : Aspect Ratio of the wing.

α : Pitch motion of airfoil.

b : Semichord length.

c : Nondimensional distance between the hinge line and the midchord, chord length.

C(k) : Theodorsen's function.

$C_{Lα}$: Lift curve slope.

d : Density for material.

DoF : Degree of freedom.

E : Modulus of elasticity.

F : Center of mass of the control surface, external excitation force.

g : Damping

h : Plunge motion of airfoil.

H : Moment about the hinge line.

H_h, H_α H_β: Aerodynamic coefficients:

$H(k)$: Henkel's function.

I : Identity matrix.

I_α : Mass moment of inertia of the typical section.

I_β : Mass moment of inertia of the control surface about the hinge line.

k : Reduced frequency.

K : Stiffness matrix.

K_h : Flexural stiffness of the typical section.

K_α : Torsional stiffness of the typical section.

K_β : Stiffness of the control surface.

l : Span of the wing.

l_h, l_α, L_h, L_α L_β: Aerodynamic coefficients:

L : Aerodynamic lift force acting at the elastic axis.

L_c : Circulatory lift.

L_{nc} : Non-circulatory lift.

m : Mass of the typical section.

m_β : Mass of the control surface.

m_h, m_α, M_h, M_α, M_β : Aerodynamic coefficients:

M : Mass matrix.

M, M_y : Aerodynamic moment about the elastic axis.

M_∞ : Mach number.

$\boldsymbol{q}$: Generalized coordinates vector.

r_α : nondimensional radius of gyration about the elastic axis.

r_β : nondimensional radius of gyration of the control surface about the hinge line.

s : Laplace parameter.

S_α : Static mass moment of the unit span about the elastic axis.

S_β : Static mass moment of the control surface about the hinge line.

t : Time.

t_w : Thickness of the wing.

T_i : T-functions.

U, U_∞ : Free stream flow speed.

V : Reduced velocity.

w : Downwash.

X_α : Nondimensional distance between the elastic axis and the center of mass.

X_β : Nondimensional distance between the hinge line and the center of mass of the control surface.

α : Pitch motion of airfoil.

β : Control surface motion of airfoil.

γ : Transient decay parameter

δ : Logarithmic decrement.

λ : Eigenvalue parameter.

μ : Mass ratio.

ρ_∞ : Density of air.

σ : Ratio of natural frequencies.

τ : Nondimensional time.

υ : Poisson's ratio

ϕ : Wagner's function.

ω : Frequency

ω_h : Natural pitching frequency

ω_β : Natural plunging frequency

ω_α : Natural control surface frequency

(.) : Differentiation with respect to time.

(') : Differentiation with respect to dimensionless time

(^) : Laplace transformed.

CHAPTER 1

INTRODUCTION

1.1.   General

Aeroelasticity basically focuses on aerodynamic, elastic and inertial forces affects on structures [1]. Collar's aeroelastic triangle given in Figure 1 summarizes the disciplines which investigates the interaction of the forces mentioned. In the scope of aeroelasticity there are static and dynamic instabilities.
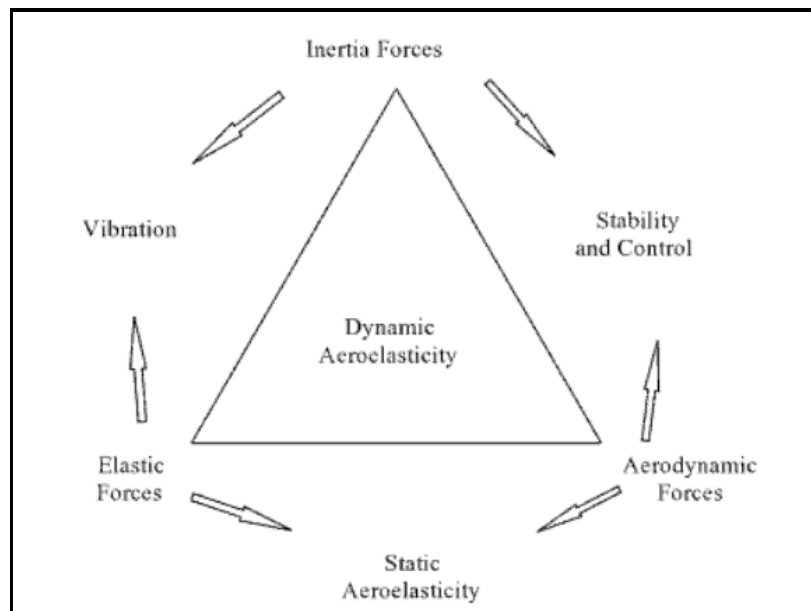
Figure 1 Collar's aeroelastic triangle [1]

The basic static instabilities may be listed as wing divergence, control surface reversal and redistribution of loads. Wing divergence is an instability which occurs when the elastic moments within the wing structure are exceeded by the aerodynamic moments. The torsional stiffness displays a vital role in wing divergence phenomenon. Control surface reversal which is known as aileron reversal as well is the situation in which the aileron twists the wing such that the gain due to control surface (aileron) deflection is less than the loss due to wing twist above critical speeds. The air vehicle facing aileron reversal has poor roll performance; it may even experience the roll in opposite direction. Load redistribution is the redistribution of aerodynamic pressures over the wing because of elastic deformation of the wing. The elastic wing may experience washout and this may result in loss of lift.

Wing flutter, control surface flutter, panel flutter, blade flutter and buffeting are some of dynamic aeroelastic instabilities. In wing flutter, wing surface experiences divergent oscillations. There are no external forcing agents present and the air flow supplies energy to the structure. Occurrence of flutter generally results in sudden catastrophic failure. Wing flutter may be classified in two: classical bending-torsion flutter and stall flutter which is more likely to be seen in rotating wings and wings at high angle of attack. Control surface flutter which is also called aileron buzz generally occurs in transonic regions. It is not catastrophic but unwanted. Panel flutter is a vital stability problem for rocket like structures where standing and travelling waves occur on the surfaces of the structure. It is generally seen in transonic and supersonic flow regimes. Structural and aerodynamic non-linearities have important effects in this type of dynamic instability. Blade flutter may be also classified as stall flutter. It may be seen in rotorcraft blades and engine blades. Buffeting occurs because of transient vibrations of the aircraft structural components due to wakes, gusts and other type of dynamic loads [2]. It results in fatigue related failures.
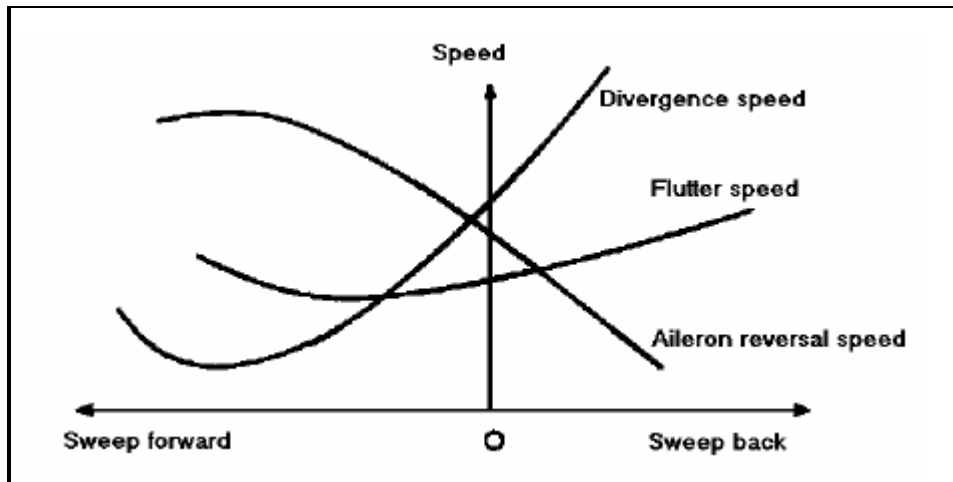
Figure 2 Comparison of critical speeds [2]

In Figure 2, the typical behavior of instability due to speed and sweep angles of the wing is shown. Although the rigid sweep forward wing creates better lifting forces one can see from the figure that it may face low divergence speeds. Sweep back wings are preferred for their better speed performances in terms of divergence speed. However, the speed limit of the sweep back wing aircraft is determined by flutter. Designing an accurate flight control system, stiffness improvements and mass balancing may be used to increase flutter speed.

The most dangerous problem of aeroelasticity is flutter in which relatively small disturbances end up with violent oscillations. Flutter is a dynamic instability problem which occurs by the interaction of the elastic, inertia and aerodynamic forces. It can result in catastrophic failure of the wing, winglet, fin, vertical and horizontal stabilizer or any aerodynamic surface that is subjected to it. In addition to air vehicles, structures like suspension bridges may also be subjected to flutter.

The structure's response to the unsteady aerodynamic forces occurs with a damping effect at low speeds. This response increases with speed up to a critical speed level. At this critical speed level the some of the structure's elastic modes are coupled by aerodynamic forces. This causes energy transfer from the airflow to the structure which results in increasing oscillations. The amplitude of these oscillations increases

violently with a little speed increment so that the person who controls the aircraft may not response before catastrophic failure occurs.

1.2.   Historical Review

History of flutter and flight flutter testing is generally described in Reference [3]. The first incident of flutter recorded happened in 1916 on a twin engine biplane bomber. The flutter occurred due to coupled torsion mode of fuselage and antisymetric elevator rotation mode. During World War I, control surface flutter occurences started, and control surface problems are solved by addition of mass balances about the hinge lines. Cantilevered wings and higher speeds resulted in more wing flutter incidents after World War I. In 1930's the major flutter form that was widely seen was servo tab flutter, and this form of flutter kept being a problem till the mid 1950's. Even in 1986 a trainer experienced servo tab flutter during a test flight [3].

Reaching transonic speeds in 1940's introduced a new type of aeroelastic problem: control surface buzzes. In 1944 at the test flight of P-80 aileron buzz is reported. Prototypes of fighters F-100 and F-14 experienced rudder buzz. Transonic flight regime is still the most critical flight regime in terms of flutter [3].

Supersonic speed, which was first reached in 1947 in level flight, introduced the panel flutter. In 1950's a fighter was lost because of fatigue related failure induced by panel flutter [3].

External stores like munitions, fuel tanks, engines carried by pylons also have effects on the aeroelastic stability of an aircraft. The increasing diversity of store configurations keeps store related flutter a major problem in terms of flutter today. Much effort has been spent to confirm the dedicated flight envelope is flutter safe during the integration of an external store to an aircraft [3].

The first formal flight flutter test was performed by Von Schlippe in 1935 in Germany [3]. Von Schlippe used an unbalance weight which is rotating as an exciter and recorded the amplitude responses. He recorded the amplitudes as a function of airspeed at subcritical speeds free from flutter. Then, he estimated the flutter speeds using the results. His method is described in Figure 3. His technique was successfully used till 1938 when a JU90 crashed due to unpredictable flutter. The probable causes were inadequate exciters and measurement systems. His technique was also used in USA in 1940's [3].
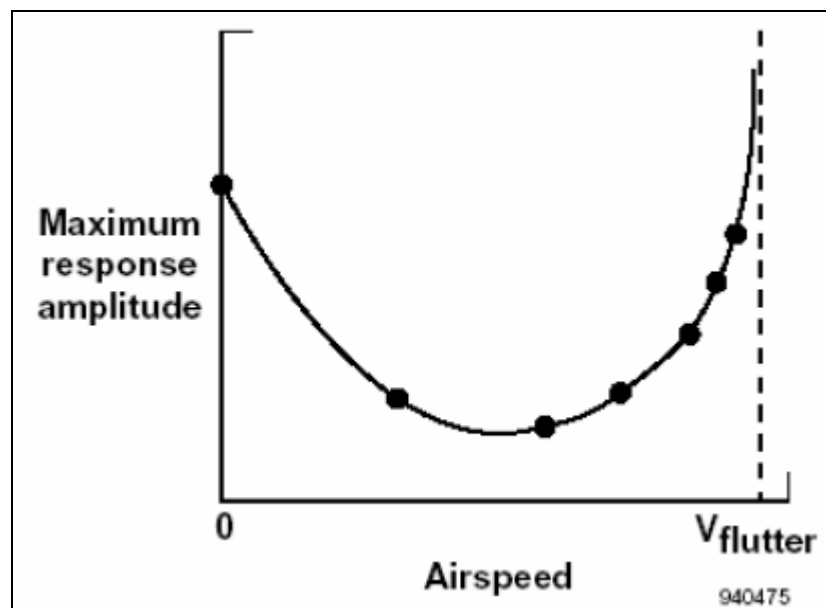
Figure 3. Von Schlippe's flutter flight test method [3]

Towards the end of 1950's flight test people recognized the severity of adequate excitation systems, measuring equipment and data recording systems. The first applications of telemetry to transmit the flight test data to the ground station for analysis were introduced. Between 1950's and 1970's many aircraft were instrumented by excitation systems and accelerometers for sweeping a frequency range to check resonance where damping was manually determined using strip charts. From 1970's till today digital computers has played significant role in flight

flutter test techniques. Use of computers allowed analysts to do fast Fourier transforms rapidly, and gave rise to algorithms of sophisticated data processing. By real time parameter identification techniques, damping and frequency are estimated as functions of airspeed or Mach number. Extrapolation is done to determine stability of the next higher speed test point. By the increasing computer speeds, the gained ability of analyzing more data at each point resulted in more sophisticated aircraft design. On the contrary, the total time to clear the flutter envelope increased [3]. In flight flutter testing, there is some specific critical weight interval of interest. To keep the air vehicle in this interval, flight refueling which increases the costs may be needed. Reducing the test steps covered in one flight and increasing the number of flights, which increases the cost as well, to cover up all the test steps for the desired weight interval may also be a solution. Modern flight flutter testing is described in Figure 4 although recently monitor displays are being used instead of strip charts. There has been substantial improvements in the instrumentation equipment, data processing techniques and real time telemetry technology. The basic estimation of damping as a function of air speed that Von Schlippe introduced is still being used.

In theoretical background, Theodore Theodorsen introduced the Theodorsen Function *C(k)*, for the steady motion and sinusoidal motion in his report [4]. In this report the wing section is modeled as a flat plate assuming it is oscillating about elastic axis. He investigates the effects of the parameters mass ratio, bending torsion frequency ratio, dimensionless static unbalance dimensionless radius of gyration to critical flutter speed and frequency. Theodorsen and Garrick suggested a numerical approach to solve flutter problem and compare their solution with wind tunnel test results in their report [5].

After the work done by Theodorsen and Garrick various flutter prediction methods are developed by researchers. k-method which is also known as American method or Air Material Comand Method in literature is used by Smilg and Wessermann [7]. In k-method an Eigenvalue problem is build and solved by the addition of an artificial damping term. In the first half of 1950's Irwin and Guyett presented p-k method which is also known as the British method in literature [8]. P-k method is an

6

approximate method constructed to find out the decay rate. In both methods for solution damping vs. speed curves are plotted though damping values determined are physically meaningless accept around flutter boundary at which the damping value is equal to zero [9].

Dimitriadis and Cooper investigates the damping variation with airspeed, flutter margin, envelope function and Autoregressive Moving Average-Based (ARMA) methods to predict flutter from flight flutter test data [10]. They introduced simulated flutter test and outlined the steps to perform it.
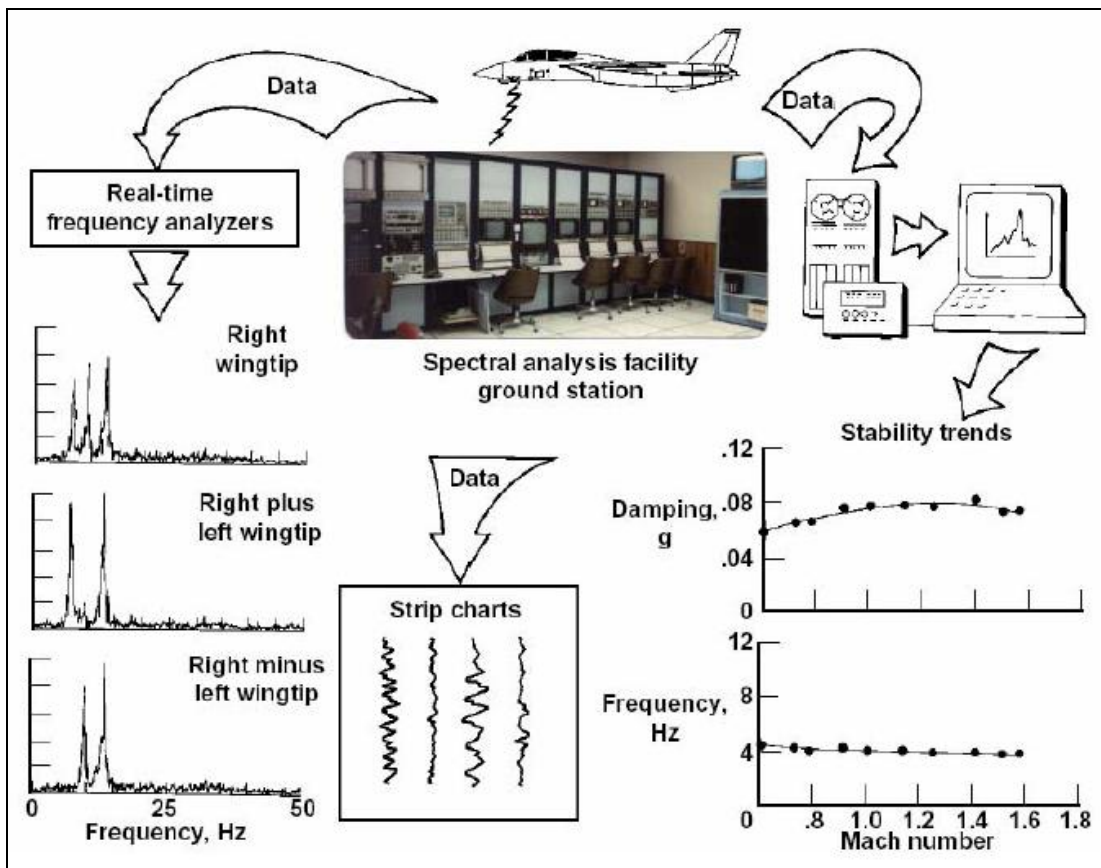
Figure 4. Typical modern flutter flight test process [3]

1.3. Scope of the Study

In this study, flutter prediction methods k method and p-k method are investigated. The 2 degree of freedom typical section model is introduced and equations of motions are derived for the model in incompressible flows. Then for 3 degree of freedom typical section model with a control surface, equations are derived. k-method and p-k method is introduced and solution process for these methods are explained. Using MATLAB a code is generated for solutions using k-method and p-k method. The code is validated by solving some known problems and the results are presented graphically. Comparison of methods are made.

A simple 3D wing is designed and flutter solutions are made in a finite elements method based commercial tool. Solutions are made for a corresponding 2D typical section model. The results of 3D and 2D solutions are compared.

The equations of motion for a 2 DoF typical section are derived in time domain and and external excitation term is added to the equations. A simulated flutter test method is introduced. Following the simulated flutter test method, for a case study flutter speed estimations are made.

CHAPTER 2

FLUTTER ANALYSIS OF A TYPICAL WING SECTION

2.1.   Mathematical Modeling of a 2 DoF Typical Section

Figure 5 shows the location and description of the coordinate system used and some dimensional quantities of primary interest in modeling an aeroelastic system. This airfoil is a representative "2 DoF typical section" used by Theodorsen and Garrick in their famous reports [4], [5]. They suggest that for purposes of theoretical flutter prediction, inertial and geometric properties of a large span and straight wing can be represented by a typical section with inertial and geometric properties of the wing at ¾ of the distance from root of the wing. This suggestion holds where the aspect ratio is large, the sweep is small, and the sectional characteristics vary smoothly across span. The typical section representation is not only suitable for cantilever wing simulation but also for missile control surface aeroelastic analysis. Control surfaces are assumed to be chordwise rigid and obey the thin airfoil assumption. Since the control surface is connected to the control unit via a torsionally less stiff shaft than the control surface, it can be assumed that elastic rotation takes place at the connecting shaft only. The mechanical components of the servo system such as links of the mechanism or the transmission box, and the nonlinearities such as free play on these components will also decrease the equivalent stiffness of the shaft further. The

difference between a cantilever wing and a control surface is that the bending stiffness of the control surface is much larger than its torsional stiffness, due to relatively low aspect ratio.

In Figure 5, z=0 line represents the undeflected airfoil centerline; b is the half-chord length; a is the ratio of the distance between the centerline and the elastic axis to the half-chord length b (one should note that positive values of a indicates that elastic axis is located at the rear half chord, while negative values of a indicates that the elastic axis is located at front half chord); x_α is the ratio of distance between the elastic axis and the center of gravity of the airfoil to the half-chord length b; h is the deflection of the airfoil in plunge direction and α is the deflection angle in pitch direction. K_h and K_α are the restraining spring stiffness values in plunge and pitch degree of freedoms, respectively. L is the aerodynamic lift force and M_y is the aerodynamic moment.
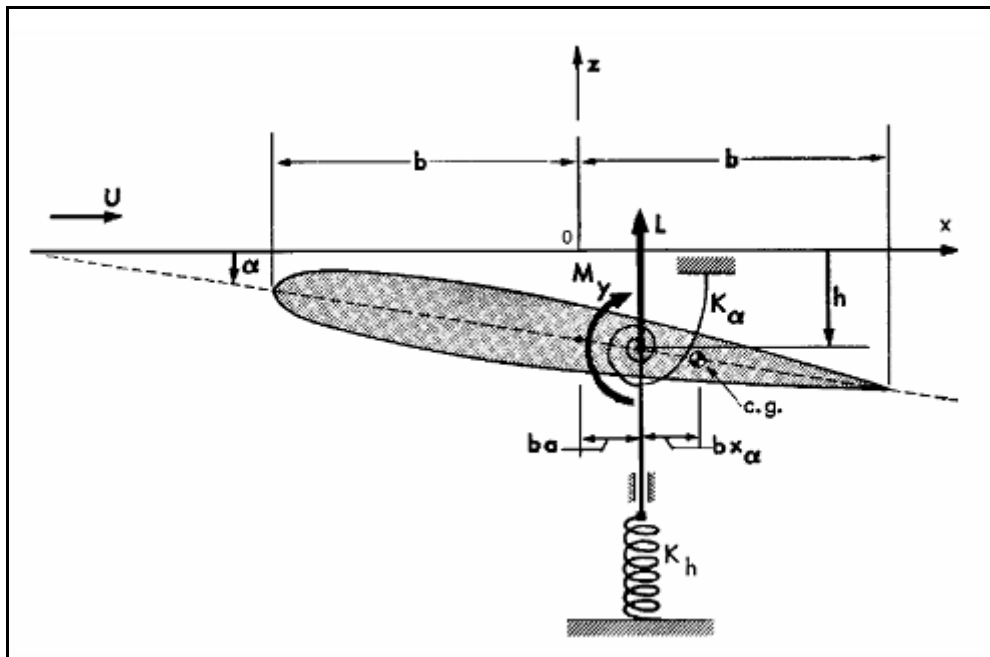
Figure 5. The 2 DoF Typical Section [6]

2.2. Equations of Motion of 2 DoF Typical Section

The notation given above is called Theodorsen's notation. The general equations of motion per unit span length for the typical section without damping and linear stiffness parameters are given as;

$$m\ddot{h} + S_\alpha \ddot{\alpha} + K_h h = -L \tag{1}$$

in plunge degree of freedom, and

$$S_\alpha \ddot{h} + I_\alpha \ddot{\alpha} + K_\alpha \alpha = M \tag{2}$$

in pitch degree of freedom, where

$$S_\alpha = mbX_\alpha \tag{3}$$

is the static mass moment per unit span, I_α is the mass moment of inertia of the airfoil, K_h is the plunge stiffness, K_α is the pitch stiffness, L is the aerodynamic lift, and M is the aerodynamic moment.

The harmonic motion is modeled as

$$h = \bar{h} e^{i\omega t} \tag{4}$$

$$\alpha = \bar{\alpha} e^{i\omega t} \tag{5}$$

The corresponding lift and moment can be written as

$$L = \overline{L} e^{i\omega t} \tag{6}$$

$$M = \overline{M} e^{i\omega t} \tag{7}$$

Substituting these into equations of motion we have

$$-\omega^2 m \overline{h} - \omega^2 mbX_\alpha \overline{\alpha} + m\omega_h^2 \overline{h} = -\overline{L} \tag{8}$$

$$-\omega^2 mbX_\alpha \overline{h} - \omega^2 I_\alpha \overline{\alpha} + I_\alpha \omega_\alpha^2 \overline{\alpha} = \overline{M} \tag{9}$$

Lift and moment equations are given below;

$$\overline{L} = -\pi \rho_\infty b^3 \omega^2 \left[\ell_h(k, M_\infty) \frac{\overline{h}}{b} + \ell_\alpha(k, M_\infty) \overline{\alpha} \right] \tag{10}$$

$$\overline{M} = \pi \rho_\infty b^4 \omega^2 \left[m_h(k, M_\infty) \frac{\overline{h}}{b} + m_\alpha(k, M_\infty) \overline{\alpha} \right] \tag{11}$$

where k is the reduced frequency: $b\omega/U$. l_h, l_α, m_h and m_α are the complex dimensionless aerodynamic lift and moment coefficients. These unsteady lift and moment coefficients act on a wing which performs oscillatory plunging and pitching motions[8]. It should be noted that these coefficients are dependant on reduced frequency and Mach number. The dependency on Mach number reflects the compressibility effects, in incompressible flow the expressions are only dependant on reduced frequency. The content of these coefficients will be investigated in following pages.

Substituting Equations (10) and (11) into Equations (8) and (9) and rearranging we have a pair of homogeneous, linear, algebraic equations for $\overline{h}$ and $\overline{\alpha}$;

$$\left\{ \frac{m}{\pi \rho_\infty b^2}\left[1-\left(\frac{\omega_h}{\omega}\right)^2\right]+\ell_h\left(k,M_\infty\right)\right\}\frac{\bar{h}}{b}+\left[\frac{mX_\alpha}{\pi \rho_\infty b^2}+\ell_\alpha\left(k,M_\infty\right)\right]\bar{\alpha}=0 \tag{12}$$

$$\left[\frac{mX_\alpha}{\pi \rho_\infty b^2}+m_h\left(k,M_\infty\right)\right]\frac{\bar{h}}{b}+\left\{\frac{I_P}{\pi \rho_\infty b^4}\left[1-\left(\frac{\omega_\alpha}{\omega}\right)^2\right]+m_\alpha\left(k,M_\infty\right)\right\}\bar{\alpha}=0 \tag{13}$$

To simplify the equations dimensionless radius of gyration about the reference point r_α, the ratio of uncoupled bending to torsional frequencies σ, mass ratio parameter reflecting the relative importance of the modal mass to the mass of the air affected by the model μ, and dimensionless freestream speed of the air (reduced velocity) V are defined. [8]

$$r_\alpha^2=\frac{I_\alpha}{mb^2} \tag{14}$$

$$\sigma=\frac{\omega_h}{\omega_\alpha} \tag{15}$$

$$\mu=\frac{m}{\rho_\infty \pi b^2} \tag{16}$$

$$V=\frac{U}{b\omega_\alpha} \tag{17}$$

Simplifying the equations by substituting the Equations (14), (15), (16) and (17) into Equations (12) and (13) we have;

$$\left\{ \mu \left[1 - \sigma^2 \left(\frac{\omega_h}{\omega} \right)^2 \right] + \ell_h \right\} \frac{\bar{h}}{b} + \left[\mu x_\alpha + \ell_\alpha \right] \bar{\alpha} = 0 \tag{18}$$

$$\left(\mu x_\alpha + m_h \right) \frac{\bar{h}}{b} + \left\{ \mu r_\alpha^2 \left[1 - \left(\frac{\omega_\alpha}{\omega} \right)^2 \right] + m_\alpha \right\} \bar{\alpha} = 0 \tag{19}$$

The next step is solving these algebraic equations for flight conditions. The Equations (18) and (19) are linear and homogeneous in $\bar{h}/b$ and $\bar{\alpha}$ so the determinant of their coefficients must be zero for a nontrivial solution for the motion to exist. This condition can be written as [8]

$$\begin{vmatrix} \mu \left[1 - \sigma^2 \left(\frac{\omega_h}{\omega} \right)^2 + \ell_h \right] & \mu x_\alpha + \ell_\alpha \\ \\ \mu x_\alpha + m_h & \mu r^2 \left[1 - \left(\frac{\omega_\alpha}{\omega} \right)^2 \right] + m_\alpha \end{vmatrix} = 0 \tag{20}$$

This determinant is called the flutter determinant. After expanding the determinant one can get $(\omega_\alpha/\omega)^2$ in quadratic polynomial form.

2.3.   Solution of Flutter Determinant

To complete the solution of flutter for the flight condition, one should see that there are four unknowns: ω_α/ω, μ, M_∞ and $b\omega/U$. One of the equations available for their solutions is a second degree polynomial. Because the aerodynamic coefficients are complex, this complex equation contains two real equations. For solution to be obtained both the real and imaginary parts must be equal to zero. One should note that there are 4 unknown parameters and two equations, to obtain the solution two

parameters must be predicted for the calculation of the other two. The solution can be summarized in 9 steps which are given below;

1. To fix the parameter μ specify an altitude

2. Specify M_∞, accept it is equal to zero to start with

3. Specify a set of trial values for $b\omega/U$ which is denoted as k, the reduced frequency

4. Calculate the functions ℓ_h, ℓ_α, m_h and m_α for each value of k

5. Solve the flutter determinant for the corresponding values of $(\omega_\alpha/\omega)^2$ for each values of k. The real part of the root represents $(\omega_\alpha/\omega)^2$, and the imaginary parts is related to the damping of the mode.

6. To find out the k value at which the imaginary part of one of the roots becomes zero do an interpolation. This is the condition of zero damping which corresponds to the so-called cross over point meaning that damping crosses the zero line. For this value of k there is a corresponding real value of $(\omega_\alpha/\omega)^2$ from which ω can be determined.

7. Using this determined ω and corresponding k value, determine U and M_∞.

8. Repeat the steps from 3 to 7 until the value of M_∞ obtained in step 7 converges to $M_{\infty F}$, k_F and U_F for flutter for the dedicated μ.

9. To determine the flutter boundary in terms of altitude versus $M_{\infty F}$, k_F and U_F, repeat the procedure for different values of μ.

2.4. Solution of 2 DoF Model Equations for Subsonic Incompressible Flow

Lift equation for a typical section exhibiting simple harmonic oscillation in unsteady incompressible flow per unit span is given as [7];

$$L = \pi p_{\infty} b^2 \left[\ddot{h} + U\dot{\alpha} - ba\ddot{\alpha} \right] + 2\pi p_{\infty} UbC(k)\left[U\alpha + \dot{h} + b\left(\frac{1}{2} - a\right)\dot{\alpha} \right] \qquad (21)$$

and the moment equation for a typical section exhibiting simple harmonic oscillation in unsteady subsonic incompressible flow per unit span is [7];

$$\begin{aligned} M = \pi p_{\infty} b^2 &\left[ba\ddot{h} - Ub\left(\frac{1}{2} - a\right)\dot{\alpha} - b^2\left(\frac{1}{8} + a^2\right)\ddot{\alpha} \right] \\ &+ 2\pi p_{\infty} Ub^2\left(a + \frac{1}{2}\right)C(k)\left[U\alpha + \dot{h} + b\left(\frac{1}{2} - a\right)\dot{\alpha} \right] \end{aligned} \qquad (22)$$

where $C(k)$ is the Theoorsen's function which is expressed as [7]:

$$C(k) = F(k) + iG(k) = \frac{H_1^{(2)}(k)}{H_1^{(2)}(k) + iH_0^{(2)}(k)} \qquad (23)$$

where $H(k)$ is the Henkel function which consists of first and second kinds of Bessel functions.

Substituting Equation (4)and Equation (5) into Equation (21), lift equation can be written as:

$$\begin{aligned} L = \Big\{ \pi p_{\infty} b^2 &\left[-\omega^2\overline{h} + i\omega U\overline{\alpha} + ba\omega^2\overline{\alpha} \right] \\ &+ 2\pi p_{\infty} UbC(k)\left[U\overline{\alpha} + i\omega\overline{h} - ib\left(\frac{1}{2} - a\right)\omega\overline{\alpha} \right] \Big\} e^{i\omega t} \end{aligned} \qquad (24)$$

U can be expressed as a function of reduced frequency: $U=b\omega/k$. Substituting this expression into the equation above and reorganizing the equation;

16

$$L = \left\{ (-b\omega^2)\pi\rho_\infty b^2 \frac{\left[-\omega^2\bar{h} + i\omega\frac{b\omega}{k}\bar{\alpha} + ba\omega^2\bar{\alpha} \right]}{(-b\omega^2)} \right.$$

$$\left. + (b\omega)2\pi\rho_\infty \frac{b\omega}{k} bC(k) \frac{\left[\frac{b\omega}{k}\bar{\alpha} + i\omega\bar{h} - ib\left(\frac{1}{2} - a\right)\omega\bar{\alpha} \right]}{(b\omega)} \right\} e^{i\omega t} \tag{25}$$

$$L = -\pi\rho b^3\omega^2 \left\{ \left(\frac{1}{b}\bar{h} - i\frac{1}{k}\bar{\alpha} - a\bar{\alpha} \right) - 2\frac{1}{k}C(k)\left[\frac{1}{k}\bar{\alpha} + i\frac{1}{b}\bar{h} - i\left(\frac{1}{2} - a\right)\bar{\alpha} \right] \right\} e^{i\omega t}$$

$$= -\pi\rho b^3\omega^2 \left\{ \left(1 - \frac{2iC(k)}{k} \right)\frac{\bar{h}}{b} + \left[-a - \frac{i[1 + (1 - 2a)C(k)]}{k} - \frac{2C(k)}{k^2} \right]\bar{\alpha} \right\} e^{i\omega t} \tag{26}$$

and similarly Equation (22) can be written as;

$$M = \left\{ \pi\rho_\infty b^2 \left[-ba\omega^2\bar{h} - iUb\left(\frac{1}{2} - a\right)\omega\bar{\alpha} + b^2\left(\frac{1}{8} + a^2\right)\omega^2\bar{\alpha} \right] \right.$$

$$\left. + 2\pi\rho_\infty Ub^2\left(a + \frac{1}{2} \right)C(k)\left[U\bar{\alpha} + i\omega\bar{h} + ib\left(\frac{1}{2} - a\right)\omega\bar{\alpha} \right] \right\} e^{i\omega t} \tag{27}$$

Again *U* can be expressed as a function of reduced frequency *U=bω/k*. Substituting this expression into the equation above and reorganizing the equation;

17

$$M = \left\{ (b^2\omega^2)\pi\rho_\infty b^2 \frac{\left[-ba\,\omega^2\bar{h} - i\frac{b\omega}{k}b\left(\frac{1}{2}-a\right)\omega\bar{\alpha} + b^2\left(\frac{1}{8}+a^2\right)\omega^2\bar{\alpha} \right]}{(b^2\omega^2)} \right.$$

$$\left. + (b\omega)2\pi\rho_\infty \frac{b\omega}{k}b^2\left(a+\frac{1}{2}\right)C(k)\frac{\left[\frac{b\omega}{k}\bar{\alpha} + i\omega\bar{h} + ib\left(\frac{1}{2}-a\right)\omega\bar{\alpha} \right]}{(b\omega)} \right\}e^{i\omega t} \tag{28}$$

$$M = \pi\rho_\infty b^4\omega^2\left\{ \left[-a\frac{\bar{h}}{b} - i\frac{1}{k}\left(\frac{1}{2}-a\right)\bar{\alpha} + \left(\frac{1}{8}+a^2\right)\bar{\alpha} \right] \right.$$

$$\left. + \frac{1}{k}(2a+1)C(k)\left[\frac{1}{k}\bar{\alpha} + i\frac{\bar{h}}{b} + i\left(\frac{1}{2}-a\right)\bar{\alpha} \right] \right\}e^{i\omega t} \tag{29}$$

$$M = \pi\rho_\infty b^4\omega^2\left\{ \left[-a + \frac{i(2a+1)C(k)}{k} \right]\frac{\bar{h}}{b} \right.$$

$$\left. + \left[\frac{1}{8}+a^2 - \frac{i\left(\frac{1}{2}-a\right)[1-(2a+1)C(k)]}{k} + \frac{(2a+1)C(k)}{k^2} \right]\bar{\alpha} \right\}e^{i\omega t} \tag{30}$$

One can notice that Equation (26) and (30) takes the form which is suggested in Equation (10) and (11). So, the equations of lift and moment of a 2 DoF typical section in incompressible flow can be expressed as

18

$$L = -\pi \rho_\infty b^3 \omega^2 \left[L_h \frac{\overline{h}}{b} + L_\alpha \overline{\alpha} \right] e^{i\omega t} \tag{31}$$

$$M = \pi \rho_\infty b^4 \omega^2 \left[M_h \frac{\overline{h}}{b} + M_\alpha \overline{\alpha} \right] e^{i\omega t} \tag{32}$$

where;

$$L_h = 1 - \frac{i2C(k)}{k}$$

$$L_\alpha = -a - \frac{i\left[1 + (1 - 2a)C(k)\right]}{k} - \frac{2C(k)}{k^2}$$

$$M_h = -a + \frac{i(2a+1)C(k)}{k} \tag{33}$$

$$M_\alpha = \frac{1}{8} + a^2 - \frac{i\left(\frac{1}{2} - a\right)\left[1 - (2a+1)C(k)\right]}{k} + \frac{(2a+1)C(k)}{k^2}$$

The equations of motion which were defined in the beginning of this section can be written as:

$$mb\frac{\ddot{h}}{b} + S_\alpha \ddot{\alpha} + bK_h \frac{h}{b} + L = 0 \tag{34}$$

$$S_\alpha \frac{\ddot{h}}{b} + \frac{I_\alpha}{b}\ddot{\alpha} + \frac{K_\alpha}{b}\alpha - \frac{M}{b} = 0 \tag{35}$$

Substituting Equations (31) and (32) into Equations (34) and (35):

$$mb\frac{\ddot{h}}{b} + S_\alpha\ddot{\alpha} + K_h h - \pi\rho_\infty b^3\omega^2\left[L_h\frac{\bar{h}}{b} + L_\alpha\bar{\alpha}\right]e^{i\omega t} = 0 \tag{36}$$

$$S_\alpha\frac{\ddot{h}}{b} + \frac{I_\alpha}{b}\ddot{\alpha} + \frac{K_\alpha}{b}\alpha - \pi\rho_\infty b^3\omega^2\left[M_h\frac{\bar{h}}{b} + M_\alpha\bar{\alpha}\right]e^{i\omega t} = 0 \tag{37}$$

Rewriting Equations (36) and (37) in matrix form we have:

$$\begin{bmatrix} mb & S_\alpha \\ S_\alpha & I_\alpha/b \end{bmatrix}\begin{Bmatrix} \ddot{h}/b \\ \ddot{\alpha} \end{Bmatrix} + \begin{bmatrix} K_h & 0 \\ 0 & K_\alpha/b \end{bmatrix}\begin{Bmatrix} h/b \\ \alpha \end{Bmatrix} - \pi\rho_\infty b^3\omega^2\begin{bmatrix} L_h & L_\alpha \\ M_h & M_\alpha \end{bmatrix}\begin{Bmatrix} \bar{h}/b \\ \bar{\alpha} \end{Bmatrix} = 0 \tag{38}$$

Equation (38) is the equation of motion of a 2 DoF typical wing section exhibiting simple harmonic oscillation in unsteady subsonic incompressible flow.

2.5.   Mathematical Modeling of a 3 DoF Typical Section

Similarly to the previous part Figure 6 shows the location and description of the coordinate system used and some dimensional quantities of primary interest in modeling an aeroelastic system with 3 degrees of freedom. This airfoil is a representative "3 DoF typical section" taken from Reference [12], with the third degree of freedom representing the rotatin of the control surface with respect to the wing. A little change of notation has been made in the original figure. Like in 2 DoF model, a large span and straight wing can be represented by the 3 DoF typical section model using the inertial and geometric properties of the wing at about ¾ of the distance from the root of the wing ([9]p.194).

In Figure 6, similar to Figure 5, z=0, b is the half-chord length; a is the ratio of the distance between the centerline and the elastic axis to the half-chord length b; x_α is the ratio of distance between the elastic axis and the center of gravity of the airfoil to

the half-chord length b; h is the deflection of the airfoil in plunge direction and α is the deflection angle in pitch direction; K_h and K_α are the restraining spring stiffness values in plunge and pitch degree of freedoms, respectively. In addition, β is the DoF representing control surface motion; K_β is the spring constant associated with the control surface motion; c is the nondimensional distance between the hinge line of the control surface and the midchord; F is the center of mass of the control surface; X_β is the nondimensional distance between F and hinge line [12].
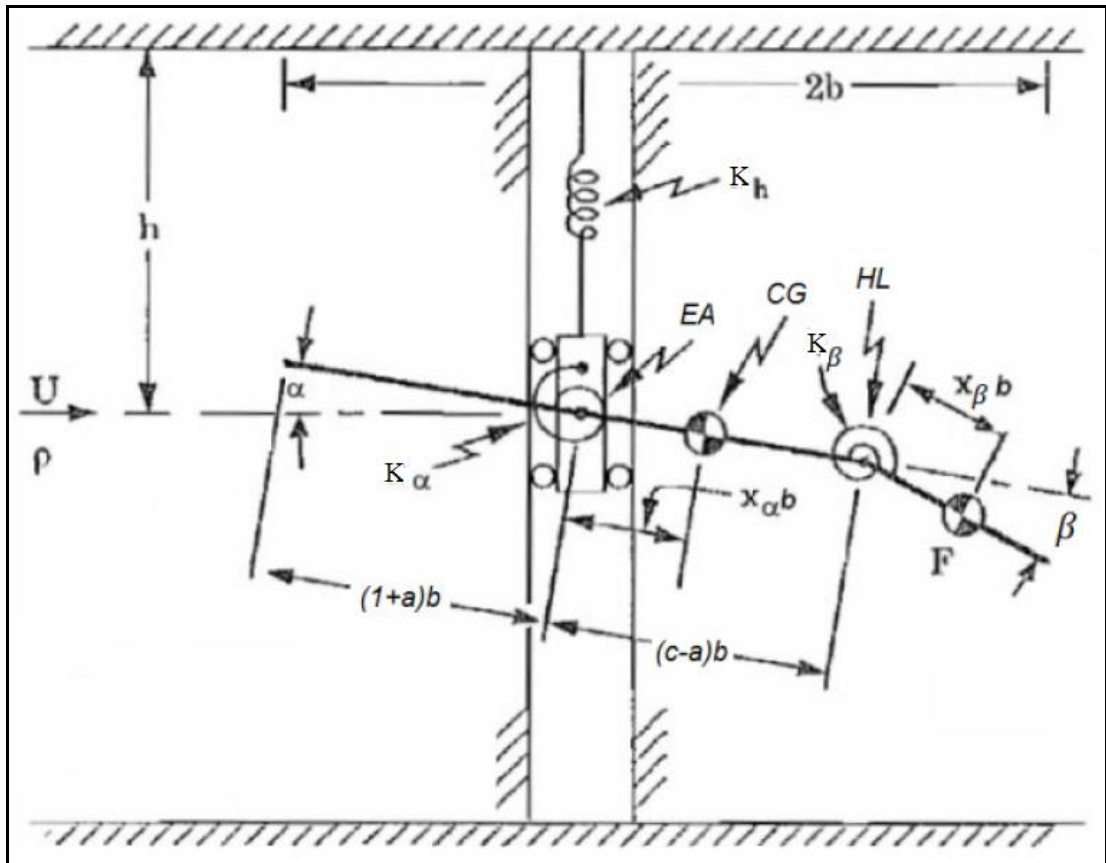
Figure 6. The 3 DoF Typical Wing Section [12]

2.6.   3 DoF Model Equations and Solution for Subsonic Incompressible Flow

The general equations of motion per unit span length for the typical section without damping and linear stiffness parameters are given as [9];

$$m\ddot{h} + S_\alpha\ddot{\alpha} + S_\beta\ddot{\beta} + K_h h = -L \tag{39}$$

$$S_\alpha\ddot{h} + I_\alpha\ddot{\alpha} + \left[(c-a)bS_\beta + I_\beta\right]\ddot{\beta} + K_\alpha\alpha = M \tag{40}$$

$$S_\beta\ddot{h} + \left[(c-a)bS_\beta + I_\beta\right]\ddot{\alpha} + I_\beta\ddot{\beta} + K_\beta\beta = H \tag{41}$$

where;

$$S_\beta = m_\beta b X_\beta \tag{42}$$

is the control surface's static mass moment about the hinge line, I_β and H are the mass moment of inertia of the control surface and the moment about the hinge line respectively.

The harmonic motion of the control surface is modeled similarly to pitch and plunge motions as;

$$\beta = \overline{\beta}e^{i\omega t} \tag{43}$$

The corresponding moment can be expressed as;

$$H = \overline{H}e^{i\omega t} \tag{44}$$

Lift and moment expressions about the elastic axis of the wing and hinge moment expression for a typical section exhibiting simple harmonic oscillation in incompressible flow per unit span are given, without derivation, by Equations (45), (46) and (47) [9].

$$L = \rho_\infty b^2\left[\pi\ddot{h} + \pi U\dot{\alpha} - \pi ba\ddot{\alpha} - UT_4\dot{\beta} - T_1 b\ddot{\beta}\right] \\ + 2\pi\rho_\infty UbC(k)\left[U\alpha + \dot{h} + b\left(\frac{1}{2} - a\right)\dot{\alpha} + \frac{T_{10}U\beta}{\pi} + \frac{bT_{11}\dot{\beta}}{2\pi}\right] \tag{45}$$

22

$$M = \rho_\infty b^2 \left\{ \pi ba\, \ddot{h} - \pi Ub \left(\frac{1}{2} - a \right) \dot{\alpha} - \pi b^2 \left(\frac{1}{8} + a^2 \right) \ddot{\alpha} - (T_4 + T_{10})U^2\beta \right.$$

$$\left. - \left[T_1 - T_8 - (c - a)T_4 + \frac{T_{11}}{2} \right] Ub\, \dot{\beta} + \left[T_7 + (c - a)T_1 \right] b^2 \ddot{\beta} \right\} \qquad (46)$$

$$+ 2\pi \rho_\infty Ub^2 \left(a + \frac{1}{2} \right) C(k) \left[U\alpha + \dot{h} + b \left(\frac{1}{2} - a \right) \dot{\alpha} + \frac{T_{10}U\beta}{\pi} + \frac{bT_{11}\dot{\beta}}{2\pi} \right]$$

$$H = \rho_\infty b^2 \left\{ T_1 b \ddot{h} - \left[-2T_9 - T_1 + T_4 \left(a - \frac{1}{2} \right) \right] Ub\, \dot{\alpha} - 2T_{13} b^2 \ddot{\alpha} - \frac{U^2(T_5 - T_4 T_{10})\beta}{\pi} \right.$$

$$\left. + \frac{UbT_4 T_{10}\dot{\beta}}{2\pi} + \frac{T_4 b^2 \ddot{\beta}}{\pi} \right\} - \rho_\infty Ub^2 T_{12} C(k) \left[U\alpha + \dot{h} + b \left(\frac{1}{2} - a \right) \dot{\alpha} + \frac{T_{10}U\beta}{\pi} + \frac{bT_{11}\dot{\beta}}{2\pi} \right] \qquad (47)$$

where, the constants denoted with *T* are the T-functions of the geometry of the system which will be given in next pages. Substituting Equations (4), (5), (43) and (44) into Equations (45),(46) and (47), the updated relations for lift, pithing moment and hinge moment expressions become:

$$L = \left\{ \rho_\infty b^2 \left[-\omega^2 \pi \overline{h} + i\omega\pi U\overline{\alpha} + \omega^2 \pi ba\, \overline{\alpha} - i\omega U T_4 \overline{\beta} + \omega^2 T_1 b\overline{\beta} \right] \right.$$

$$\left. + 2\pi \rho_\infty UbC(k) \left[U\overline{\alpha} + i\omega\overline{h} + i\omega b \left(\frac{1}{2} - a \right) \overline{\alpha} + \frac{T_{10}U\overline{\beta}}{\pi} + i\omega \frac{bT_{11}\overline{\beta}}{2\pi} \right] \right\} e^{i\omega t} \qquad (48)$$

$$M = \left\{ \rho_\infty b^2 \left\{ -\omega^2 \pi ba\, \overline{h} - i\omega\pi Ub \left(\frac{1}{2} - a \right) \overline{\alpha} + \omega^2 \pi b^2 \left(\frac{1}{8} + a^2 \right) \overline{\alpha} - (T_4 + T_{10})U^2\overline{\beta} \right. \right.$$

$$\left. - i\omega \left[T_1 - T_8 - (c - a)T_4 + \frac{T_{11}}{2} \right] Ub\, \overline{\beta} - \omega^2 \left[T_7 + (c - a)T_1 \right] b^2 \overline{\beta} \right\} \qquad (49)$$

$$\left. + 2\pi \rho_\infty Ub^2 \left(a + \frac{1}{2} \right) C(k) \left[U\overline{\alpha} + i\omega\overline{h} + i\omega b \left(\frac{1}{2} - a \right) \overline{\alpha} + \frac{T_{10}U\overline{\beta}}{\pi} + i\omega \frac{bT_{11}\overline{\beta}}{2\pi} \right] \right\} e^{i\omega t}$$

23

$$H = \left\{ \rho_\infty b^2 \left\{ -\omega^2 T_1 b\bar{h} - i\omega\left[-2T_9 - T_1 + T_4\left(a - \frac{1}{2}\right)\right]Ub\,\bar{\alpha} + 2\omega^2 T_{13} b^2 \bar{\alpha} \right.\right.$$

$$\left. - \frac{U^2(T_5 - T_4 T_{10})\bar{\beta}}{\pi} + i\omega\frac{UbT_4 T_{11}\bar{\beta}}{2\pi} - \omega^2\frac{T_3 b^2 \bar{\beta}}{\pi} \right\} \tag{50}$$

$$\left. - \rho_\infty Ub^2 T_{12} C(k)\left[U\bar{\alpha} + i\omega\bar{h} + i\omega b\left(\frac{1}{2} - a\right)\bar{\alpha} + \frac{T_{10}U\bar{\beta}}{\pi} + i\omega\frac{bT_{11}\bar{\beta}}{2\pi}\right] \right\} e^{i\omega t}$$

Similar to 2DoF equations U can be expressed as a function of reduced frequency $U=b\omega/k$. Substituting this expression into the lift, pitching moment and hinge moment expressions above and reorganizing them one gets:

$$L = \left\{ (-b\omega^2)\rho_\infty b^2 \left[\frac{-\omega^2\pi\bar{h} + i\omega\pi\dfrac{b\omega}{k}\bar{\alpha} + \omega^2\pi ba\,\bar{\alpha} - i\omega\dfrac{b\omega}{k}T_4\bar{\beta} + \omega^2 T_1 b\bar{\beta}}{(-b\omega^2)} \right] \right.$$

$$\left. + (b\omega)2\pi\rho_\infty\frac{b\omega}{k}bC(k)\left[\frac{\dfrac{b\omega}{k}\bar{\alpha} + i\omega\bar{h} + i\omega b\left(\dfrac{1}{2} - a\right)\bar{\alpha} + \dfrac{T_{10}b\omega\bar{\beta}}{\pi k} + i\omega\dfrac{bT_{11}\bar{\beta}}{2\pi}}{b\omega} \right] \right\} e^{i\omega t} \tag{51}$$

$$M = \left\{ (b^2\omega^2)\rho_\infty b^2 \left\{ \frac{-\omega^2\pi ba\,\bar{h} - i\omega\pi\dfrac{b\omega}{k}b\left(\dfrac{1}{2} - a\right)\bar{\alpha} + \omega^2\pi b^2\left(\dfrac{1}{8} + a^2\right)\bar{\alpha}}{b^2\omega^2} \right.\right.$$

$$\left. + \frac{-(T_4 + T_{10})\left(\dfrac{b\omega}{k}\right)^2\bar{\beta} - i\omega\left[T_1 - T_8 - (c - a)T_4 + \dfrac{T_{11}}{2}\right]\dfrac{b\omega}{k}b\bar{\beta} - \omega^2\left[T_7 + (c - a)T_1\right]b^2\bar{\beta}}{b^2\omega^2} \right\} \tag{52}$$

$$\left. + (b\omega)2\pi\rho_\infty\frac{b\omega}{k}b^2\left(a + \frac{1}{2}\right)C(k)\left[\frac{\dfrac{b\omega}{k}\bar{\alpha} + i\omega\bar{h} + i\omega b\left(\dfrac{1}{2} - a\right)\bar{\alpha} + \dfrac{T_{10}b\omega\bar{\beta}}{\pi k} + i\omega\dfrac{bT_{11}\bar{\beta}}{2\pi}}{b\omega} \right] \right\} e^{i\omega t}$$

$$H = \left\{ (\pi b^2 \omega^2) \rho_\infty b^2 \left\{ \frac{-\omega^2 T_1 b \overline{h} - i\omega \left[-2T_9 - T_1 + T_4 \left(a - \frac{1}{2} \right) \right] \frac{b\omega}{k} b \overline{\alpha} + \omega^2 2 T_{13} b^2 \overline{\alpha}}{\pi b^2 \omega^2} \right. \right.$$

$$\left. + \frac{\frac{-(b\omega)^2 (T_5 - T_4 T_{10}) \overline{\beta}}{\pi k^2} + i\omega \frac{b\omega b T_4 T_{11} \overline{\beta}}{2\pi k} - \omega^2 \frac{T_3 b^2 \overline{\beta}}{\pi}}{\pi b^2 \omega^2} \right\} \tag{53}$$

$$\left. - (\pi b \omega) \rho_\infty \frac{b\omega}{k} b^2 T_{12} C(k) \left[\frac{\frac{b\omega}{k} \overline{\alpha} + i\omega \overline{h} + i\omega b \left(\frac{1}{2} - a \right) \overline{\alpha} + \frac{T_{10} b\omega \overline{\beta}}{\pi k} + i\omega \frac{b T_{11} \overline{\beta}}{2\pi}}{\pi b \omega} \right] \right\} e^{i\omega t}$$

The lift, pitching moment and hinge moment expressions of the oscillating wing with a control surface can be reorganized one more time.

$$L = -\pi \rho_\infty b^3 \omega^2 \left\{ \frac{1}{b} \overline{h} - i \frac{1}{k} \overline{\alpha} - a \overline{\alpha} + i \frac{1}{\pi k} T_4 \overline{\beta} - \frac{1}{\pi} T_1 \overline{\beta} - \right.$$

$$\left. 2 \frac{1}{k} C(k) \left[\frac{1}{k} \overline{\alpha} + i \frac{1}{b} \overline{h} + i \left(\frac{1}{2} - a \right) \overline{\alpha} + \frac{T_{10} \overline{\beta}}{\pi k} + i \frac{T_{11} \overline{\beta}}{2\pi} \right] \right\} e^{i\omega t} \tag{54}$$

$$M = \pi \rho_\infty b^4 \omega^2 \left\{ -a \frac{1}{b} \overline{h} - i \frac{1}{k} \left(\frac{1}{2} - a \right) \overline{\alpha} + \left(\frac{1}{8} + a^2 \right) \overline{\alpha} - (T_4 + T_{10}) \frac{1}{\pi k^2} \overline{\beta} \right.$$

$$- i \left[T_1 - T_8 - (c - a) T_4 + \frac{T_{11}}{2} \right] \frac{1}{\pi k} \overline{\beta} - \frac{1}{\pi} [T_7 + (c - a) T_1] \overline{\beta} \tag{55}$$

$$\left. + 2 \frac{1}{k} \left(a + \frac{1}{2} \right) C(k) \left[\frac{1}{k} \overline{\alpha} + i \frac{1}{b} \overline{h} + i \left(\frac{1}{2} - a \right) \overline{\alpha} + \frac{T_{10} \overline{\beta}}{\pi k} + i \frac{T_{11} \overline{\beta}}{2\pi} \right] \right\} e^{i\omega t}$$

$$H = \pi \rho_\infty b^4 \omega^2 \left\{ \left\{ -\frac{T_1}{\pi}\frac{1}{b}\bar{h} - i\left[-2T_9 - T_1 + T_4\left(a - \frac{1}{2}\right)\right]\frac{1}{\pi k}\bar{\alpha} + 2\frac{1}{\pi}T_{13}\bar{\alpha} \right.\right.$$

$$\left. -\frac{1}{\pi^2 k^2}(T_5 - T_4 T_{10})\bar{\beta} + i\frac{1}{2\pi^2 k}T_4 T_{11}\bar{\beta} - \frac{T_3\bar{\beta}}{\pi^2} \right\} \tag{56}$$

$$\left. -\pi \rho_\infty b^4 \omega^2 \frac{1}{k}T_{12}C(k)\left[\frac{1}{\pi k}\bar{\alpha} + i\frac{1}{\pi b}\bar{h} + i\frac{1}{\pi}\left(\frac{1}{2} - a\right)\bar{\alpha} + T_{10}\frac{1}{\pi^2 k}\bar{\beta} + i\frac{T_{11}\bar{\beta}}{2\pi^2}\right] \right\}e^{i\omega t}$$

Finally, lift, pitching moment and hinge moment expressions of the oscillating wing with a control surface is brought into the forms given by Equations (57), (58)   and (59).

$$L = -\pi \rho_\infty b^3 \omega^2 \left\{ \left(1 - \frac{2iC(k)}{k}\right)\frac{\bar{h}}{b} + \left(-a - \frac{i[1 + (1 - 2a)C(k)]}{k} - \frac{2C(k)}{k^2}\right)\bar{\alpha} \right.$$

$$\left. + \left(-\frac{T_1}{\pi} + \frac{iT_4}{\pi k} - \frac{iT_{11}C(k)}{\pi k} - \frac{2T_{10}C(k)}{\pi k^2}\right)\bar{\beta} \right\}e^{i\omega t} \tag{57}$$

$$M = \pi \rho_\infty b^4 \omega^2 \left\{ \left[-a + \frac{i(2a+1)C(k)}{k}\right]\frac{\bar{h}}{b} + \left[\frac{1}{8} + a^2 + \frac{(2a+1)C(k)}{k^2}\right.\right.$$

$$\left. -\frac{i(0.5-a)[1 - (2a+1)C(k)]}{k}\right]\bar{\alpha} + \left[-\frac{T_4 + T_{10} - (2a+1)T_{10}C(k)}{\pi k^2}\right.$$

$$\left.\left. -\frac{T_7 + (c-a)T_1}{\pi} - \frac{i[T_8 - T_1 + (c-a)T_4 - 0.5T_{11} + (a+0.5)T_{11}C(k)]}{\pi k}\right]\bar{\beta} \right\}e^{i\omega t} \tag{58}$$

$$H = \pi \rho_\infty b^4 \omega^2 \left\{ \left(-\frac{T_1}{\pi} - \frac{iT_{12}C(k)}{\pi k}\right)\frac{\bar{h}}{b} + \left(\frac{i[2T_9 + T_1 + (0.5-a)(T_4 - T_{12}C(k))]}{\pi k}\right.\right.$$

$$\left. + \frac{2T_{13}}{\pi} - \frac{T_{12}C(k)}{\pi k^2}\right)\bar{\alpha} + \left(-\frac{T_3}{\pi^2} + \frac{iT_4 T_{11}}{2\pi^2 k} - \frac{iT_{11}T_{12}C(k)}{2\pi^2 k} - \frac{(T_5 - T_4 T_{10})}{\pi^2 k^2}\right.$$

$$\left.\left. - \frac{T_{10}T_{12}C(k)}{\pi^2 k^2}\right)\bar{\beta} \right\}e^{i\omega t} \tag{59}$$

It can be noticed that Equations (57) and (58) take the similar form which is suggested in Equations (10) and (11). So, the equations of lift and moments of a 3 DoF typical Section in incompressible flow can be expressed as:

$$L = -\pi \rho_\infty b^3 \omega^2 \left[L_h \frac{\overline{h}}{b} + L_\alpha \overline{\alpha} + L_\beta \overline{\beta} \right] e^{i\omega t} \tag{60}$$

$$M = \pi \rho_\infty b^4 \omega^2 \left[M_h \frac{\overline{h}}{b} + M_\alpha \overline{\alpha} + M_\beta \overline{\beta} \right] e^{i\omega t} \tag{61}$$

$$H = \pi \rho_\infty b^4 \omega^2 \left[H_h \frac{\overline{h}}{b} + H_\alpha \overline{\alpha} + H_\beta \overline{\beta} \right] e^{i\omega t} \tag{62}$$

where the new coefficients appearing in Equations (60), (61) and (62) are defined in Equation (63).

$$L_\beta = -\frac{T_1}{\pi} + \frac{iT_4}{\pi k} - \frac{iT_{11}C(k)}{\pi k} - \frac{2T_{10}C(k)}{\pi k^2}$$

$$M_\beta = -\frac{T_7 + (c-a)T_1}{\pi} - \frac{i\left[T_8 - T_1 + (c-a)T_4 - 0.5T_{11} + (a+0.5)T_{11}C(k)\right]}{\pi k}$$
$$\quad - \frac{T_4 + T_{10} - (2a+1)T_{10}C(k)}{\pi k^2}$$

$$H_h = \left(-\frac{T_1}{\pi} - \frac{iT_{12}C(k)}{\pi k} \right)$$

$$H_\alpha = \frac{2T_{13}}{\pi} + \frac{i\left[2T_9 + T_1 + (0.5-a)(T_4 - T_{12}C(k))\right]}{\pi k} - \frac{T_{12}C(k)}{\pi k^2}$$

$$H_\beta = -\frac{T_3}{\pi^2} + \frac{iT_4 T_{11}}{2\pi^2 k} - \frac{iT_{11}T_{12}C(k)}{2\pi^2 k} - \frac{(T_5 - T_4 T_{10})}{\pi^2 k^2} - \frac{T_{10}T_{12}C(k)}{\pi^2 k^2}$$

$$\tag{63}$$

It should be noted that the expressions of L_h, L_α, M_h, and M_α were previously given in Equation (33). T_i terms are constants specific for a typical section model which are functions of the nondimensional distance between the hinge line and the midchord

and the nondimensional distance of the elastic axis from the midchord. T_i terms are given as [4];

$$T_1 = -\tfrac{1}{3}\sqrt{1-c^2}\left(2+c^2\right)+c\left(\cos^{-1}c\right)$$

$$T_2 = c\left(1-c^2\right)-\sqrt{1-c^2}\left(1+c^2\right)\cos^{-1}c+c\left(\cos^{-1}c\right)^2$$

$$T_3 = -\left(\tfrac{1}{8}+c^2\right)\left(\cos^{-1}c\right)^2+\tfrac{1}{4}c\sqrt{1-c^2}\cos^{-1}c\left(7+2c^2\right)-\tfrac{1}{8}\left(1-c^2\right)\left(5c^2+4\right)$$

$$T_4 = -\cos^{-1}c+c\sqrt{1-c^2}$$

$$T_5 = -\left(1-c^2\right)-\left(\cos^{-1}c\right)^2+2c\sqrt{1-c^2}\cos^{-1}c$$

$$T_6 = T_2$$

$$T_7 = -\left(\tfrac{1}{8}+c^2\right)\cos^{-1}c+\tfrac{1}{8}c\sqrt{1-c^2}\left(7+2c^2\right)$$

$$T_8 = -\tfrac{1}{3}\sqrt{1-c^2}\left(2c^2+1\right)+c\left(\cos^{-1}c\right)$$

$$T_9 = \tfrac{1}{2}\left(\tfrac{1}{3}\sqrt{1-c^2}+aT_4\right)$$

$$T_{10} = \sqrt{1-c^2}+\cos^{-1}c$$

$$T_{11} = \cos^{-1}c\left(1-2c\right)+\sqrt{1-c^2}\left(2-c\right)$$

$$T_{12} = \sqrt{1-c^2}\left(2+c\right)-\cos^{-1}c\left(2c+1\right)$$

$$T_{13} = \tfrac{1}{2}\left[-T_7-\left(c-a\right)T_1\right]$$

$$T_{14} = \tfrac{1}{16}+\tfrac{1}{2}ac \qquad\qquad (64)$$

The equations of motion for 3 DoF typical section model which were defined in Equation (39), (40) and (41), can be written as:

$$mb\frac{\ddot{h}}{b}+S_\alpha\ddot{\alpha}+S_\beta\ddot{\beta}+bK_h\frac{h}{b}+L=0 \qquad\qquad (65)$$

$$S_\alpha\frac{\ddot{h}}{b}+\frac{I_\alpha}{b}\ddot{\alpha}+\frac{\left[(c-a)bS_\beta+I_\beta\right]}{b}\ddot{\beta}+\frac{K_\alpha}{b}\alpha-\frac{M}{b}=0 \qquad\qquad (66)$$

$$S_\beta\frac{\ddot{h}}{b}+\frac{\left[(c-a)bS_\beta+I_\beta\right]}{b}\ddot{\alpha}+\frac{I_\beta}{b}\ddot{\beta}+\frac{K_\beta}{b}\beta-\frac{H}{b}=0 \qquad\qquad (67)$$

Rewriting Equations, (65), (66) and (67) in matrix form we have the equation which defines an aeroelastic system in which structural damping is ignored:

$$
\begin{bmatrix} mb & S_\alpha & S_\beta \\ S_\alpha & I_\alpha/b & \dfrac{(c-a)bS_\beta + I_\beta}{b} \\ S_\beta & \dfrac{(c-a)bS_\beta + I_\beta}{b} & I_\beta/b \end{bmatrix} \begin{Bmatrix} \ddot{h}/b \\ \ddot{\alpha} \\ \ddot{\beta} \end{Bmatrix} + \begin{bmatrix} bK_h & 0 & 0 \\ 0 & K_\alpha/b & 0 \\ 0 & 0 & K_\beta/b \end{bmatrix} \begin{Bmatrix} h/b \\ \alpha \\ \beta \end{Bmatrix}
$$

$$
- \pi \rho_\infty b^3 \omega^2 \begin{bmatrix} L_h & L_\alpha & L_\beta \\ M_h & M_\alpha & M_\beta \\ H_h & H_\alpha & H_\beta \end{bmatrix} \begin{Bmatrix} \overline{h}/b \\ \overline{\alpha} \\ \overline{\beta} \end{Bmatrix} = 0
\tag{68}
$$

Equation (68) can be expressed as;

$$
[M]\{\ddot{q}\} + [K]\{q\} - \pi \rho_\infty b^3 \omega^2 [A(k)]\{\overline{q}\} = 0
\tag{69}
$$

where [M], [K], [A], {q} are the mass, stiffness and aerodynamic coefficient matrix and generalized coordinates vector respectively.

$$
[M] = \begin{bmatrix} mb & S_\alpha & S_\beta \\ S_\alpha & I_\alpha/b & \dfrac{(c-a)bS_\beta + I_\beta}{b} \\ S_\beta & \dfrac{(c-a)bS_\beta + I_\beta}{b} & I_\beta/b \end{bmatrix}, \qquad \{q\} = \begin{Bmatrix} h/b \\ \alpha \\ \beta \end{Bmatrix},
$$

$$
[A] = \begin{bmatrix} L_h & L_\alpha & L_\beta \\ M_h & M_\alpha & M_\beta \\ H_h & H_\alpha & H_\beta \end{bmatrix}, \qquad [K] = \begin{bmatrix} bK_h & 0 & 0 \\ 0 & K_\alpha/b & 0 \\ 0 & 0 & K_\beta/b \end{bmatrix}
\tag{70}
$$

To find out the flutter boundaries for a constant flight condition, the aeroelastic system equation should be solved. Generally the real parts of the eigenvalues determined from the solution define the damping. If the real parts of the eigenvalues are negative then it means the motion is stable, if they are positive, it means the motion is unstable. In this study two flutter prediction methods are used: k-Method and P-k Method [12], [13].

2.7.   k-Method

In this method an artificial damping term is introduced and added to the aeroelastic system equation. The terms in the equation are simplified by nondimensionalizing and then the simplified equation is solved and the eigenvalues for aeroelastic modes which were defined as a function of artificial dampings are obtained. The values of damping are obtained for a range of reduced frequencies. The point where the value of this damping goes to positive from negative is the point of flutter. Flutter speed and flutter frequency are achieved after determining this point [12].

An artificial structural damping coefficient which is indicated by letter g is introduced to the aeroelastic system equation (69).

$$[M]\{\ddot{q}\} + (1 + ig)[K]\{q\} - \pi\rho_\infty b^3 \omega^2 [A(k)]\{\overline{q}\} = 0 \qquad (71)$$

For harmonic oscillation Equation (71) becomes

$$-\omega^2 [M]\{\overline{q}\} + (1 + ig)[K]\{\overline{q}\} - \pi\rho_\infty b^3 \omega^2 [A(k)]\{\overline{q}\} = 0 \qquad (72)$$

Dividing all terms by $(-\omega^2)$;

$$\left\{ [M] + \pi\rho_\infty b^3 [A(k)] - \frac{(1+ig)}{\omega^2} [K] \right\} \{\bar{q}\} = 0 \qquad (73)$$

where $\dfrac{(1+ig)}{\omega^2}$ is the eigenvalue parameter λ. Note that;

$$\text{Re}(\lambda) = \frac{1}{\omega^2}, \qquad \text{Im}(\lambda) = \frac{g}{\omega^2}, \quad \Rightarrow \quad \omega = \frac{1}{\sqrt{\text{Re}(\lambda)}}, \quad g = \frac{\text{Im}(\lambda)}{\text{Re}(\lambda)} \qquad (74)$$

Multiplying Equation (73) with $\dfrac{1}{\pi\rho_\infty b^3}$, one non-dimensionalizes the the equation;

$$\left\{ \begin{bmatrix} \dfrac{mb}{\pi\rho_\infty b^3} & \dfrac{S_\alpha}{\pi\rho_\infty b^3} & \dfrac{S_\beta}{\pi\rho_\infty b^3} \\[2mm] \dfrac{S_\alpha}{\pi\rho_\infty b^3} & \dfrac{I_\alpha}{\pi\rho_\infty b^4} & \dfrac{(c-a)bS_\beta + I_\beta}{\pi\rho_\infty b^4} \\[2mm] \dfrac{S_\beta}{\pi\rho_\infty b^3} & \dfrac{(c-a)bS_\beta + I_\beta}{\pi\rho_\infty b^4} & \dfrac{I_\beta}{\pi\rho_\infty b^4} \end{bmatrix} + \begin{bmatrix} L_h & L_\alpha & L_\beta \\ M_h & M_\alpha & M_\beta \\ H_h & H_\alpha & H_\beta \end{bmatrix} \cdots \right.$$

$$\left. - \lambda \begin{bmatrix} \dfrac{K_h}{\pi\rho_\infty b^2} & 0 & 0 \\[2mm] 0 & \dfrac{K_\alpha}{\pi\rho_\infty b^4} & 0 \\[2mm] 0 & 0 & \dfrac{K_\beta}{\pi\rho_\infty b^4} \end{bmatrix} \right\} \left\{ \begin{array}{c} \bar{h}/b \\ \bar{\alpha} \\ \bar{\beta} \end{array} \right\} = 0 \qquad (75)$$

Note that;

$$r_\beta^2 = \frac{I_\beta}{m_\beta b^2}, \qquad K_h = m\omega_h^2, \qquad K_\alpha = I_\alpha \omega_\alpha^2, \qquad K_\beta = I_\beta \omega_\beta^2 \qquad (76)$$

where m_β is the mass of the control surface and r_β is the control surface's nondimensional radius of gyration about the hinge line. Combining Equation (14), (75), (16) and (76) nondimensional form of the equation associated with the k-method can be written as:

$$
\left\{
\begin{bmatrix}
\mu & \mu X_\alpha & \dfrac{m_\beta}{m}\mu X_\beta \\[2mm]
\mu X_\alpha & \mu r_\alpha^{\,2} & \dfrac{m_\beta}{m}\mu\big[(c-a)X_\beta + r_\beta^{\,2}\big] \\[2mm]
\dfrac{m_\beta}{m}\mu X_\beta & \dfrac{m_\beta}{m}\mu\big[(c-a)X_\beta + r_\beta^{\,2}\big] & \dfrac{m_\beta}{m}\mu r_\beta^{\,2}
\end{bmatrix}
+
\begin{bmatrix}
L_h & L_\alpha & L_\beta \\
M_h & M_\alpha & M_\beta \\
H_h & H_\alpha & H_\beta
\end{bmatrix}
\cdots
\right.
$$

$$
\left.
-\lambda
\begin{bmatrix}
\omega_h^2\mu & 0 & 0 \\[2mm]
0 & \omega_\alpha^2\mu r_\alpha^{\,2} & 0 \\[2mm]
0 & 0 & \omega_\beta^2\dfrac{m_\beta}{m}\mu r_\beta^{\,2}
\end{bmatrix}
\right\}
\left\{
\begin{array}{c}
\overline{h}/b \\[1mm]
\overline{\alpha} \\[1mm]
\overline{\beta}
\end{array}
\right\} = 0
\tag{77}
$$

$$
\big\{[\overline{M}] + [\overline{A}] - \lambda[\overline{K}]\big\}\{\overline{q}\} = 0
\tag{78}
$$

where nondimensionalized mass, aerodynamic coefficient and stiffness matrices are defined in Equation (79).

$$
[\overline{M}] =
\begin{bmatrix}
\mu & \mu X_\alpha & \dfrac{m_\beta}{m}\mu X_\beta \\[2mm]
\mu X_\alpha & \mu r_\alpha^{\,2} & \dfrac{m_\beta}{m}\mu\big[(c-a)X_\beta + r_\beta^{\,2}\big] \\[2mm]
\dfrac{m_\beta}{m}\mu X_\beta & \dfrac{m_\beta}{m}\mu\big[(c-a)X_\beta + r_\beta^{\,2}\big] & \dfrac{m_\beta}{m}\mu r_\beta^{\,2}
\end{bmatrix},
$$

$$
[\overline{A}(k)] = [A(k)], \qquad
[\overline{K}] =
\begin{bmatrix}
\omega_h^2\mu & 0 & 0 \\[2mm]
0 & \omega_\alpha^2\mu r_\alpha^{\,2} & 0 \\[2mm]
0 & 0 & \omega_\beta^2\dfrac{m_\beta}{m}\mu r_\beta^{\,2}
\end{bmatrix}
\tag{79}
$$

Multiplying both sides of Equation (78) by $[K]^{-1}$, we have the eigenvalue problem:

$$\left\{ [\overline{K}]^{-1} \left\{ [\overline{M}] + [\overline{A}(k)] \right\} - [I]\lambda \right\} \{\overline{q}\} = 0 \tag{80}$$

Following the steps defined below k-method equation can be solved.

1. Specify a range of interest for reduced frequency k. k-method would not allow k to be chosen as 0 because U is calculated as a function of $\dfrac{1}{k}$.

2. For all k values specified;

   a. Compute the aerodynamic coefficient matrix $[\overline{A}(k)]$.

   b. Solve the eigenvalue problem given in Equation (80) and determine the eigenvalue parameters λ_i for each mode.

   c. Determine the frequencies ω_i and damping parameters g_i for each mode using the formulation given in Equation (74). The corresponding speed can be determined as $U_i = \dfrac{b\omega_i}{k}$.

3. Plot the graphs U_i vs ω_i and U_i vs g_i for each mode.

4. Using the graphs determine the flutter speed U_f at the point where g=0 (where the damping changes sign from negative to positive) and corresponding flutter frequency ω_f [12].

2.8. p-k Method

In comparison to k-method p-k method is more sophisticated, because in p-k method frequency matching process is performed. It is an iterative process which includes the calculation of the eigenvalue p for a preassumed reduced frequency k, and

computation of k from the calculated p value until the k values converges. This process is performed for the whole speed range of interest. Then, similar to k-method the graphs U vs. ω and U vs. g are plotted to find out flutter speed and frequency.

Dividing all terms to $\pi p_\infty b^3$ in Equation (69) we have the equation of motion in the form below:

$$
\begin{bmatrix} \mu & \mu X_\alpha & \dfrac{m_\beta}{m}\mu X_\beta \\ \mu X_\alpha & \mu r_\alpha^2 & \dfrac{m_\beta}{m}\mu\big[(c-a)X_\beta + r_\beta^2\big] \\ \dfrac{m_\beta}{m}\mu X_\beta & \dfrac{m_\beta}{m}\mu\big[(c-a)X_\beta + r_\beta^2\big] & \dfrac{m_\beta}{m}\mu r_\beta^2 \end{bmatrix} \begin{Bmatrix} \ddot{h}/b \\ \ddot{\alpha} \\ \ddot{\beta} \end{Bmatrix}
$$

$$
+ \begin{bmatrix} \omega_h^2 \mu & 0 & 0 \\ 0 & \omega_\alpha^2 \mu r_\alpha^2 & 0 \\ 0 & 0 & \omega_\beta^2 \dfrac{m_\beta}{m}\mu r_\beta^2 \end{bmatrix} \begin{Bmatrix} h/b \\ \alpha \\ \beta \end{Bmatrix} - \omega^2 \begin{bmatrix} L_h & L_\alpha & L_\beta \\ M_h & M_\alpha & M_\beta \\ H_h & H_\alpha & H_\beta \end{bmatrix} \begin{Bmatrix} \overline{h}/b \\ \overline{\alpha} \\ \overline{\beta} \end{Bmatrix} = 0 \tag{81}
$$

which can be written as:

$$
[\overline{M}]\{\ddot{q}\} + [\overline{K}]\{q\} - \omega^2 [\overline{A}(k)]\{\overline{q}\} = 0 \tag{82}
$$

The term p introduced as:

$$
p = \omega(\gamma + i) \tag{83}
$$

where γ is the transient decay parameter which is relatively small to ω. The relation between the structural damping term g of the k-method and transient decay parameter γ is given by the expression $g \cong 2\gamma$ for lightly damped conditions[8]. So the generalized coordinates vector can be written in terms of p:

$${q} = {\overline{q}}e^{pt} \qquad (84)$$

Assuming simple harmonic motion in Equation (82) and allocating the term $\left[\overline{A}(k)\right]$ to real and imaginary parts:

$$\left\{p^2\left[\overline{M}\right]+\left[\overline{K}\right]-\omega^2\,\mathrm{Re}\left[\overline{A}(k)\right]-i\omega^2\,\mathrm{Im}\left[\overline{A}(k)\right]\right\}\{\overline{q}\}=0 \qquad (85)$$

Here it should be noted that in the p-k method aerodynamic is still assumed to be due to simple harmonic motion as in the k method. However, in the p-k method both p and k methods are somewhat combined. Generalized coordinate vector q multiplying the mass and stiffness matrices in Equation (82) is assumed to have an oscillatory part and a transient decay part.

Writing the first ω term multiplying the real part of the aerodynamic matrix in Equation (85) in terms of k, U and b, and than multiplying the second ω term multiplying the imaginary part of the aerodynamic matrix with p over $i\omega$, Equation (85) becomes:

$$\left\{p^2\left[\overline{M}\right]+\left[\overline{K}\right]-k^2\left(\frac{U}{b}\right)^2\mathrm{Re}\left[\overline{A}(k)\right]-i\omega^2\left(\frac{p}{i\omega}\right)\mathrm{Im}\left[\overline{A}(k)\right]\right\}\{\overline{q}\}=0 \qquad (86)$$

It should be noted that since γ is relatively small compared to ω, multiplying the imaginary part of the aerodynamic matrix by p over $i\omega$ can be assumed to have not much effect on the resulting equation.

Rewriting the ω term in terms of k, U and b once again:

35

$$\left\{ p^2 \left[\overline{M} \right] + \left[\overline{K} \right] - k^2 \left(\frac{U}{b} \right)^2 \operatorname{Re} \left[\overline{A}(k) \right] - k \frac{U}{b} p \operatorname{Im} \left[\overline{A}(k) \right] \right\} \{ \overline{q} \} = 0 \qquad (87)$$

Remembering Equation (84):

$$\left[\overline{M} \right] \{ \ddot{q} \} - k \frac{U}{b} \operatorname{Im} \left[\overline{A}(k) \right] \{ \dot{q} \} + \left\{ \left[\overline{K} \right] - k^2 \left(\frac{U}{b} \right)^2 \operatorname{Re} \left[\overline{A}(k) \right] \right\} \{ q \} = 0 \qquad (88)$$

So $\{ \ddot{q} \}$ is:

$$\{ \ddot{q} \} = k \frac{U}{b} \left[\overline{M} \right]^{-1} \operatorname{Im} \left[\overline{A}(k) \right] \{ \dot{q} \} - \left[\overline{M} \right]^{-1} \left\{ \left[\overline{K} \right] - k^2 \left(\frac{U}{b} \right)^2 \operatorname{Re} \left[\overline{A}(k) \right] \right\} \{ q \} \qquad (89)$$

which can be written as:

$$\{ \ddot{q} \} = \left[-\left[\overline{M} \right]^{-1} \left\{ \left[\overline{K} \right] - k^2 \left(\frac{U}{b} \right)^2 \operatorname{Re} \left[\overline{A}(k) \right] \right\} \quad \vdots \quad k \frac{U}{b} \left[\overline{M} \right]^{-1} \operatorname{Im} \left[\overline{A}(k) \right] \right] \begin{Bmatrix} \{ q \} \\ \cdots \\ \{ \dot{q} \} \end{Bmatrix} \qquad (90)$$

So Equation (87) can be written in state space form to get the eigenvalue problem for p-k method solution which is:

$$\{ [A] - [I] p \} \begin{Bmatrix} q \\ \cdots \\ \dot{q} \end{Bmatrix} = \{ 0 \} \qquad (91)$$

36

where;

$$[A] = \begin{bmatrix} [0] & \vdots & [I] \\ \cdots & & \cdots \\ -[\overline{M}]^{-1}\left\{[\overline{K}] - k^2\left(\dfrac{U}{b}\right)^2 \mathrm{Re}\,[\overline{A}(k)]\right\} & \vdots & k\dfrac{U}{b}[\overline{M}]^{-1}\,\mathrm{Im}\,[\overline{A}(k)] \end{bmatrix} \tag{92}$$

To solve the eigenvalue problem and determine flutter speeds and frequencies an iterative method is applied. Steps given below should be followed to determine the flutter speed and the flutter frequency in the p-k method.

1. Specify a range of speed parameter U/b of interest.

2. Set an initial k_1 value and a *tolerance* for k to converge.

3. For each U/b value specified;

    a. Using the initial k_1 value, solve the eigenvalue problem given in Equation (91) to determine a p_1 value. Note that the imaginary part of the determined p_1 stands for ω_1. Dividing the ω_1 value determined by U/b value specified, get a value for k_2

    b. Repeat the step above until the condition $(k_{n+1}-k_n) < $ *tolerance* is satisfied.

    c. For the k_i value which satisfies the above condition Calculate the corresponding p_i value which gives the frequency ω_i and the damping g_i ($g = 2\gamma$) for the specified U_i/b.

4. Plot the graphs U_i vs ω_i and U_i vs g_i for each mode.

5. Using the graphs determine the flutter speed U_f at the point where g=0 (where the damping changes sign from negative to positive) and corresponding flutter frequency ω_f [12].

2.9. Code Validation

Using MATLAB, codes are generated to predict the flutter speed and flutter using k-method and p-k method. The examples below are considered to prove the code generated works properly.

The first example is a 2 DoF typical section problem given in Reference [8]. The properties of the typical section given in Figure 5, and the flight condition are given as nondimensional parameters which are:

$$
\begin{aligned}
a &= -0.2, \\
x_\alpha &= 0.1, \\
\mu &= 20, \\
r_\alpha^2 &= 0.24, \\
\omega_h / \omega_\alpha &= 0.4.
\end{aligned}
\tag{93}
$$

In k-method solution, Equation (77) can be written for 2 DoF. Since ω_h and ω_α are not known separately, but the ratio is known, a new eigenvalue parameter and a new stiffness matrix should be defined.

$$
\left\{ \begin{bmatrix} \mu & \mu X_\alpha \\ \mu X_\alpha & \mu r_\alpha^2 \end{bmatrix} + \begin{bmatrix} L_h & L_\alpha \\ M_h & M_\alpha \end{bmatrix} - \omega_\alpha^2 \lambda \begin{bmatrix} \dfrac{\omega_h^2}{\omega_\alpha^2}\mu & 0 \\ 0 & \mu r_\alpha^2 \end{bmatrix} \right\} \begin{Bmatrix} \bar{h}/b \\ \bar{\alpha} \\ \bar{\beta} \end{Bmatrix} = 0
\tag{94}
$$

The new eigenvalue parameter is $\bar{\lambda} = \dfrac{\omega_\alpha^{\;2}(1+ig)}{\omega^2}$. Solving the eigenvale problem for

each k of interest and using:

$$\mathrm{Re}(\bar{\lambda}) = \frac{\omega_\alpha^{\;2}}{\omega^2}, \qquad \mathrm{Im}(\bar{\lambda}) = \frac{\omega_\alpha^{\;2}g}{\omega^2}, \qquad \Rightarrow \qquad \frac{\omega}{\omega_\alpha} = \frac{1}{\sqrt{\mathrm{Re}(\bar{\lambda})}}, \qquad g = \frac{\mathrm{Im}(\bar{\lambda})}{\mathrm{Re}(\bar{\lambda})} \qquad (95)$$

$\dfrac{\omega}{\omega_\alpha}$, g and $\dfrac{U}{b\omega_\alpha} = \dfrac{\omega}{\omega_\alpha}\dfrac{1}{k}$ are calculated for each k value. The graphs $\dfrac{U}{b\omega_\alpha}$ vs $\dfrac{\omega}{\omega_\alpha}$

and $\dfrac{U}{b\omega_\alpha}$ vs g are plotted. Figure 7 gives speed vs. frequency curve, and Figure 8
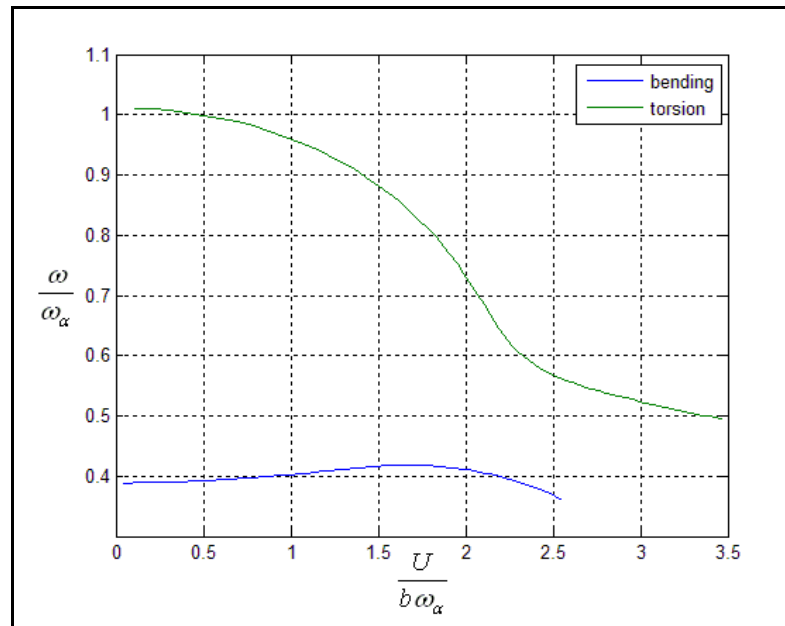
gives the damping vs. speed curve.

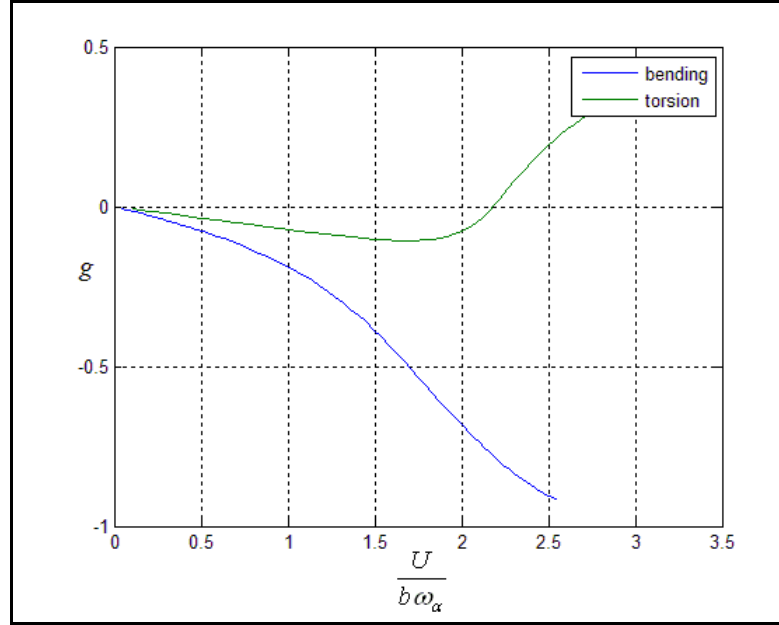**Figure 7.** Frequency vs speed plot of the 2DoF typical section (k-method).

Figure 8. Damping vs. speed plot of the 2DoF typical section (k-method).

For p-k method solution if Equation is rewritten for 2 DoF:

$$
\begin{bmatrix} \mu & \mu X_\alpha \\ \mu X_\alpha & \mu r_\alpha^2 \end{bmatrix} \begin{Bmatrix} \ddot{h}/b \\ \ddot{\alpha} \end{Bmatrix} + \begin{bmatrix} \omega_h^2 \mu & 0 \\ 0 & \omega_\alpha^2 \mu r_\alpha^2 \end{bmatrix} \begin{Bmatrix} h/b \\ \alpha \end{Bmatrix} - \omega^2 \begin{bmatrix} L_h & L_\alpha \\ M_h & M_\alpha \end{bmatrix} \begin{Bmatrix} \overline{h}/b \\ \overline{\alpha} \end{Bmatrix} = 0 \qquad (96)
$$

In p-k method solution of the same example, similar to the solution process in k-method a new stiffness matrix and eigenvalues parameter needs to be defined. They are:

$$
\overline{p} = \frac{\omega}{\omega_\alpha}(\gamma + i) \qquad (97)
$$

$$
\left[\overline{\overline{K}} \right] = \begin{bmatrix} \dfrac{\omega_h^2}{\omega_\alpha^2} \mu & 0 \\ 0 & \mu r_\alpha^2 \end{bmatrix} \qquad (98)
$$

40

For these new eigenvalues parameters and stiffness matrix Equation (87) and (92) becomes:

$$\left\{ \overline{p}^{2}\left[\overline{M}\right] + \left[\overline{\overline{K}}\right] - k^{2}\left(\frac{U}{b\,\omega_{\alpha}}\right)^{2} \text{Re}\left[\overline{A}\left(k\right)\right] - k\,\frac{U}{b\,\omega_{\alpha}}\,\overline{p}\,\text{Im}\left[\overline{A}\left(k\right)\right]\right\}\left\{\overline{q}\right\} = 0 \qquad (99)$$

$$\left[\overline{A}\right] = \begin{bmatrix} [0] & \vdots & [I] \\ \cdots & & \cdots \\ -\left[\overline{M}\right]^{-1}\left\{\left[\overline{\overline{K}}\right] - k^{2}\left(\frac{U}{b\,\omega_{\alpha}}\right)^{2}\text{Re}\left[\overline{A}\left(k\right)\right]\right\} & \vdots & k\,\frac{U}{b\,\omega_{\alpha}}\left[\left[\overline{M}\right]^{-1}\text{Im}\left[\overline{A}\left(k\right)\right]\right] \end{bmatrix} \qquad (100)$$

The eigenvalue problem to get the solutions is:

$$\left\{\left[\overline{A}\right] - [I]\overline{p}\right\}\left\{\begin{array}{c} q \\ \cdots \\ \dot{q} \end{array}\right\} = \{0\} \qquad (101)$$

We specify the range for velocity $\dfrac{U}{b\,\omega_{\alpha}}$, set k_{initial} as 0.35 and convergence tolerance value for k as 0.0001. For each $\dfrac{U}{b\,\omega_{\alpha}}$ value, eigenvalues $\overline{p}$ are calculated. The imaginary part of $\overline{p}$ stands for $\dfrac{\omega}{\omega_{\alpha}}$. By dividing this term to corresponding $\dfrac{U}{b\,\omega_{\alpha}}$ a new k value is calculated. This step is repeated until the convergence criterion above is satisfied. When the convergence criterion is satisfied we store the corresponding frequency and damping value and continue to the next $\dfrac{U}{b\,\omega_{\alpha}}$ point. After all $\dfrac{U}{b\,\omega_{\alpha}}$

41

values are held. The graphs $\dfrac{U}{b\omega_\alpha}$ vs $\dfrac{\omega}{\omega_\alpha}$ and $\dfrac{U}{b\omega_\alpha}$ vs g are plotted. Figure 9 gives

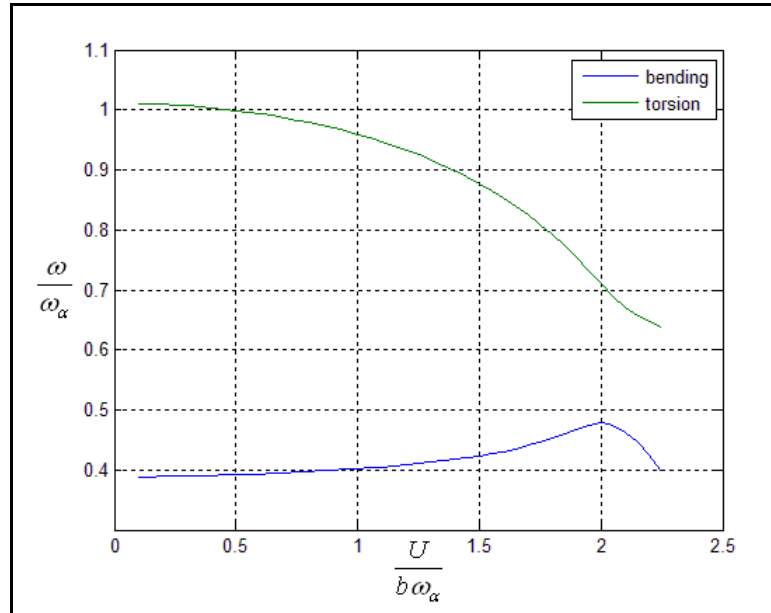the curve speed vs frequency and Figure 10 gives speed vs damping.

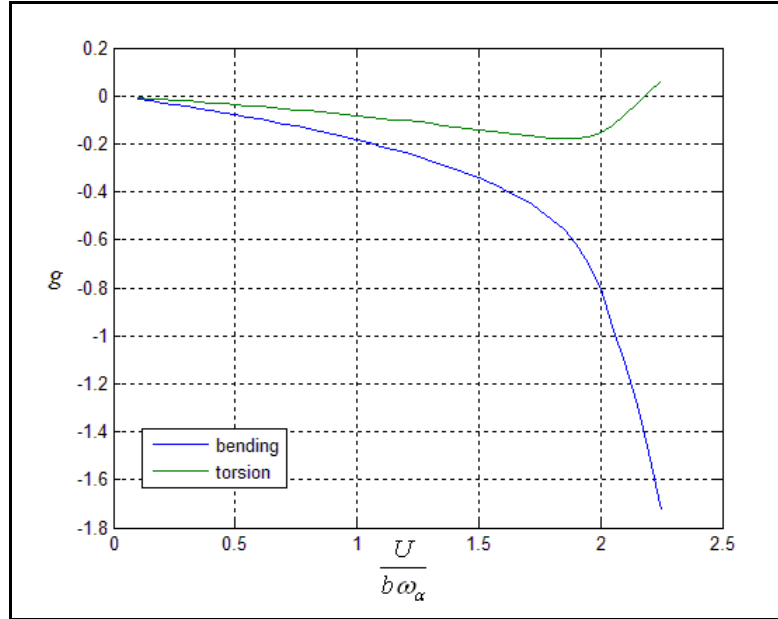**Figure 9.** Frequency vs.speed plot of the 2DoF typical section (p-k method).

Figure 10. Damping vs. speed plot of the 2DoF typical section (p-k method).

As seen from the figures above, although there are minor changes in the graphics, both k-method and p-k method solutions give the same results for flutter speed and flutter frequency with excellent agreement. Flutter is predicted to occur in torsion mode due to both methods. Flutter speed and frequency are:

$$\frac{U_f}{b\,\omega_\alpha} \approx 2.18, \qquad \frac{\omega_f}{\omega_\alpha} \approx 0.65 \qquad (102)$$

The results are in consistence with the reference.

The second example is a 3 DoF typical section problem given in Reference [14]. The properties of the typical section and the flight condition are given as nondimensional parameters which are:

$$a = -0.4,$$
$$x_\alpha = 0.2,$$
$$c = 0.6,$$
$$\mu = 40,$$
$$m_\beta / m = 0.2,$$
$$r_\alpha^2 = 0.25,$$
$$r_\beta^2 = 0.05,$$
$$x_\beta = 0.0125,$$
$$\omega_h / \omega_\alpha = 0.5,$$
$$\omega_h / \omega_\beta = 0.2108.$$

(103)

Following the similar steps as mentioned in the solution of 2 DoF Typical Section Model problem above, The graphics shown in Figure 11 and Figure 12 are generated for the k-method solution and the graphics shown in Figure 13 and Figure 14 are generated for p-k method solution.
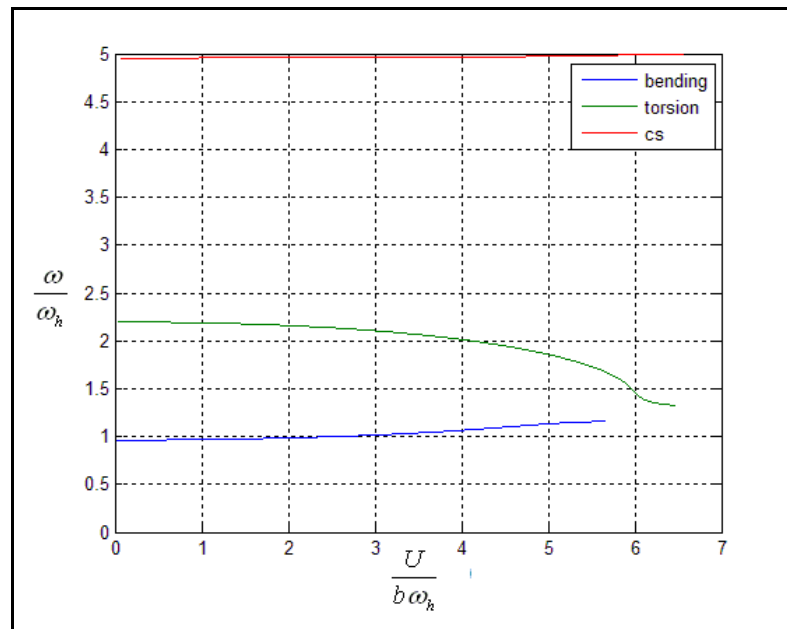

Figure 11. Frequency vs.speed plot of the second example (k-method).
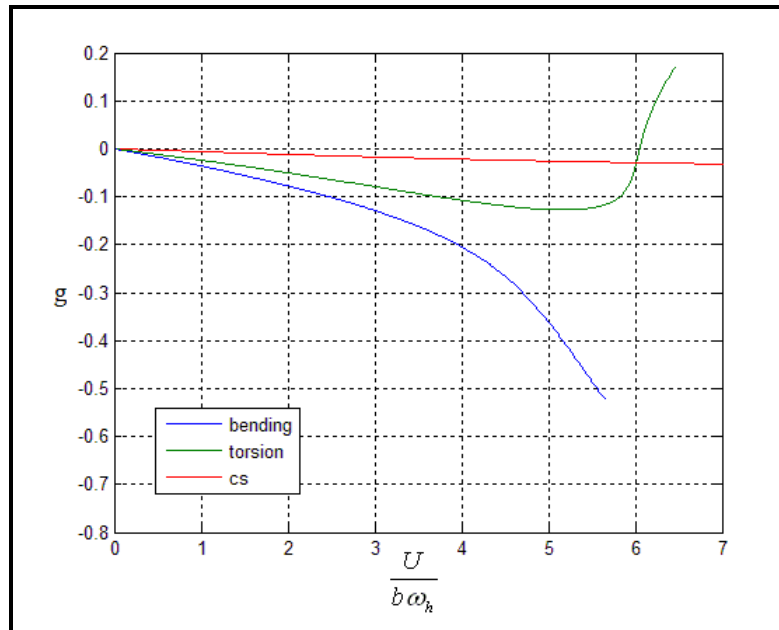
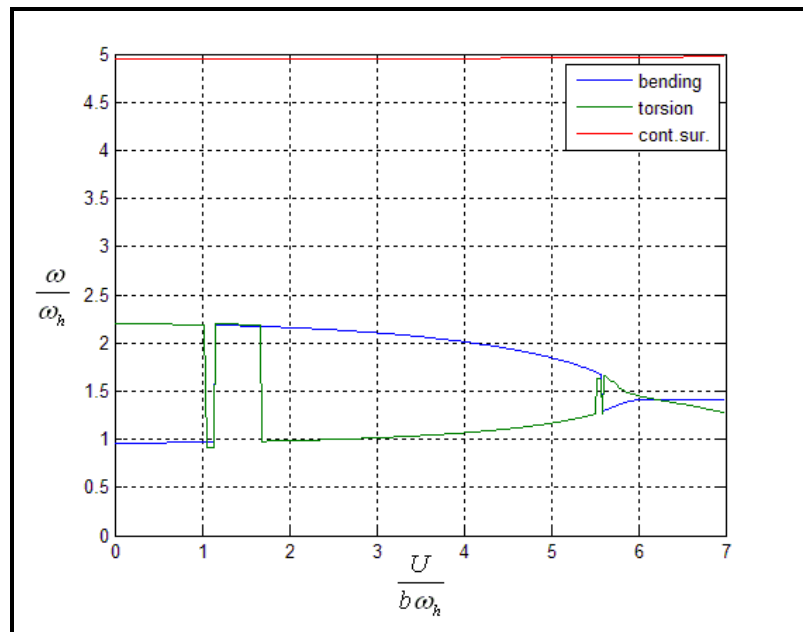**Figure 12.** Damping vs. speed plot of the second example (k-method).

Figure 13. Frequency vs.speed plot of the second example (p-k method).
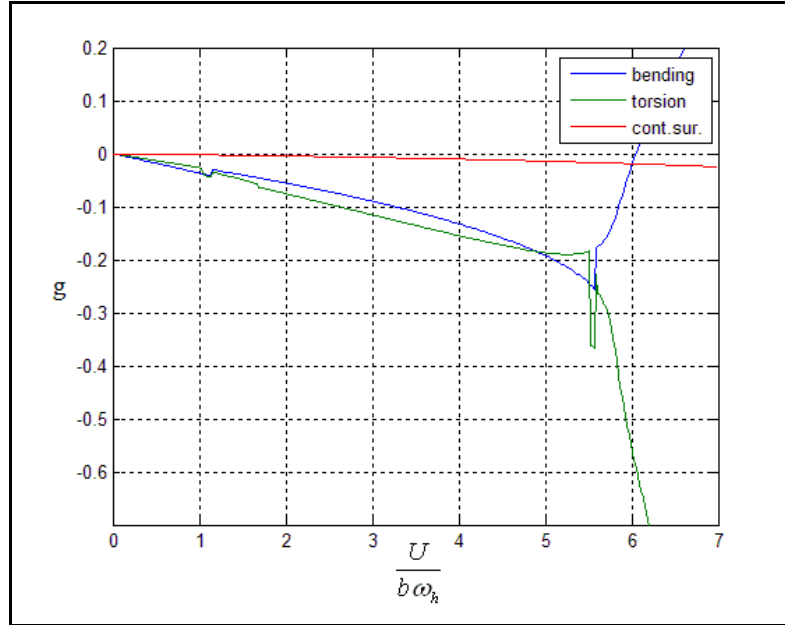
45

Figure 14. Damping vs. speed plot of the second example (p-k method).

Both k-method and p-k method solutions give the same results for flutter speed and flutter frequency with excellent agreement. However p-k method indicates that flutter occurance would be in bending mode while k-method indicates flutter occurance would be in torsional mode. p-k method may produce discontinuities in U vs g and U vs ω plots which generally occurs as jumps between modes. One can track the modes in p-k method, examining U vs g and U vs ω plots together. Flutter speed and frequency are:

$$\frac{U_f}{b\omega_h} \approx 6.05, \qquad \frac{\omega_f}{\omega_h} \approx 1.41 \qquad (104)$$

The third example is a 3 DoF typical section problem given in Reference [15]. The properties of the typical section and the flight condition are given as nondimensional parameters which are:

46

$$a = -0.4,$$
$$x_\alpha = 0.2,$$
$$c = 0.6,$$
$$\mu = 40,$$
$$r_\alpha^2 = 0.25, \tag{105}$$
$$r_\beta^2 = 0.00625,$$
$$x_\beta = 0.0125,$$
$$\omega_h / \omega_\alpha = 0.5,$$
$$\omega_h / \omega_\beta = 0.1667.$$

The graphics shown in Figure 15 and Figure 16 are generated for the k-method solution and the graphics shown in Figure 17 and Figure 18 are generated for p-k method solution.
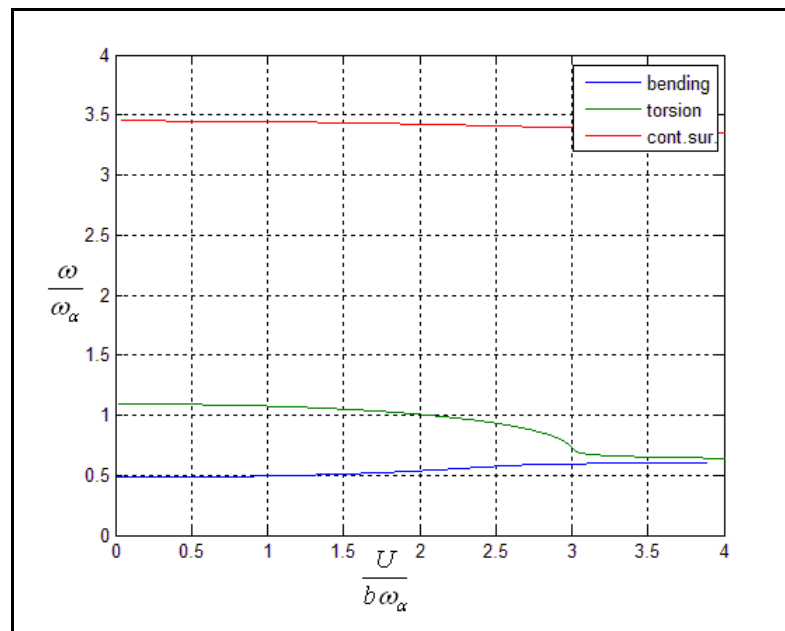

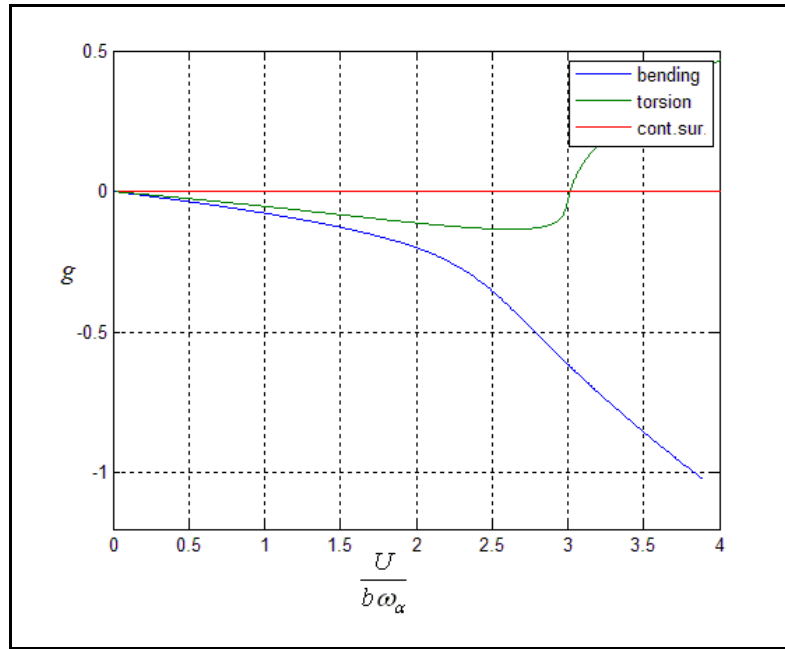**Figure 15.** Frequency vs.speed plot of the third example (k-method).

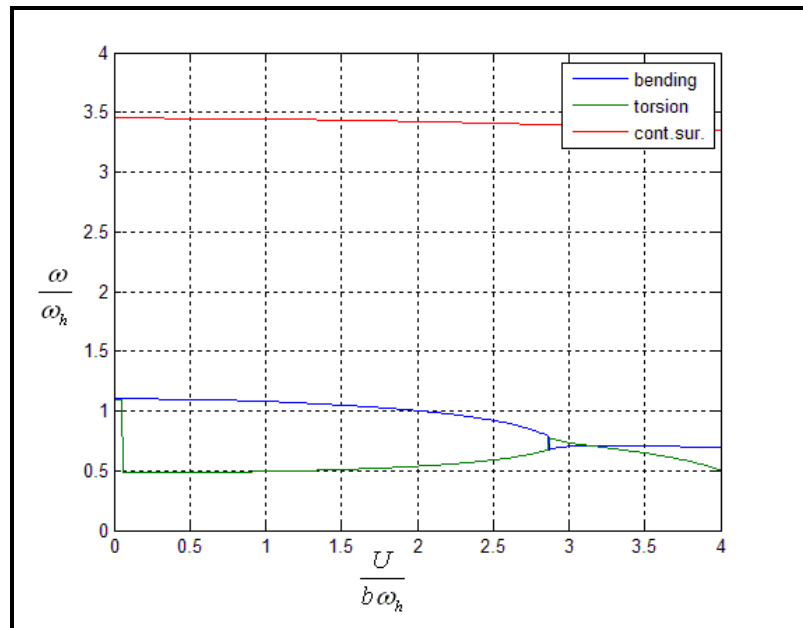**Figure 16.** Damping vs. speed plot of the third example (k-method).

Figure 17. Frequency vs.speed plot of the third example (p-k method).
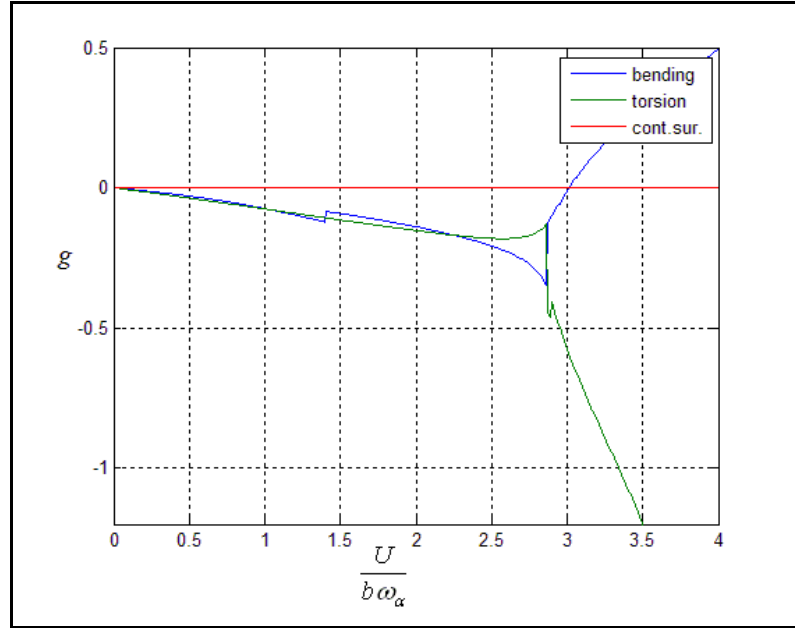
48

Figure 18. Damping vs. speed plot of the third example (p-k method).

Both k-method and p-k method solutions give the same results for flutter speed and flutter frequency with excellent agreement. However p-k method indicates that flutter occurance would be in bending mode while k-method indicates flutter occurance would be in torsional mode. Flutter speed and frequency are:

$$\frac{U_f}{b\,\omega_\alpha} \approx 3.02, \qquad\qquad \frac{\omega_f}{\omega_\alpha} \approx 0.7 \qquad\qquad (106)$$

2.10. Comparison of Methods

k-method is a straightforward, and robust method which is computationally efficient to predict flutter by solving complex eigenvalue problem. An artificial damping term is used in k-method to point out the needed damping for the harmonic motion. Although the damping values are not physically correct except flutter boundary, mild flutter and explosive flutter can be detected using U vs g plots. Figure 8 designates a mild flutter case, whereas Figure 16 is an example of explosive flutter. The

inclination to flutter occurance is indicated in the U vs g plots as well. When the frequency curves gets closer to each other the flutter is likely to occur as can be seen in the figures above.[13]

Due to $1/k$ term used in the solution procedure, solution process can not be performed at $k=0$ in k-method. k-method excludes rigid body modes and can not predict divergence.

p-k method is an approximation method to expose the decay rate. P-k method is mathematically inconsistent since the eigenvalue problem is expressed as damped harmonic motion whereas the aerodynamic coefficient matrix is based on undamped simple harmonic motion.[13]

Using p-k method flutter speeds of configurations with rigid body modes can be found so divergence can be predicted. ($1/k$ term is not used in solution process). Divergence occurs at the speed where ω is equal to zero. If the U vs ω graph is replotted for a wide range of speed for the first example held in the code validation part, divergence speed can be found.
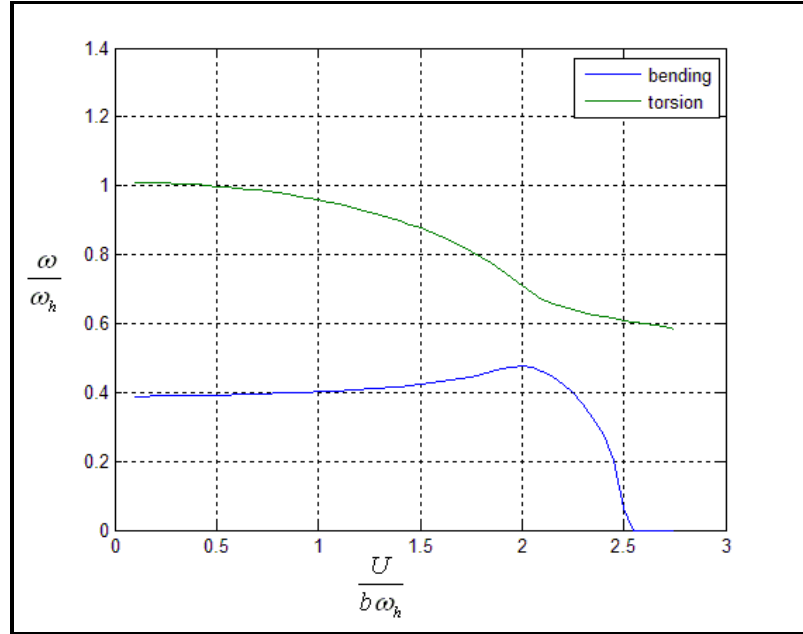
Figure 19. Frequency vs. speed plot of the 2DoF typical section (divergence).

$$\frac{U_d}{b\omega_\alpha} \approx 2.55 \qquad (107)$$

Damping calculated in p-k method is more accurate. However p-k method may produce discontinuities in U vs g and U vs ω plots which generally occurs as jumps between modes as seen in Figure 13, Figure 14, Figure 17 and Figure 18. This may be due to "aerodynamic lag roots" [13].

The solution takes more computational time in p-k method compared to k-method. k method provides a faster solution.

Although k-method and p-k method uses different approaches for the solutions as seen from the results of the examples held in this section, the solutions of both k-method and p-k method shows an excellent agreement at the flutter boundary for predicted flutter speeds. However, flutter occurance may be predicted in different

modes by k-method and p-k method. The advantages of methods are shown in Table 1.

Table 1 Advantages of methods

	k-method	**p-k method**
Less computational time	√	
Divergence prediction		√
More efficient damping prediction		√
Continuous damping and frequency plots	√	

CHAPTER 3

COMPARISON OF FINITE ELEMENTS BASED FLUTTER ANALYSIS OF 3D WINGS WITH 2D TYPICAL SECTION ANALYSIS

3.1.   General

In this chapter, the flutter problem is solved for 3D wings using finite elements method and doublet lattice aerodynamics to examine the efficiency of the methods that are introduced in previous chapter. In Chapter 2, k-method and p-k method solutions are derived for a 2D typical Section oscillating harmonically in unsteady incompressible flow. As mentioned before, for purposes of theoretical flutter prediction, inertial and geometric properties of a large span and straight wing can be represented by a typical section especially when the aspect ratio is large.

Doublet lattice aerodynamics is widely used in finite element based method of flutter analysis [16]. The process of solution is involved with the pressure differences across the wing. The unknown pressure functions are solved by Doublet-Lattice Method by dividing the pressure doublet sheet into finite number of elements on which the pressure is assumed to be constant initially [17]. The method is suitable for subsonic incompressible and compressible speeds [17].

In this section a very simple 3D wing is modeled using PATRAN, structural analysis are made by NASTRAN to find the the natural frequencies of the first bending and torsional modes. Natural frequencies are used to do the calculations for the 2D typical section using p-k method. NASTRAN's aeroelasticity module, which is based on Doublet Lattice Aerodynamics, is also used to calculate the flutter speed for the 3D wing and the results are compared to the 2D typical section results. This procedure is repeated by changing the span of the 3D wing. The primary goal of such a study is to examine how closely two dimensional typical section analysis can estimate flutter speeds compared to the flutter speeds obtained from a three dimensional analysis. It is considered that since two dimensional typical section analysis is very fast, this method can be used in the preliminary design stage to get a rough idea about the flutter speed and the flutter frequency.

3.2.   Modeling

In this section a very simple wing is designed and meshed using PATRAN. As seen in Figure 20, the wing consists of a thin aluminium rectangular plate and two aluminium I profiles located at leading edge and trailing edge to increase the stiffness. These profiles can be assumed to model the spars of the wing. Modulus of elasticity, Poisson's ratio and density of the aluminium used is given below:

$$E = 7 \times 10^{10} \text{ Pa} \qquad \upsilon = 0.3 \qquad d = 2710 \text{ kg/m}^3 \qquad (108)$$

Wingspan, chordlength and the thickness of the 3D wing modeled is given below:

$$l = 1 \text{ m}, \qquad c = 0.5 \text{ m}, \qquad t_w = 0.004 \text{ m} \qquad (109)$$
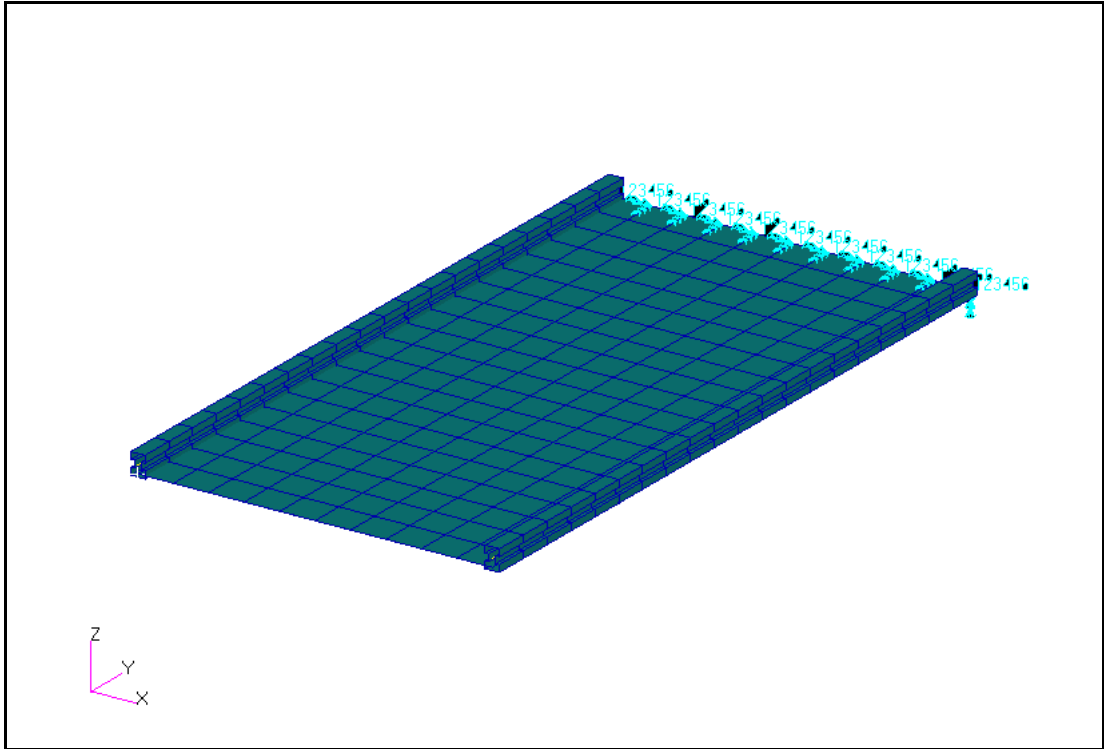
Figure 20. Wing Model

The wing's natural frequencies for first bending mode and torsional mode are found out using modal analysis module of NASTRAN. Natural frequencies for the first bending mode and torsional mode of vibration are given below respectively.

$$\omega_h = 16.954 \ Hz \qquad \omega_\alpha = 27.988 \ Hz \qquad (110)$$

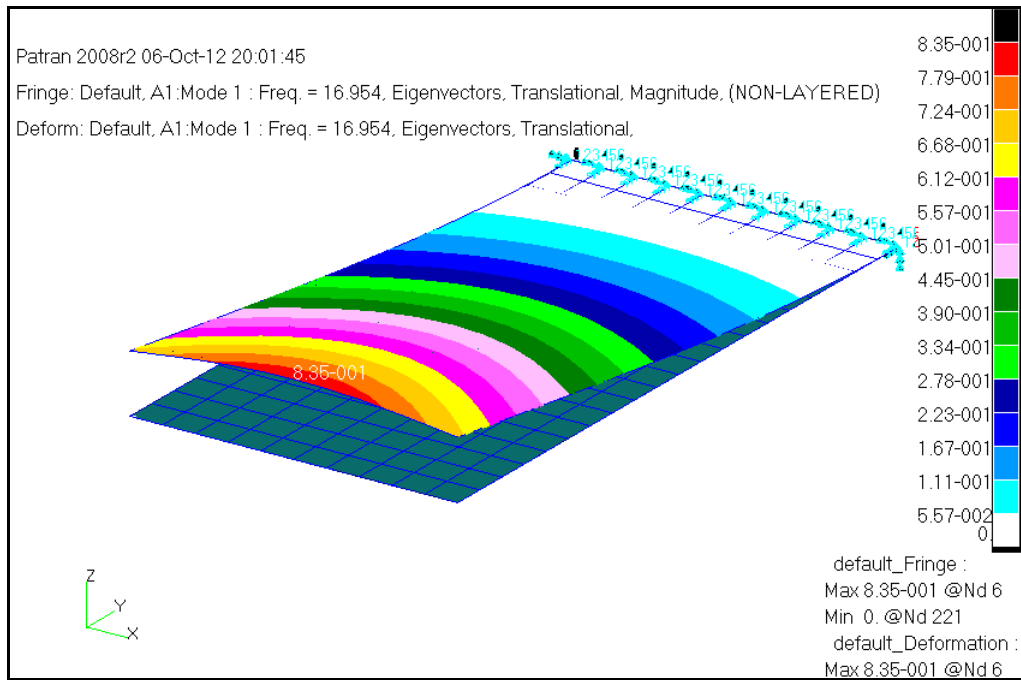Solutions for first bending mode and torsional mode are given in Figure 21 and Figure 22 respectively.
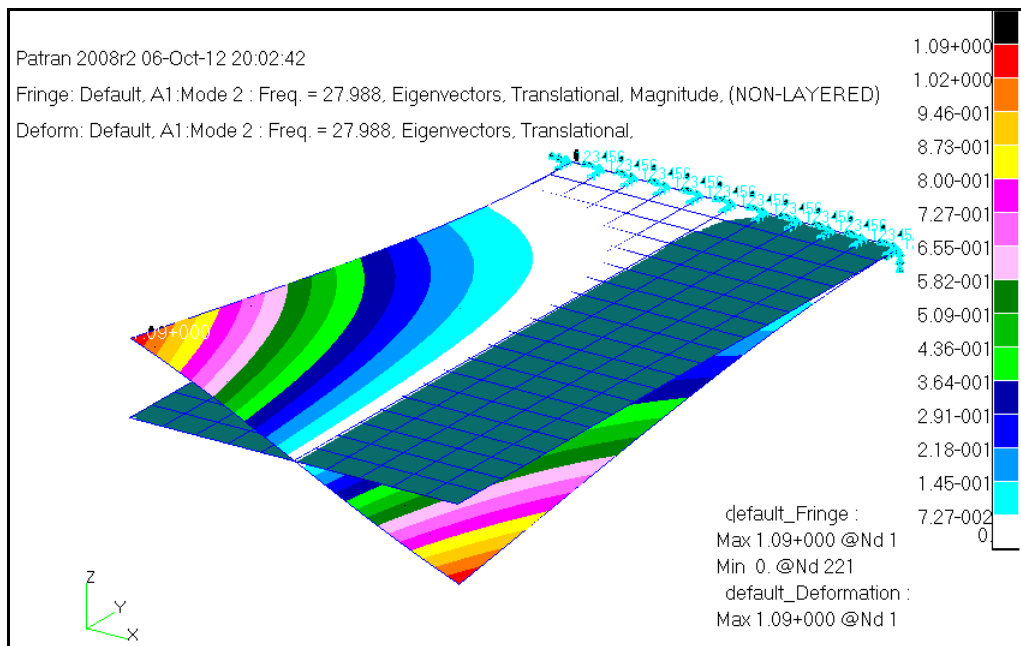
Figure 21. Modal Solution for Bending Mode

Figure 22. Modal Solution for Torsional Mode

3.3. Solutions for the 2D Wing

From the geometric and material properties of the 3D wing defined previously, mass per unit span and moment of inertia per unit span is calculated for a 2D wing which is modeled as shown in Figure 23.
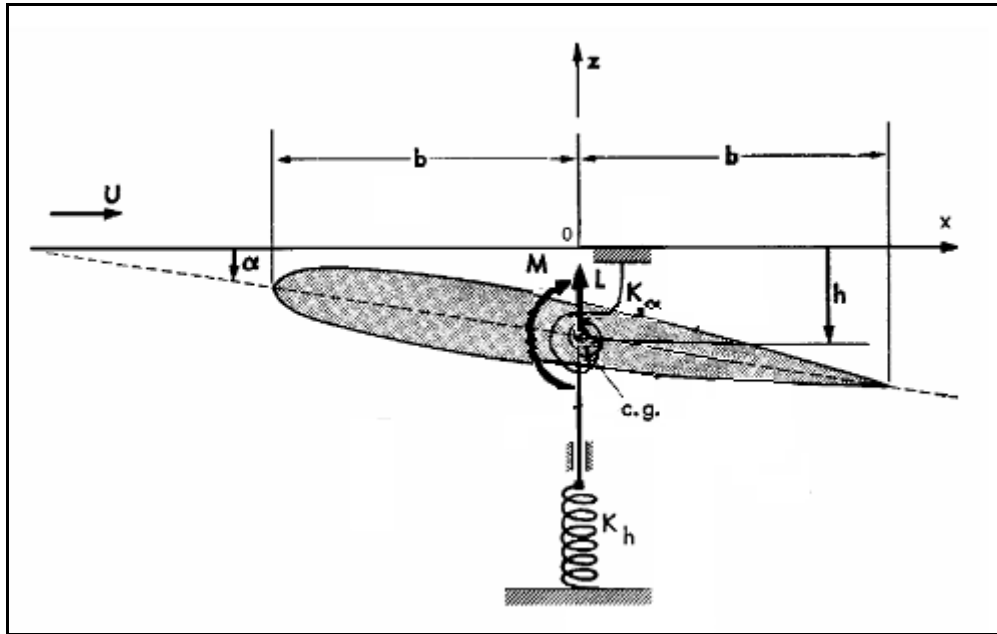

Figure 23. 2D Model of the 3D wing.

One should note that due to the symmetry of the 3D wing, the elastic axis, and mass center coincide at the same point located at the middle chord in the 2D model. Mass per unit span, and moment of inertia for unit span is calculated as:

$$m = dct_w + 2d(A_I) \qquad I_\alpha = \frac{1}{12}(dct_w)c^2 + 2(dA_I)b^2 \qquad (111)$$

$$m = 6.7208 \ \text{kg/m} \qquad I_\alpha = 0.1942 \ \text{kg m} \qquad (112)$$

where A_I is the area of the cross section of I profile and t_w is the thickness of the plate.

57

Having the natural frequencies for bending and torsion mode of vibration from NASTRAN, all the required parameters are determined to do the calculations using the p-k method for a 2D model corresponding to a 3D wing.

Following the steps described in detail in the second Chapter flutter determinant is solved for the 2D wing model, The curves shown in Figure 24 and Figure 25 are generated for the p-k method solution.
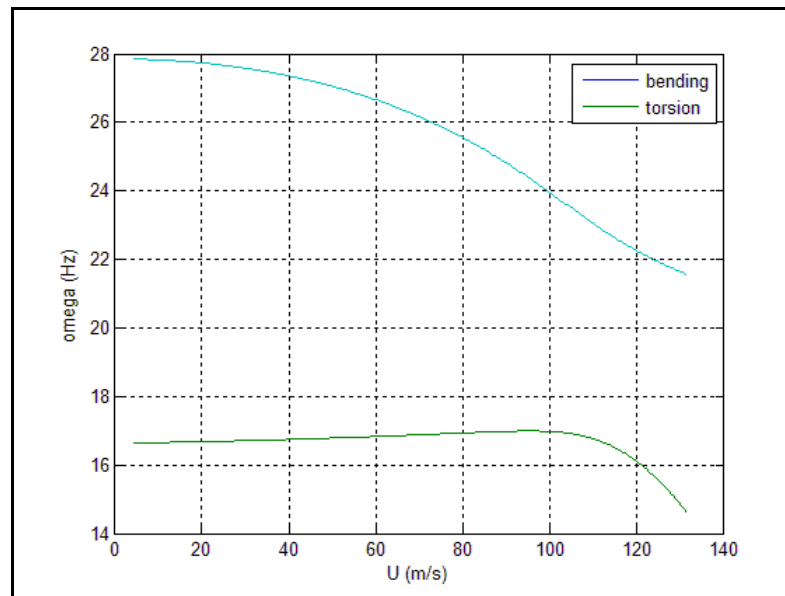

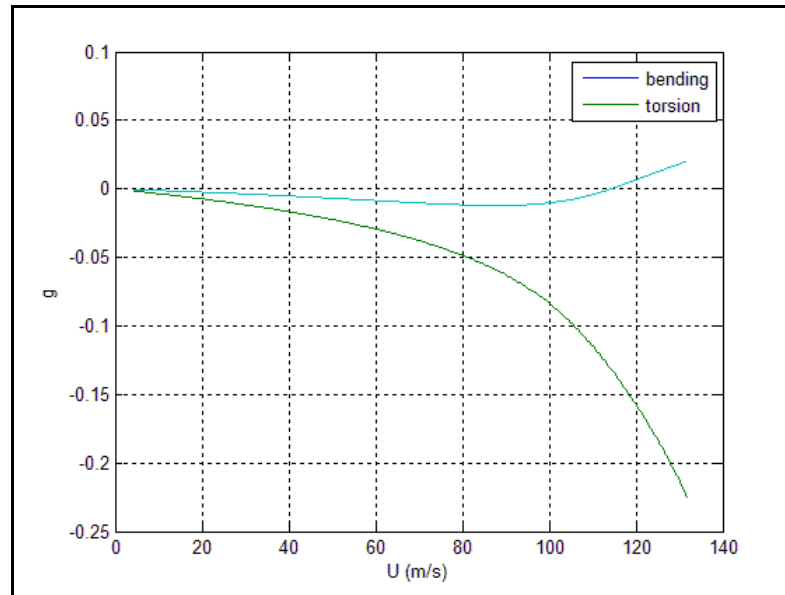**Figure 24.** Frequency vs. speed plot of the 2D wing (p-k method).

Figure 25. Damping vs. speed plot of the 2D wing (p-k method).

As seen from the plots the estimated flutter speed parameter is about 1114 m/s for 2D solution using p-k method.

3.4. Flutter Solution Using NASTRAN's Aeroelasticity Module

The 3D wing model with 0.5m chord length and 1m span length shown in Figure 20 is used for solving the flutter problem using NASTRAN's aeroelasticity module. Supergroup is created using flat plate type. The model is meshed and lifting suface is created. Mach number- reduced frequency pairs are composed using the results above. The solutions are determined using the first bending and torsion modes in the flutter analysis. P-k method is chosen as analysis method in NASTRAN. For the speed range of interest frequency and damping values shown in Table 2 are generated.

59

Table 2 Damping and Frequency Values of a 3D Wing with 0.5m Chord Length and
1 m span length

	Bending Mode		Torsion Mode	
Speed (m/s)	Damping	Frequency (Hz)	Damping	Frequency (Hz)
5.0000E+00	1.9735E-02	1.6941E+01	4.8761E-02	2.7953E+01
1.0000E+01	8.2193E-03	1.6915E+01	4.2163E-02	2.7948E+01
1.5000E+01	-3.4519E-03	1.6881E+01	3.5571E-02	2.7922E+01
2.0000E+01	-1.5371E-02	1.6841E+01	2.9026E-02	2.7874E+01
2.5000E+01	-2.7666E-02	1.6794E+01	2.2572E-02	2.7805E+01
3.0000E+01	-4.0458E-02	1.6741E+01	1.6318E-02	2.7714E+01
3.5000E+01	-5.3883E-02	1.6682E+01	1.0217E-02	2.7600E+01
4.0000E+01	-6.8086E-02	1.6616E+01	4.3706E-03	2.7462E+01
4.5000E+01	-8.3234E-02	1.6546E+01	-1.1523E-03	2.7301E+01
5.0000E+01	-9.9515E-02	1.6470E+01	-6.2660E-03	2.7116E+01
5.5000E+01	-1.1715E-01	1.6388E+01	-1.0867E-02	2.6905E+01
6.0000E+01	-1.3636E-01	1.6302E+01	-1.4828E-02	2.6668E+01
6.5000E+01	-1.5752E-01	1.6212E+01	-1.7986E-02	2.6404E+01
7.0000E+01	-1.8093E-01	1.6116E+01	-2.0137E-02	2.6112E+01
7.5000E+01	-2.0714E-01	1.6016E+01	-2.1016E-02	2.5792E+01
8.0000E+01	-2.3666E-01	1.5910E+01	-2.0285E-02	2.5442E+01
8.5000E+01	-2.7019E-01	1.5797E+01	-1.7507E-02	2.5064E+01
9.0000E+01	-3.0834E-01	1.5674E+01	-1.2133E-02	2.4658E+01
9.5000E+01	-3.5239E-01	1.5536E+01	-3.5002E-03	2.4228E+01
1.0000E+02	-4.0339E-01	1.5378E+01	9.0354E-03	2.3778E+01
1.0500E+02	-4.6266E-01	1.5186E+01	2.6372E-02	2.3318E+01
1.1000E+02	-5.3139E-01	1.4949E+01	4.8823E-02	2.2859E+01
1.1500E+02	-6.1063E-01	1.4655E+01	7.6373E-02	2.2411E+01
1.2000E+02	-7.0140E-01	1.4294E+01	1.0854E-01	2.1983E+01
1.2500E+02	-8.0501E-01	1.3862E+01	1.4457E-01	2.1578E+01
1.3000E+02	-9.2353E-01	1.3356E+01	1.8379E-01	2.1195E+01
1.3500E+02	-1.0602E+00	1.2774E+01	2.2570E-01	2.0831E+01

The tabulated data above is shown in graphical form in Figure 26 and Figure 27. As seen from Figure 26 flutter occurance is predicted at about 97 m/s in torsional mode. Flutter speed was predicted at about 114 m/s in Figure 24 using for 2D model using p-k method.
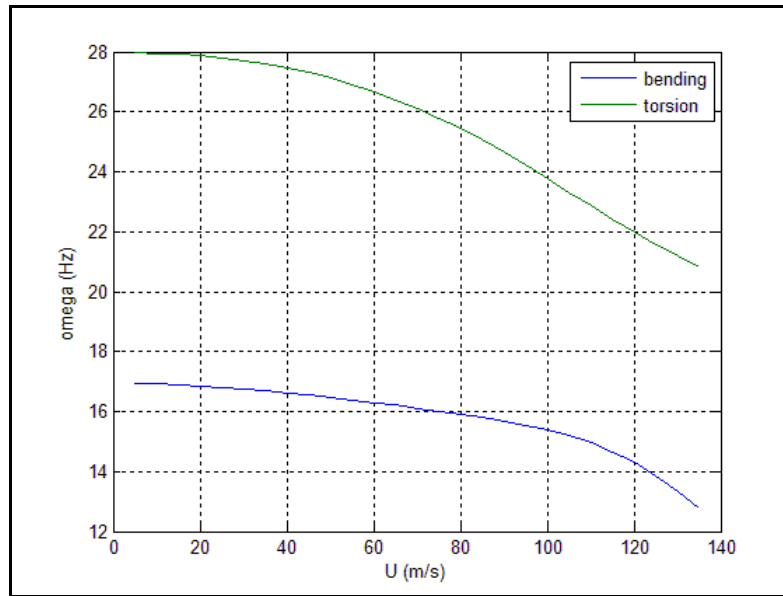
Figure 26. Frequency vs. speed plot of the 2D wing (NASTRAN).
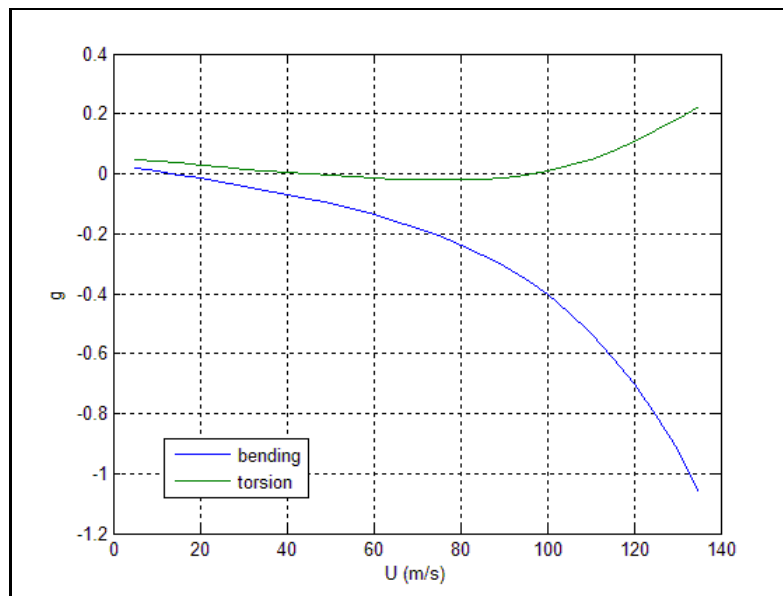

Figure 27. Damping vs. speed plot of the 2D wing (NASTRAN).

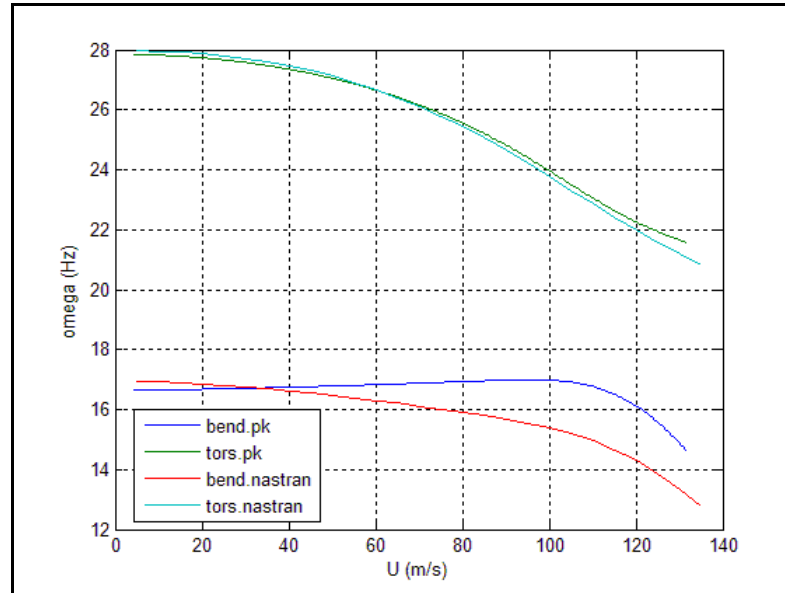For better comparison the plots are given in the same graph in Figure 28 and Figure 29.

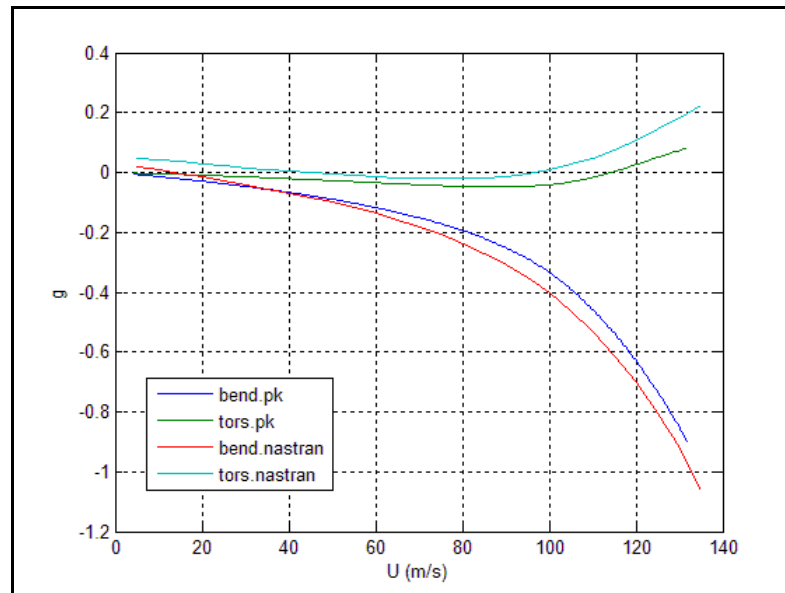**Figure 28.** Frequency vs. speed plot of the 2D wing (p-k and NASTRAN).

Figure 29. Damping vs. speed plot of the 2D wing (p-k and NASTRAN).

3.5. Solutions for Wings with Various Aspect Ratios

In this section, flutter solutions are investigated for wings with various aspect ratios. In previous sections a rectangular uniform wing with 0.5 m chord length and 1 m span length is modeled. Keeping the cross sectional properties the same and changing the span length flutter solutions are made and the results are compared. One should note that the effect of 3D wing is modeled by using the stiffness parameters, natural frequencies in the 2D solutions. The results of the 2D typical section method and Nastran flutter analyses are compared in Table 3.

Table 3 Flutter solutions for various aspect ratio wings

l (m)	c (m)	AR	NASTRAN			p-k method
			ω_h (Hz)	ω_α (Hz)	U_f (m/s)	U_f (m/s)
1	0.5	2	16.95	37.99	97	114
1.5	0.5	3	7.93	14.29	54	61
2	0.5	4	4.51	9.27	37	41
2.5	0.5	5	2.90	6.75	28	31
3	0.5	6	2.02	5.26	22	24

In Table 3 *AR* indicates the aspect ratio of the wing (semi-span), and U_f indicates the predicted flutter speed. In all the cases above flutter is predicted in the torsional mode. One can see that as the span increases, stiffness of the total wing decreases as expected. As the aspect ratio of the wing increases, zero air speed natural frequencies and flutter speeds decrease. From the results given in Table 3, it is seen that flutter speeds predicted with the 2D typical section model are about %10 higher than the flutter speeds predicted by Nastran.

3.6. Solutions for a Tapered Wing

In Chapter 2, it is stated that the inertial and geometric properties of a large span and straight wing can be represented by a typical section with inertial and geometric properties of the wing at the ¾ of the distance from root of the wing. In this section a tapered wing is modeled as a plate of uniform thickness with two I profile stiffeners at the leading edge and trailing edge. The I section stiffeners are taken as same in the previous section, but the plate has a thickness of 1 cm, and the tapered wing has 1 m chord length at the root and 0.6 m chord length at the tip. The tapered wing modeled is shown in Figure 30.
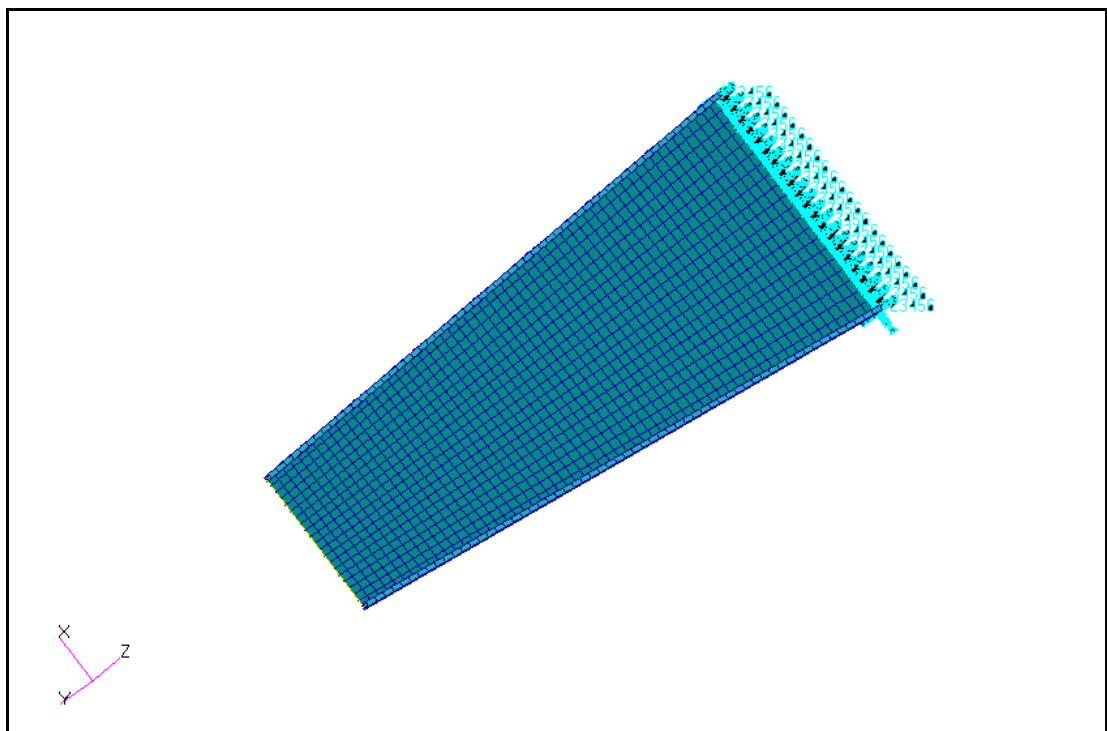

Figure 30. Tapered Wing Model

At ¾ of the distance from root of the wing the chord length is 0.7 m.Using this value mass per unit span and moment of inertia about midchord is calculated. Natural frequencies for the first bending and torsional mode are found using NASTRAN modal analysis, and using these values p-k method is employed to determine the

flutter speed using the typical section method. The results are given in Figure 31 and Figure 32.
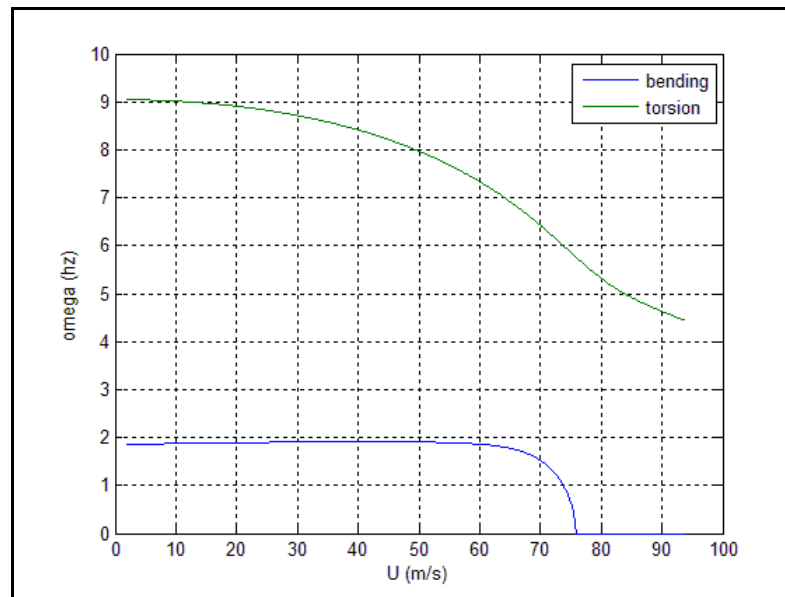

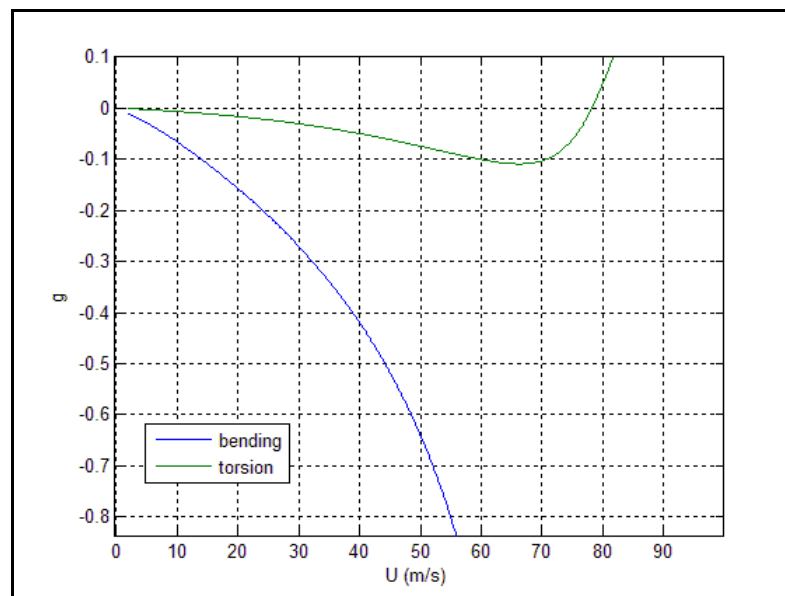**Figure 31.** Frequency vs. speed plot of the tapered wing (p-k method).

Figure 32. Damping vs. speed plot of the tapered wing (p-k method).

As one can see from the plots above, in both methods flutter occurance is predicted in torsional mode at a speed of 78 m/s. However, in Figure 31 at a speed of 76 m/s bending frequency becomes zero which indicates divergence. One may notice that getting close to the predicted divergence speed in bending mode, the damping grows extremely large in the same mode.

Using NASTRAN the results given in Table 4 are obtained for the 3D tapered wing.

Table 4 Damping and Frequency Values of the 3D Tapered Wing

Speed (m/s)	Bending Mode		Torsion Mode	
	Damping	Frequency (Hz)	Damping	Frequency (Hz)
5.00E+00	-1.976E-02	1.879E+00	1.047E-01	9.068E+00
1.00E+01	-5.553E-02	1.876E+00	9.013E-02	9.062E+00
1.50E+01	-9.240E-02	1.873E+00	7.551E-02	9.031E+00
2.00E+01	-1.310E-01	1.870E+00	6.082E-02	8.975E+00
2.50E+01	-1.722E-01	1.866E+00	4.606E-02	8.894E+00
3.00E+01	-2.170E-01	1.862E+00	3.127E-02	8.787E+00
3.50E+01	-2.666E-01	1.856E+00	1.649E-02	8.651E+00
4.00E+01	-3.229E-01	1.848E+00	1.838E-03	8.486E+00
4.50E+01	-3.884E-01	1.838E+00	-1.250E-02	8.289E+00
5.00E+01	-4.666E-01	1.823E+00	-2.617E-02	8.058E+00
5.50E+01	-5.628E-01	1.803E+00	-3.856E-02	7.790E+00
6.00E+01	-6.865E-01	1.773E+00	-4.852E-02	7.479E+00
6.50E+01	-8.550E-01	1.726E+00	-5.390E-02	7.123E+00
7.00E+01	-1.105E+00	1.644E+00	-5.052E-02	6.717E+00
7.50E+01	-1.533E+00	1.488E+00	-3.028E-02	6.262E+00
8.00E+01	-2.561E+00	1.135E+00	2.061E-02	5.777E+00
8.50E+01	-1.088E-01	0.000E+00	1.159E-01	5.307E+00
9.00E+01	-5.281E-02	0.000E+00	2.514E-01	4.901E+00
9.50E+01	-2.580E-02	0.000E+00	4.088E-01	4.557E+00
1.00E+02	-6.784E-03	0.000E+00	5.770E-01	4.246E+00

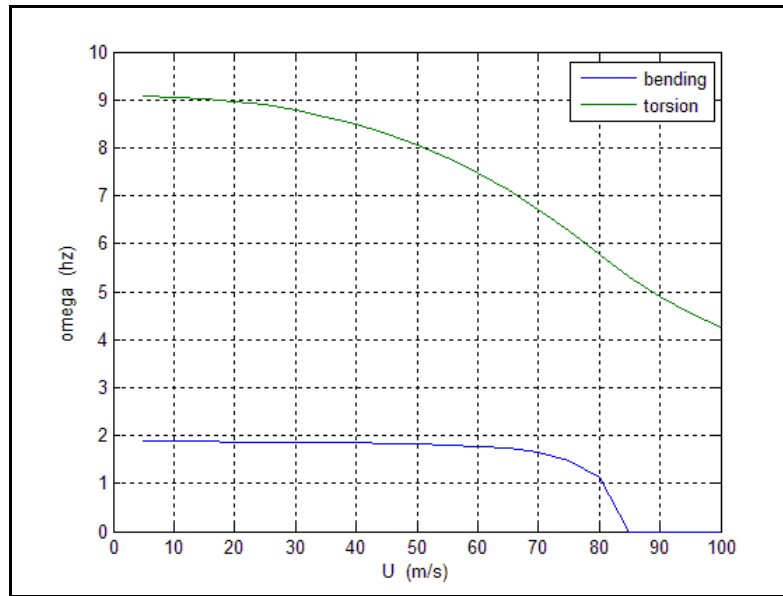The tabulated data above can be shown graphically in Figure 33 and Figure 34.

Figure 33. Frequency vs. speed plot of the tapered wing (NASTRAN).
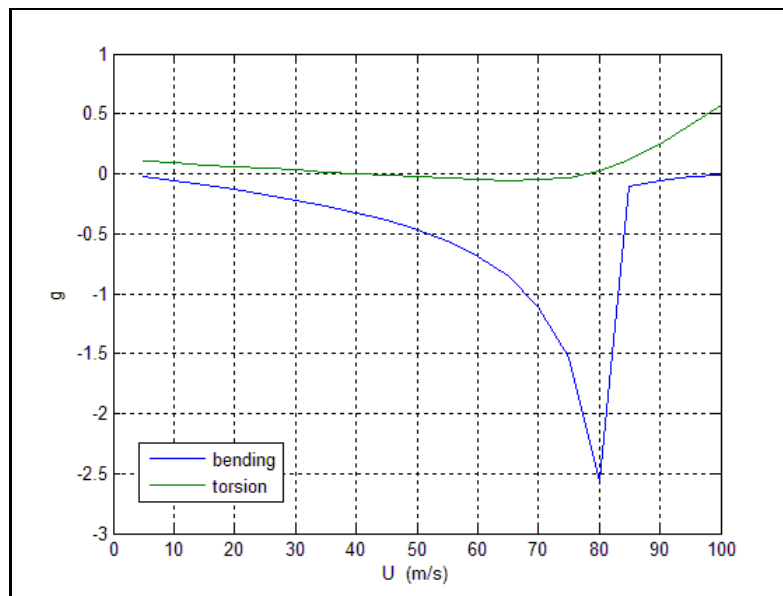
Figure 34. Damping vs. speed plot of the tapered wing (NASTRAN).

67

The flutter occurance is predicted in torsional mode at about a speed of 78 m/s using NASTRAN, however divergence occurance is predicted in bending mode at about 83 m/s. The predicted flutter speed parameter using 3D model is in a good agreement with the results determined for ¾ span chord modeled 2D model. However the predicted divergence speeds shows a little difference. For better comparison of the 2D And 3D solutions, the plots are given in the same graph in Figure 35 and Figure 36.
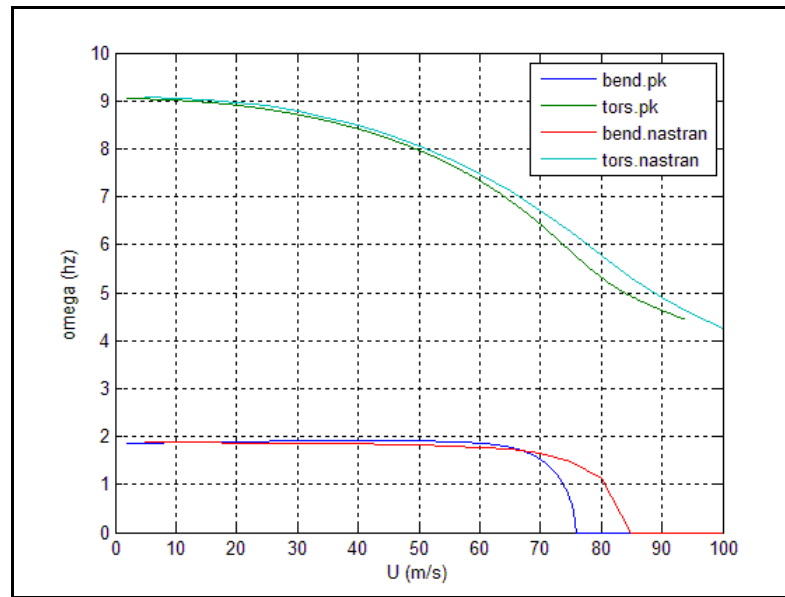
Figure 35. Frequency vs. speed plot of the tapered wing (p-k and NASTRAN).
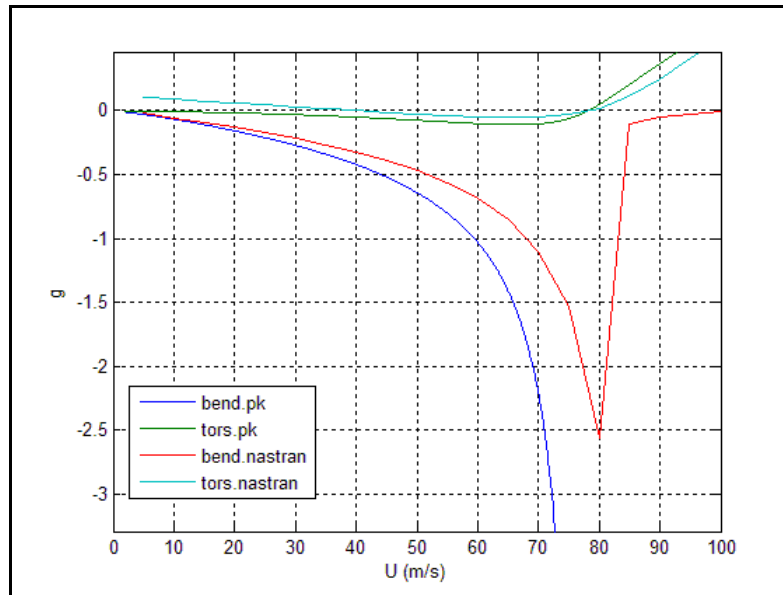
Figure 36. Damping vs. speed plot of the tapered wing (p-k and NASTRAN).

One can notice that frequency curves of 2D and 3D solutions especially at low speeds are in good agreement. However damping curves only gets closer to each other about flutter point, at the mode that flutter is estimated. In Chapter 2 it was stated that the damping values for typical sections does not have a physical meaning except the region about flutter.

Flutter solutions with 2D models which are modeled using various sections along the wing span are made. The results are tabulated in Table 5. As one can see best approximations are obtained about 75%-80% span.

69

Table 5 Flutter solutions for various sections along wing span

Span%	Chord length (m)	p-k method U_f (m/s)
95	0.62	75
90	0.64	76
85	0.66	77
80	0.68	78
75	0.7	78
70	0.72	79
65	0.74	80
60	0.76	81
55	0.78	82
50	0.8	83

Generally using 2D wing model based solutions flutter speeds are found at about 10% higher values than the flutter speeds found using 3D wing model NASTRAN solutions. In preliminary design stage the flutter speeds predicted using 2D typical section model may give an idea about what the flutter speed would be. However in detailed design process and planning flight flutter tests the results found using 2D typical section model may be inaccurate.

However in some cases, flutter prediction using 2D typical section model may be in excellent agreement with 3D results like the tapered wing case represented in this study.

CHAPTER 4

SIMULATED FLUTTER TEST OF WING BASED ON A TYPICAL WING SECTION

4.1. General

In this chapter simulated flutter test is performed using a typical section model of a wing. The main aim of this study is to get the sub-critical damping trend from a simple analysis to aid the actual flutter test planning. In the actual flutter test of aircraft, critical structures such as wing, tail plane are excited by external exciters and damping is estimated either online or off-line for each test speed until dive speed. The damping trend obtained until dive speed is then extrapolated to zero damping to predict the flutter speed. Obviously, in simulated flutter test damping estimates can be made until flutter speed. The critical issue in the damping trend is to decide whether the flutter is mild flutter with gradually decreasing damping or explosive flutter with sharp decrease of damping once the flutter speed is approached. Deciding on the flutter type, mild or explosive, is very important to make appropriate plans for the flutter test. Explosive flutter is very dangerous since damping decreases suddenly with slight increases in airspeed. Therefore, with simple 2D typical section models one can study the sub-critical damping trend and decide on the flutter type.

In this section, lift and moment equations are derived in time domain f or a typical wing section model which is used in the simulated flutter test. Nondimensional time parameter is introduced and the equations of motion for a 2 DoF typical Section Model given in Chapter-2, are defined in non-dimensional time domain. A time dependent external excitation is introduced and the aeroelastic response equations of a two dimensional lifting surface subjected to this external excitation is derived in time domain. To have the response in time domain first Laplace transform of the equations of motions including the aerodynamic terms and, excitation terms are taken. Then, the equations of pitch and plunge responses in Laplace domain are determined. Finally, by taking the inverse laplace transform of the pitch and plunge responses, time domain solutions are obtained. A case study is introduced and the flutter speed parameter is calculated for the case study using p-k method which is described in Chapter 2. A code is generated in MATLAB to calculate the responses in time domain for a case study by performing the inverse Laplace transforms for a range of velocities starting from a subcritical speed getting closer to the flutter speed. For each velocity case amplitude vs. time plots are determined. Damping for each velocity case is calculated using logarithmic decrement method using the amplitude vs. time plots of the pitch and plunge responses. After performing this process for all velocities, damping vs. velocity plots are established. Extrapolating the plots, the velocity value corresponding to zero damping is found out and the results are compared to those determined using p-k method.

4.2. Lift and Moment Equations

In this section, the aerodynamic forces are defined. Lift and moment equations consist of two major parts which are generally called circulatory part and non-circulatory part in the literature. The lift effect caused by the apperent mass forces are generally called non-circulatory lift [18].

The circulation is defined by the downwash velocity at the third quarter chord point of the airfoil from the leading edge. The downwash consists of three main terms due

72

to pitch, vertical translation and $d\alpha/dt$, respectively [18]. Equation (113) gives each of the components of the downwash.

$$w_1 = U_\infty \sin \alpha \cong U_\infty \alpha(t), \quad w_2 = \frac{dh}{dt} = \dot{h}, \quad w_3 = \left(\frac{1}{2} - a\right)b\frac{d\alpha}{dt} = \left(\frac{1}{2} - a\right)b\dot{\alpha} \quad (113)$$

In Equation (113) dot denotes to differentiation with respect to time. The total downwash is then calculated as:

$$w = w_1 + w_2 + w_3 = U_\infty \alpha(t) + \dot{h}(t) + \left(\frac{1}{2} - a\right)b\dot{\alpha}(t) \quad (114)$$

The dimensionless time term τ is introduced as:

$$\tau = \frac{tU_\infty}{b} \quad (115)$$

Rewriting Equation (113) by substituting the dimensionless time one gets:

$$w = U_\infty \alpha(t) + \frac{dh}{d\tau}\frac{d\tau}{dt} + \left(\frac{1}{2} - a\right)b\frac{d\alpha}{d\tau}\frac{d\tau}{dt} \quad (116)$$

One should note that $\dfrac{d\tau}{dt} = \dfrac{U_\infty}{b}$. The total downwash becomes:

$$w = U_\infty \alpha(\tau) + U_\infty \frac{h'(\tau)}{b} + \left(\frac{1}{2} - a\right)U_\infty \alpha'(\tau) \quad (117)$$

73

Prime in Equation (117) above denotes differentiation with respect to dimensionless time. Between time τ_0 and $\tau_0 + d\tau_0$, there is an increment in downwash defined as $dw(\tau_0)/d\tau_0$. The unsteady aerodynamic forces can be expressed in Duhamel integral form using the Wagner's function. The corresponding increment in the circulatory lift per unit span is given by [18]:

$$dL_c(\tau) = C_{L\alpha} \rho_\infty bU_\infty \phi(\tau - \tau_0) \frac{dw(\tau)}{d\tau_0} d\tau_0 \qquad \text{for} \quad \tau \geq \tau_0 \qquad (118)$$

where $C_{L\alpha}$ is the lift curve slope and ϕ is the Wagner's function which describes the growth of circulation which starts impulsively[18]. The approximate expression of Wagner's function which is stated by R.T. Jones, is given by [19].

$$\phi(\tau) = 1 - 0.165\, e^{-0.0455\,\tau} - 0.335\, e^{-0.300\,\tau} \qquad (119)$$

Integrating Equation (118) the total circulatory lift per unit span can be found at τ.

$$L_c(\tau) = C_{L\alpha} \rho_\infty bU_\infty \int_{-\infty}^{s} \phi(\tau - \tau_0) \frac{dw(\tau)}{d\tau_0} d\tau_0 \qquad (120)$$

Substituting Equation (117) into Equation (120), Equation (120) can be rewritten as:

$$L_c(\tau) = C_{L\alpha} \rho_\infty bU_\infty \int_{-\infty}^{s} \phi(\tau - \tau_0)\left(U_\infty \alpha' + U_\infty \frac{h''}{b} + \left(\frac{1}{2} - a\right) U_\infty \alpha'' \right) d\tau_0 \qquad (121)$$

Equation (121) gives the circulatory lift component. Non-circulatory lift consists of two terms as given below in Equations (122) and (123)[18].

$$L_{nc1}(t) = \frac{1}{2} C_{L\alpha} \rho_\infty b^2 \left(\ddot{h}(t) - ab\, \ddot{\alpha}(t) \right) \tag{122}$$

$$L_{nc2}(t) = \frac{1}{2} C_{L\alpha} \rho_\infty b^2 U_\infty \dot{\alpha}(t) \tag{123}$$

Substituting Equation (115) in Equation (122) and Equation (123), one can express Equations (122) and (123) in terms of non-dimensional time.

$$L_{nc1}(\tau) = \frac{1}{2} C_{L\alpha} \rho_\infty U_\infty^2 \left(h''(\tau) - ab\, \alpha''(\tau) \right) \tag{124}$$

$$L_{nc2}(\tau) = \frac{1}{2} C_{L\alpha} \rho_\infty b U_\infty^2 \alpha'(\tau) \tag{125}$$

Total lift per unit span can then be expressed as:

$$L(\tau) = L_c(\tau) + L_{nc1}(\tau) + L_{nc2}(\tau) \tag{126}$$

The total moment about the elastic axis per unit span is can be expressed as [18]:

$$M(\tau) = \left(\frac{1}{2} + a \right) b L_c(\tau) + ab L_{nc1}(\tau) - \left(\frac{1}{2} - a \right) b L_{nc2}(\tau) + M_\alpha \tag{127}$$

where M_α is a non-circulatory term given by:

$$M_\alpha(t) = -\frac{1}{16} C_{L\alpha} \rho_\infty b^4 \ddot{\alpha}(t) \quad \Rightarrow \quad M_\alpha(\tau) = -\frac{1}{16} C_{L\alpha} \rho_\infty b^2 U_\infty^2 \alpha''(\tau) \tag{128}$$

Substituting Equation (121), Equation (124), Equation (125) and Equation (128),into Equation (126) and Equation (127) total lift and moment expressions can be written in terms of non-dimensional time as;

$$L(\tau) = C_{L\alpha}\rho_\infty b U_\infty \int_{-\infty}^{s} \phi(\tau - \tau_0)\left(U_\infty \alpha' + U_\infty \frac{h''}{b} + \left(\frac{1}{2} - a\right)U_\infty \alpha''\right)d\tau_0 \ldots$$
$$+ \frac{1}{2}C_{L\alpha}\rho_\infty U_\infty^2 \left(h''(\tau) - ab\,\alpha''(\tau)\right) + \frac{1}{2}C_{L\alpha}\rho_\infty b U_\infty^2 \alpha'(\tau) \tag{129}$$

$$M(\tau) = \left(\frac{1}{2} + a\right)C_{L\alpha}\rho_\infty b^2 U_\infty \int_{-\infty}^{s} \phi(\tau - \tau_0)\left(U_\infty \alpha' + U_\infty \frac{h''}{b} + \left(\frac{1}{2} - a\right)U_\infty \alpha''\right)d\tau_0 \ldots$$
$$+ \frac{1}{2}C_{L\alpha}\rho_\infty U_\infty^2 ab\left(h''(\tau) - ab\,\alpha''(\tau)\right) - \frac{1}{2}\left(\frac{1}{2} - a\right)C_{L\alpha}\rho_\infty b^2 U_\infty^2 \alpha'(\tau) \ldots \tag{130}$$
$$- \frac{1}{16}C_{L\alpha}\rho_\infty b^2 U_\infty^2 \alpha''(\tau)$$

For incompressible flow, lift curve slope $C_{L\alpha}$ is assumed to be *2π* for infinite aspect ratio wings [19]. Substituting *2π* in place of $C_{L\alpha}$ in Equation (129) and (130) and rearranging the equations:

$$L(\tau) = \pi\rho_\infty b U_\infty^2 \left[2\int_{-\infty}^{s}\phi(\tau - \tau_0)\left(\alpha' + \frac{h''}{b} + \left(\frac{1}{2} - a\right)\alpha''\right)d\tau_0 + \left(\frac{h''(\tau)}{b} - a\,\alpha''(\tau)\right) + \alpha'(\tau)\right] \tag{131}$$

$$M(\tau) = \pi\rho_\infty b^2 U_\infty^2 \left[(1 + 2a)\int_{-\infty}^{s}\phi(\tau - \tau_0)\left(\alpha' + \frac{h''}{b} + \left(\frac{1}{2} - a\right)\alpha''\right)d\tau_0 + a\left(\frac{h''(\tau)}{b} - a\,\alpha''(\tau)\right)\right.$$
$$\left. - \left(\frac{1}{2} - a\right)\alpha'(\tau) - \frac{1}{8}\alpha''(\tau)\right] \tag{132}$$

To have the aeroelastic response Laplace transform method will be needed. By taking the Laplace transforms of the lift and moment equations given above one gets [19]:

$$\hat{L}(s) = \pi b \rho_\infty U_\infty^2 \left[2\left(s\hat{\alpha}(s) + s^2 \frac{\hat{h}(s)}{b} + s^2\left(\frac{1}{2} - a\right)\hat{\alpha}(s) \right)\hat{\phi}(s)... \right.$$
$$\left. + s^2\left(\frac{\hat{h}(s)}{b} - a\hat{\alpha}(s) \right) + s\hat{\alpha}(s) \right] \tag{133}$$

$$\hat{M}(s) = \pi b^2 \rho_\infty U_\infty^2 \left[(1 + 2a)\left(s\hat{\alpha}(s) + s^2 \frac{\hat{h}(s)}{b} + s^2\left(\frac{1}{2} - a\right)\hat{\alpha}(s) \right)\hat{\phi}(s)... \right.$$
$$\left. + as^2\left(\frac{\hat{h}(s)}{b} - ab\hat{\alpha}(s) \right) - \left(\frac{1}{2} - a\right)s\hat{\alpha}(s) - \frac{1}{8}s^2\hat{\alpha}(s) \right] \tag{134}$$

4.3.   Equations of Motion

In Chapter 2 the equations of motion for a 2 DoF Typical Section are given. An external excitation *F* applied on the elastic axis in the plunge direction is introduced in addition to the terms given in equations of motion derived in Chapter 2. The new set of of equations of motion are given by Equations (135) and (136).

.

$$m\ddot{h}(t) + S_\alpha \ddot{\alpha}(t) + K_h h(t) = -L(t) + F(t) \tag{135}$$

$$S_\alpha \ddot{h}(t) + I_\alpha \ddot{\alpha}(t) + K_\alpha \alpha(t) = M(t) \tag{136}$$

One should note that the terms at the left hand side of the equation is in terms of time, not nondimensional time. Therefore, Equations (135) and (136) can be rewritten in terms of non-dimensional time as:

$$m \frac{d}{d\tau} \frac{d\tau}{dt} \left(\frac{dh}{d\tau} \frac{d\tau}{dt} \right) + S_\alpha \frac{d}{d\tau} \frac{d\tau}{dt} \left(\frac{d\alpha}{d\tau} \frac{d\tau}{dt} \right) + K_h h(\tau) = -L(\tau) + F(\tau) \qquad (137)$$

$$S_\alpha \frac{d}{d\tau} \frac{d\tau}{dt} \left(\frac{dh}{d\tau} \frac{d\tau}{dt} \right) + I_\alpha \frac{d}{d\tau} \frac{d\tau}{dt} \left(\frac{d\alpha}{d\tau} \frac{d\tau}{dt} \right) + K_\alpha \alpha(\tau) = M(\tau) \qquad (138)$$

Recalling that $\dfrac{d\tau}{dt} = \dfrac{U_\infty}{b}$, the two equations of motion can be rewritten as

$$m \frac{U_\infty^2}{b^2} h''(\tau) + S_\alpha \frac{U_\infty^2}{b^2} \alpha''(\tau) + K_h h(\tau) = -L(\tau) + F(\tau) \qquad (139)$$

$$S_\alpha \frac{U_\infty^2}{b^2} h''(\tau) + I_\alpha \frac{U_\infty^2}{b^2} \alpha''(\tau) + K_\alpha \alpha(\tau) = M(\tau) \qquad (140)$$

One should note that prime in Equations (139) and (140), denotes derivation with respect to dimensionless time. Recalling that the terms S_α, I_α, K_h and K_α are defined in Equations (3), (14) and (76) respectively, substituting these into Equations (139) and (140) one gets

$$m \frac{U_\infty^2}{b} \frac{h''(\tau)}{b} + mX_\alpha \frac{U_\infty^2}{b} \alpha''(\tau) + m \omega_h^2 h(\tau) = -L(\tau) + F(\tau) \qquad (141)$$

$$mX_\alpha U_\infty^2 \frac{h''(\tau)}{b} + mr_\alpha^2 U_\infty^2 \alpha''(\tau) + mr_\alpha^2 b^2 \omega_\alpha^2 \alpha(\tau) = M(\tau) \qquad (142)$$

It should also be noted that for non-dimensional speed term V was defined in Equation (17). Thus, free stream velocity U_∞ can be expressed as $Vb\omega_\alpha$. Substituting this expression in Equations (141) and (142):

$$m\omega_\alpha^2 bV^2 \frac{h''(\tau)}{b} + mX_\alpha \omega_\alpha^2 bV^2 \alpha''(\tau) + m\omega_h^2 h(\tau) = -L(\tau) + F(\tau) \qquad (143)$$

$$mX_\alpha \omega_\alpha^2 b^2 V^2 \frac{h''(\tau)}{b} + mr_\alpha^2 \omega_\alpha^2 b^2 V^2 \alpha''(\tau) + mr_\alpha^2 b^2 \omega_\alpha^2 \alpha(\tau) = M(\tau) \qquad (144)$$

Recalling the frequency rate σ given in Equaion (15), dividing both sides of (143) by $m\omega_\alpha^2 bV^2$ and dividing both sides of the Equation (144) by $mr_\alpha^2 \omega_\alpha^2 b^2 V^2$ one gets

$$\frac{h''(\tau)}{b} + X_\alpha \alpha''(\tau) + \frac{\sigma^2}{V^2}\frac{h(\tau)}{b} = -\frac{L(\tau)}{m\omega_\alpha^2 bV^2} + \frac{F(\tau)}{m\omega_\alpha^2 bV^2} \qquad (145)$$

$$\frac{X_\alpha}{r_\alpha^2}\frac{h''(\tau)}{b} + \alpha''(\tau) + \frac{1}{V^2}\alpha(\tau) = \frac{M(\tau)}{mr_\alpha^2 \omega_\alpha^2 b^2 V^2} \qquad (146)$$

Substituting the lift and moment expressions which are given in Equations (131) and (132) into Equations (145) and (146) and recalling that the mass ratio parameter μ is given by Equation (16), the two equations of motion can be expressed as

$$\frac{h''(\tau)}{b} + X_\alpha \alpha''(\tau) + \frac{\sigma^2}{V^2}\frac{h(\tau)}{b} + \frac{1}{\mu}\left[2\int_{-\infty}^{s}\phi(\tau-\tau_0)\left(\alpha' + \frac{h''}{b} + \left(\frac{1}{2}-a\right)\alpha''\right)d\tau_0 \right.$$
$$\left. + \left(\frac{h''(\tau)}{b} - a\alpha''(\tau)\right) + \alpha'(\tau)\right] = \frac{F(\tau)}{m\omega_\alpha^2 bV^2} \tag{147}$$

$$\frac{X_\alpha}{r_\alpha^2}\frac{h''(\tau)}{b} + \alpha''(\tau) + \frac{1}{V^2}\alpha(\tau) - \frac{1}{\mu r_\alpha^2}\left[(1+2a)\int_{-\infty}^{s}\phi(\tau-\tau_0)\left(\alpha' + \frac{h''}{b} + \left(\frac{1}{2}-a\right)\alpha''\right)d\tau_0 \cdots\right.$$
$$\left. + a\left(\frac{h''(\tau)}{b} - a\alpha''(\tau)\right) - \left(\frac{1}{2}-a\right)\alpha'(\tau) - \frac{1}{8}\alpha''(\tau)\right] = 0 \tag{148}$$

To solve the Equations (147) and (148) to determine the responses in time domain, one may convert the equations in Laplace transformed space and have the expressions for responses in Laplace domain. Inverse Laplace transforming the expressions for desired flight regime (for a specific speed and density) one can then get the responses in time domain.

Converting the Equations (147) and (148)in Laplace transformed space using the Equations (133) and (134) one gets:

$$s^2\frac{\hat{h}}{b} + X_\alpha s^2\hat{\alpha} + \left(\frac{\sigma}{V}\right)^2\frac{\hat{h}}{b} + \frac{2}{\mu}\left(s\hat{\alpha} + s^2\frac{\hat{h}}{b} + s^2\left(\frac{1}{2}-a\right)\hat{\alpha}\right)\hat{\phi}(s)$$
$$+ \frac{1}{\mu}s^2\left(\frac{\hat{h}}{b} - a\hat{\alpha}\right) + \frac{1}{\mu}s\hat{\alpha} = \frac{\hat{F}(s)}{m\omega_\alpha^2 bV^2} \tag{149}$$

$$\frac{X_\alpha}{r_\alpha^2}s^2\frac{\hat{h}}{b} + s^2\hat{\alpha} + \frac{1}{V^2}\hat{\alpha} - \frac{1}{\mu r_\alpha^2}(1+2a)\left(s\hat{\alpha} + s^2\frac{\hat{h}}{b} + s^2\left(\frac{1}{2}-a\right)\hat{\alpha}\right)\hat{\phi}(s)$$
$$- \frac{1}{\mu r_\alpha^2}as^2\left(\frac{\hat{h}}{b} - a\hat{\alpha}\right) + \frac{1}{\mu r_\alpha^2}\left(\frac{1}{2}-a\right)s\hat{\alpha} + \frac{1}{8}\frac{1}{\mu r_\alpha^2}s^2\hat{\alpha} = 0 \tag{150}$$

where, (^)represents parameters whose Laplace transforms are taken. Grouping the terms with $\dfrac{\hat{h}}{b}$ and $\hat{\alpha}$ together Equations (149) and (150)above can be written as:

$$A(s)\frac{\hat{h}}{b} + B(s)\hat{\alpha} = \frac{\hat{F}(s)}{m\,\omega_{\alpha}^{2}bV^{2}} \qquad (151)$$

$$C(s)\frac{\hat{h}}{b} + D(s)\hat{\alpha} = 0 \qquad (152)$$

where,

$$A(s) = s^{2} + \left(\frac{\sigma}{V}\right)^{2} + \frac{2}{\mu}s^{2}\hat{\phi}(s) + \frac{1}{\mu}s^{2} \qquad (153)$$

$$B(s) = X_{\alpha}s^{2} + \frac{2}{\mu}\left(s + s^{2}\left(\frac{1}{2} - a\right)\right)\hat{\phi}(s) - \frac{1}{\mu}as^{2}\hat{\alpha} + \frac{1}{\mu}s \qquad (154)$$

$$C(s) = \frac{X_{\alpha}}{r_{\alpha}^{2}}s^{2} - \frac{1}{\mu r_{\alpha}^{2}}(1 + 2a)s^{2}\hat{\phi}(s) - \frac{1}{\mu r_{\alpha}^{2}}as^{2} \qquad (155)$$

$$D(s) = s^{2} + \frac{1}{V^{2}} - \frac{1}{\mu r_{\alpha}^{2}}(1 + 2a)\left(s + s^{2}\left(\frac{1}{2} - a\right)\right)\hat{\phi}(s) + \frac{1}{\mu r_{\alpha}^{2}}a^{2}s^{2}$$
$$+ \frac{1}{\mu r_{\alpha}^{2}}\left(\frac{1}{2} - a\right)s + \frac{1}{8}\frac{1}{\mu r_{\alpha}^{2}}s^{2} \qquad (156)$$

81

Solving the Equations for $\dfrac{\hat{h}}{b}$ and $\hat{\alpha}$ one gets the responses in Laplace domain:

$$\frac{\hat{h}(s)}{b} = \frac{\hat{F}(s)}{m\,\omega_\alpha^2 bV^2} \frac{D(s)}{A(s)D(s) - B(s)C(s)} \tag{157}$$

$$\hat{\alpha}(s) = \frac{\hat{F}(s)}{m\,\omega_\alpha^2 bV^2} \frac{C(s)}{B(s)C(s) - A(s)D(s)} \tag{158}$$

Taking the inverse Laplace transforms of the Equations (157) and (158) one gets the responses in non-dimensional time domain.

4.4.   Simulated Flutter Test Method

Simulated flutter tests are performed for a case study using a similar method introduced in Reference [11]. The simulated flutter test method used, is performed by following the steps listed below.

1. First, p-k method is applied to a typical section model of the wing and a flutter speed is is predicted.

2. Excitation with respect to reduced time is introduced.

3. Using Equations (157) and (158) response of each mode is obtained at a speed, equal to 22.7% of the flutter speed parameter calculated in the first step [10]. The responses are analyzed to provide estimates for the damping ratios. Logarithmic decrement method is used to determine the damping ratios.

4. The flight speed is increased by an increment equal to 7% of the predicted flutter speed parameter and estimates for the damping ratio are obtained [10].

5. The flight speed is increased again by the same increment of the predicted flutter speed parameter and estimates for the damping ratio are obtained. The curve of estimated damping ratios vs. flight speed is plotted. The next flight speed would be an extra addition of 7% of the predicted flutter speed parameter predicted in the first step to the latest flight speed.

6. The plot is extrapolated using cubic piecewise polynomial method to cover the next flight speed. In cubic piecewise polynomial method a third degree polynomial is assigned for each interval. At the knot points the first and the second derivative values of the neighbor polynomials are equal to eachother.

   a. If the extrapolated curve does not intersect the zero damping line step 5 is repeated for the next flight speed and a new extrapolated curve is obtained.

   b. If the curve intersects the zero damping line at a speed, and 80% of this speed is higher than the next test speed step 5 is repeated [10].

   c. If the curve intersects the zero damping line at a speed, and 80% of this speed is lower than the next test speed, test is stopped and the speed where the curve intersects zero damping line is accepted as estimated flutter speed.

4.5. Case Study

Simulated flutter tests are performed for a 2DoF Typical Section Model. The tests are performed at the sea level. The properties of the typical section model are given below.

$$a = -0.2,$$
$$x_\alpha = 0.1,$$
$$m = 45 \text{ kg/m},$$
$$r_\alpha^2 = 0.24,$$
$$\omega_\alpha = 7.958 \text{ hz},$$
$$\omega_h = 3.183 \text{ hz}.$$

(159)

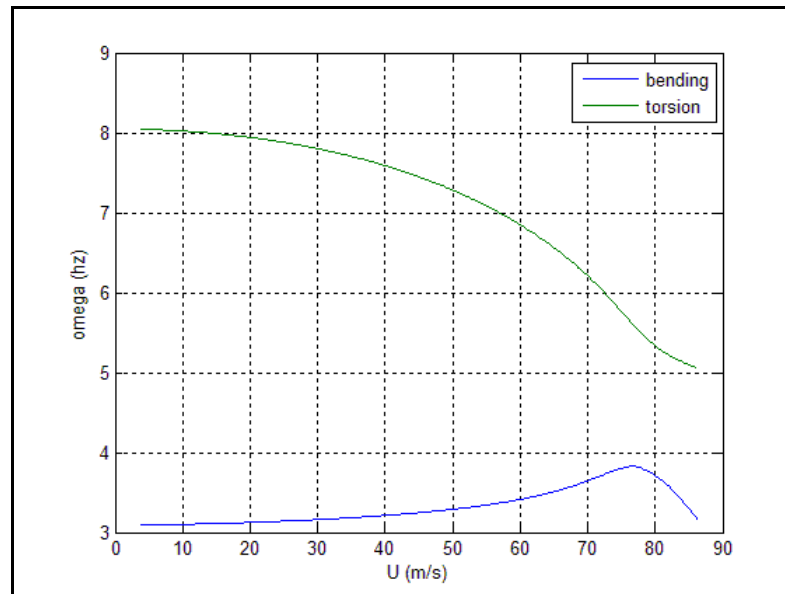Using the p-k method the plots given in Figure 37 and Figure 38 are obtained

Figure 37. Frequency vs. speed plot of the typical section model used in simulated flutter test (p-k method)
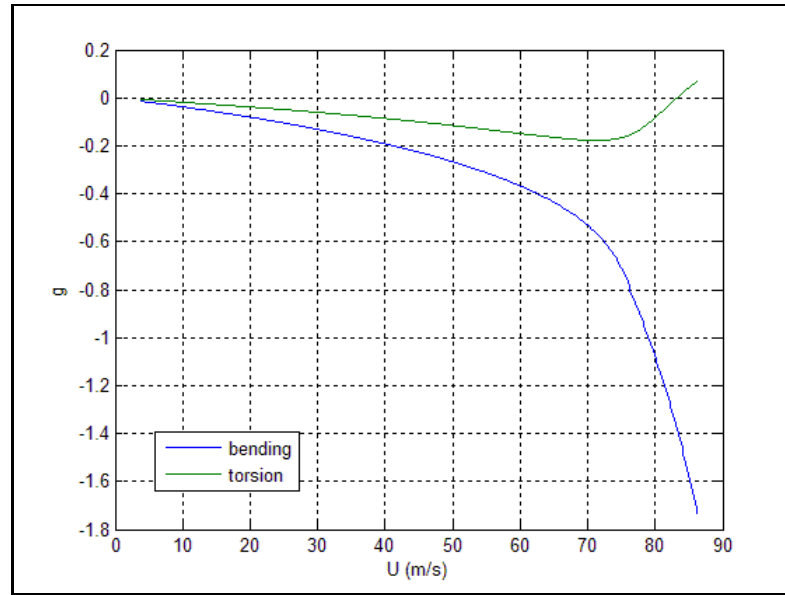
Figure 38. Damping vs. speed plot of the typical section model used in simulated flutter test (p-k method)

Predicted flutter speed parameter is 83 m/s as seen from Figure 38. This value is used in simulated flutter test to determine the test speeds.

A blast load is modeled as the external excitation. The loading which changes with respect to reduced time is given by Equation (160)

$$F(\tau) = 20\left[H(\tau)\left(1 - \frac{\tau}{15}\right) - H(\tau - 30)\left(1 - \frac{\tau}{15}\right)\right] \tag{160}$$

where, *H* is the unit step function. In Figure 39 the excitation is shown as force vs. dimensionless time plot.
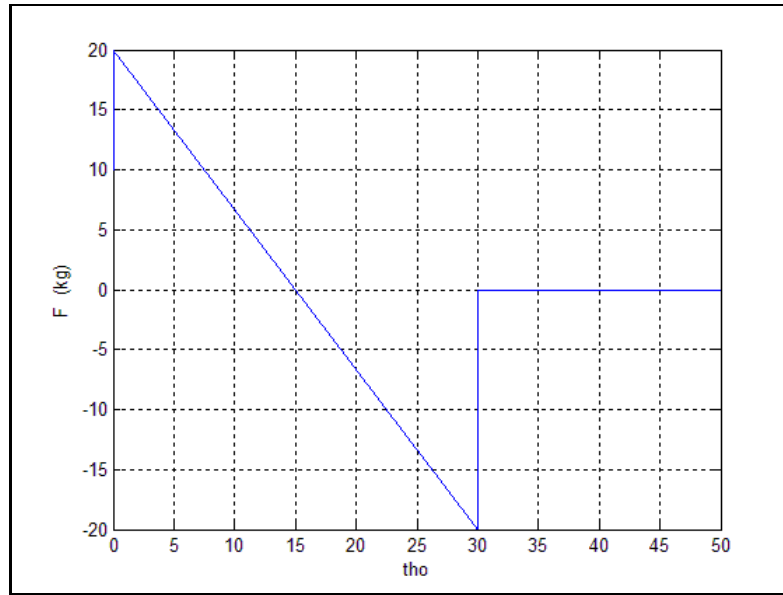
Figure 39. Blast excitation

The first test speed is taken as 18.841 m/s which is the 22.7% of the predicted flutter speed parameter 83 m/s. For the test speed of 18.841 m/s, the excitation is applied at the elastic axis and the Laplace domain responses given in Equations(157) and (158) are obtained for the excitation. The equations are first converted from Laplace transformed domain to dimensionless time domain, and then to time domain. It should be noted that taking the inverse Laplace transforms of Equations(157) and (158) by hand is almost impossible. A proper mathematical tool which has an efficient symbolic toolbox should be chosen to solve these equations since equations are very complicated and the time domain solution is performed parametrically. When the expressions for the responses are obtained in time domain, the time interval of interest is substituted into these expressions and response vs. time plots are determined. The peak points of these plots are used to estimate the damping ratios using the logarithmic decrement method. Therefore, the time interval chosen should not interfere with the time region when the excitation is being applied, to examine how the excitation induced vibration dies out.

86

One can notice that the excitation is applied between 0-30 nondimensionless time value which stands for an interval of 0-1.2 seconds for the speed 18.841m/s using the expression for the reduced time given in Equation (115). It should also be noted that this period gets shorter when the speed is increased. A MATLAB code is generated to do calculations and obtain the plots.

First, bending mode responses are analyzed. Using the generated MATLAB code, the response vs. time curve in the interval of 2-4 seconds is plotted in Figure 40, for the first test point speed 18.841 m/s. Figure 40 shows that bending response is a damped oscillation which indicates that the wing is free of flutter at the test speed of 18.841 m/s.
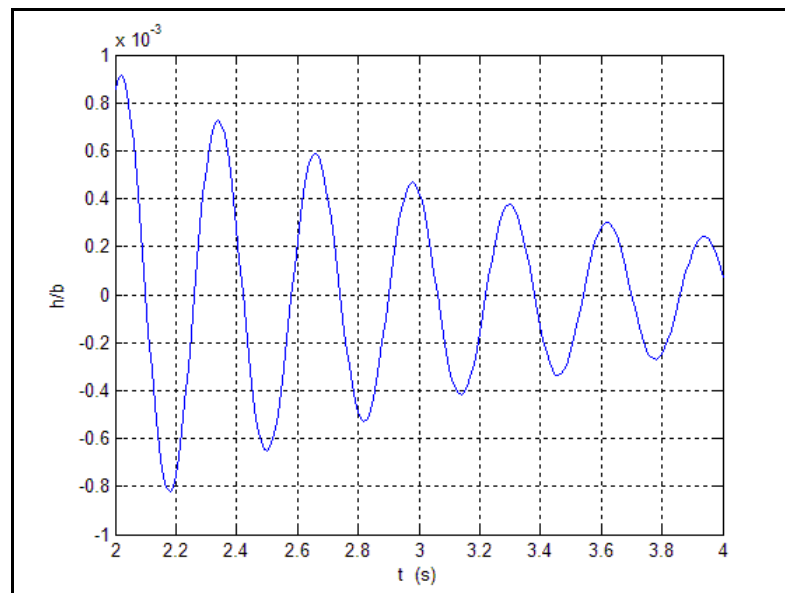

Figure 40. Bending response at 18.841 m/s, 22.7% of the predicted flutter speed.

4.6. Logarithmic Decrement Method

Logarithmic decrement is the logarithm of the ratio of two successful cycles's amplitudes of a dying out free vibration [20]. Damping ratio is expressed as a function of logarithmic decrement in the logarithmic decrement method. It is one of

87

the most popular experimental damping estimation techniques. Logarithmic decrement is expressed as [20]:

$$\delta = \frac{1}{n} \ln \left(\frac{x_1}{x_n} \right) \tag{161}$$

where n denotes the number of cycles and x denotes to the amplitudes of peaks as shown in Figure 41. The relation between logarithmic increment and the damping ratio is given as [20]:

$$g = \frac{\delta}{\sqrt{4\pi^2 + \delta^2}} \cong \frac{\delta}{2\pi} \tag{162}$$

One should note that δ^2 in the denominator can be neglected since it is very small compared to $4\pi^2$.
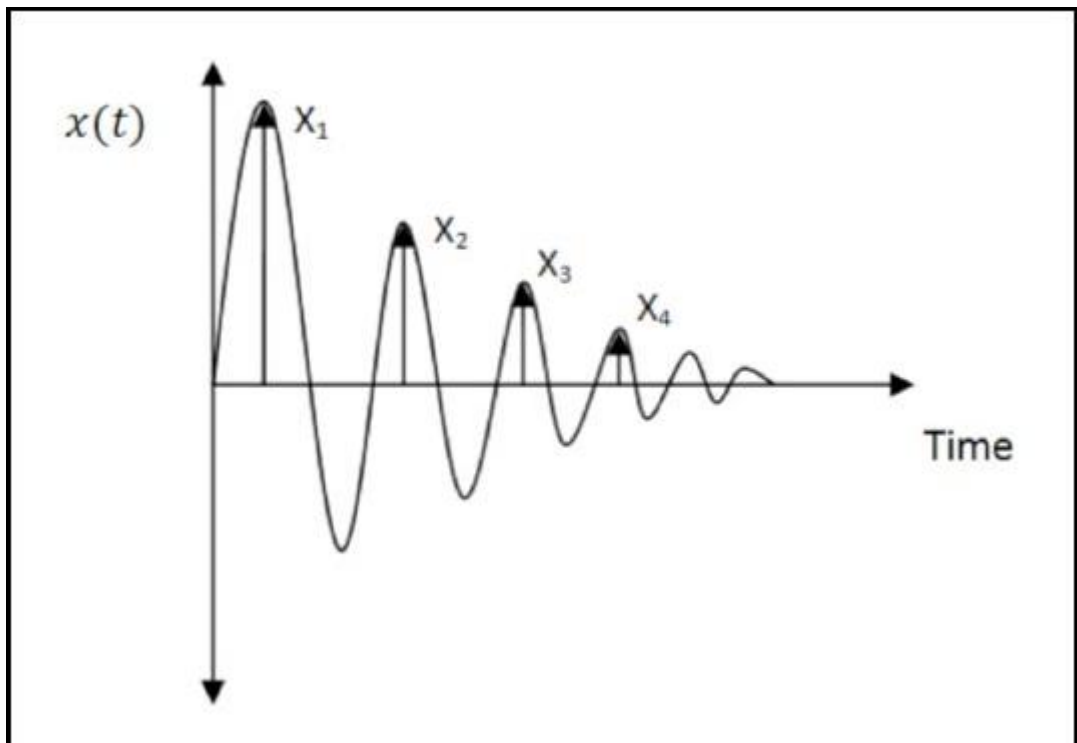

Figure 41. A decaying vibration.

Applying the logarithmic decrement method to the response vs. time plot given in Figure 40, the damping ratio for the test speed of 18.841 m/s (22.7% of the predicted flutter speed) is calculated as:

$$g_{22.7} = 0.0281 \qquad (163)$$

The second test speed is 24.651 m/s which is the 29.7% of the predicted flutter speed parameter 83 m/s. The response vs. time plot for the next test point is shown in Figure 42.
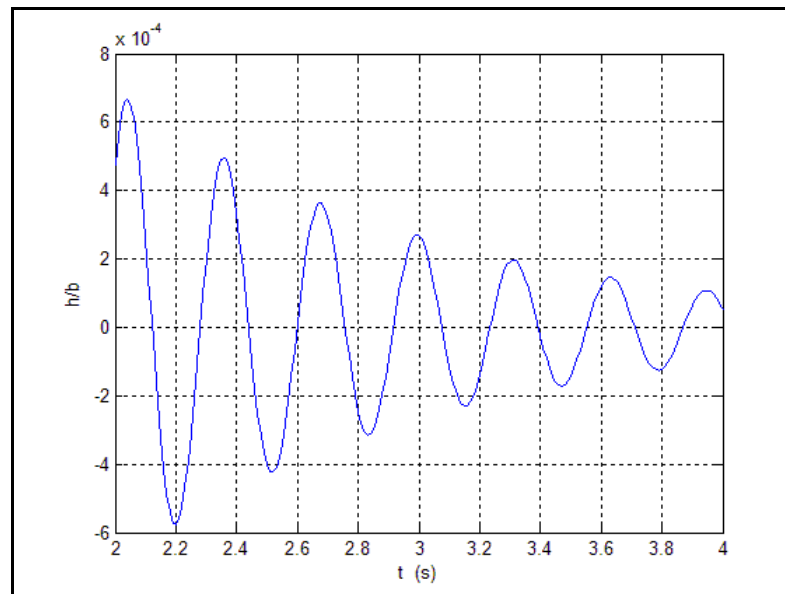

Figure 42. Bending response at 24.651 m/s, 29.7% of the predicted flutter speed.

Applying the logarithmic decrement method, the damping ratio for speed 24.651 m/s which is the 29.7% of the predicted flutter speed is calculated as:

$$g_{29.7} = 0.0387 \qquad\qquad (164)$$

Following the same steps the damping ratio for the next test speed 30.461 m/s which is the 36.7% of the predicted flutter speed is obtained as:

$$g_{36.7} = 0.0503 \ , \qquad\qquad (165)$$

The curve of estimated damping ratios vs. flight speed is plotted and extrapolated using cubic piecewise polynomial method to cover the next test point which is at 36.271 m/s to check the stability of that point. The curve is given in Figure 43. The red vertical line indicates the next test point. It can be seen that the next test speed is safe from flutter since the curve does not intersect zero damping line. So one can go for the next test point.
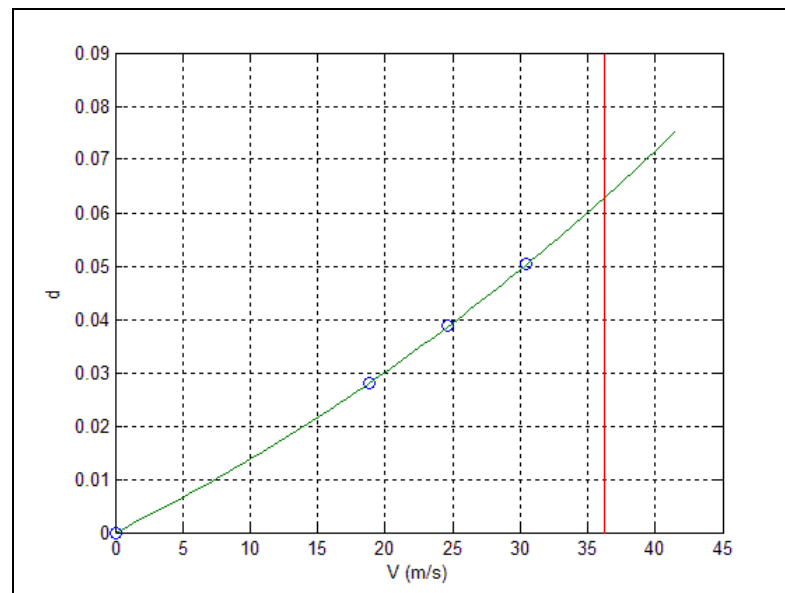

Figure 43. Extrapolated damping vs. speed curve for the first three test points

The same procedure is followed checking the stability of the next test point before going for the next point. For 4th and 5th test points the following damping ratios are obtained using logarithmic decrement method and response vs. time plots.

$$g_{43.7} = 0.0634$$
$$g_{50.7} = 0.0793$$

(166)

Extrapolated damping vs. speed curves are plotted in Figure 44, and the stability of the next test point is checked for each one.
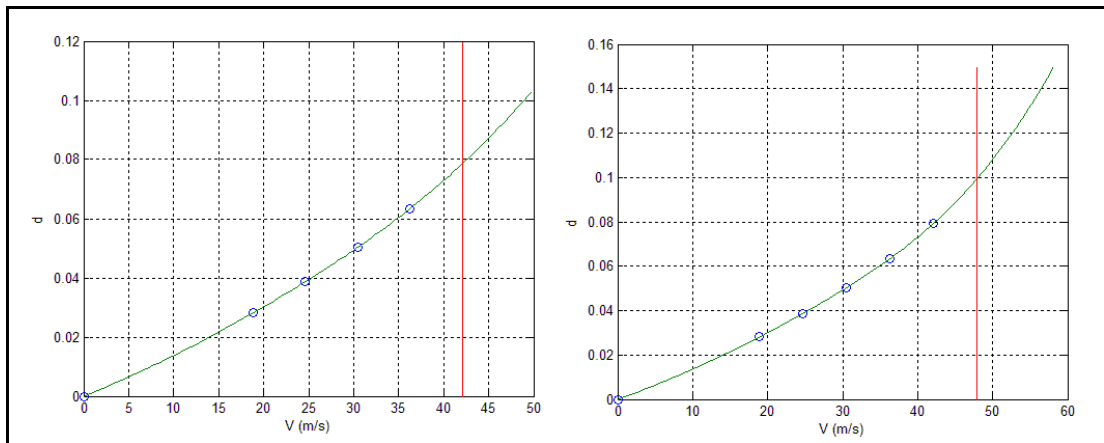

Figure 44. Extrapolated damping vs. speed curve for the first four and five test points respectively.

Damping ratio for the 6th test point is calculated as 0.0957 and the extrapolated damping vs. speed curve is ploted for the first six test points. The plot is given in Figure 45.
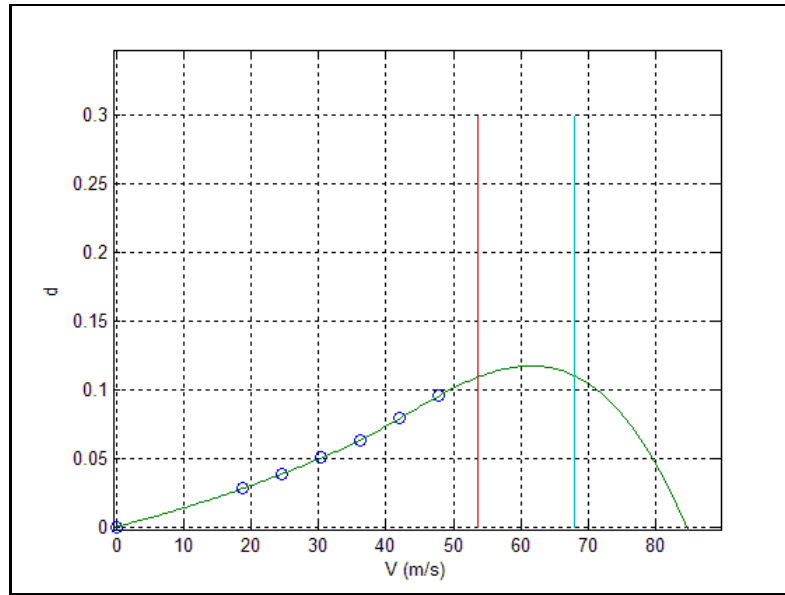
Figure 45. Extrapolated damping vs. speed curve for the first six test points.

As can be seen from Figure 45, flutter speed is estimated as 85 m/s. The vertical red line indicates the 7th test point. One should remember the stability criteria for the next test point, which is stated previously. If the curve intersects the zero damping line at a speed and 80% of this speed is lower than the next test speed, test is ended. The vertical blue line shows the 80% of the estimated flutter speed. Since 80% of the estimated flutter speed is higher than the next test point speed one can continue to the next test point which is 53.701 m/s.

The damping ratio is calculated as 0.1176 for the 7th test point and the extrapolated damping vs. speed curve is ploted for the first seven test points. The plot is given in Figure 46.
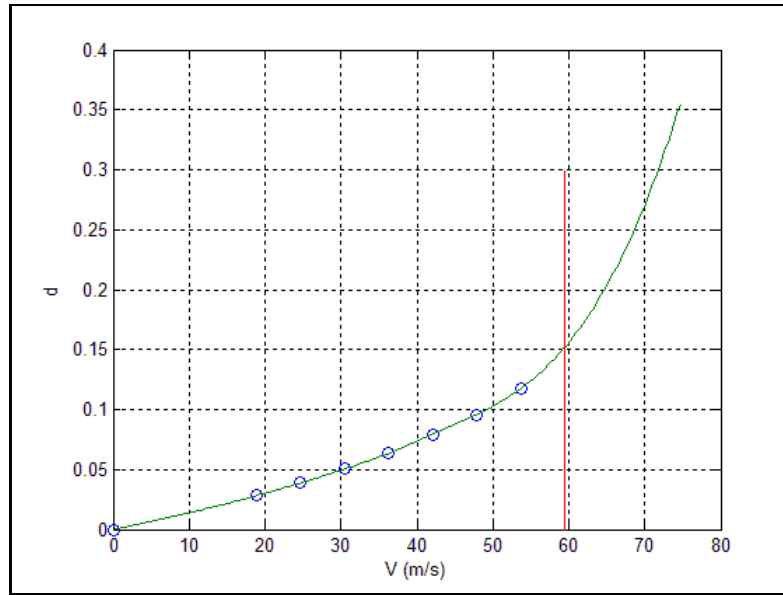
Figure 46. Extrapolated damping vs. speed curve for the first seven test points.

As can be seen from Figure 46, 59.511 m/s speed which is test point 8, is clear from flutter. So test is continued for the 8th test point. The damping ratio is calculated as 0.1387 for the 8th test point. Extrapolated damping vs. speed curve for the first eight test points is given inFigure 47.
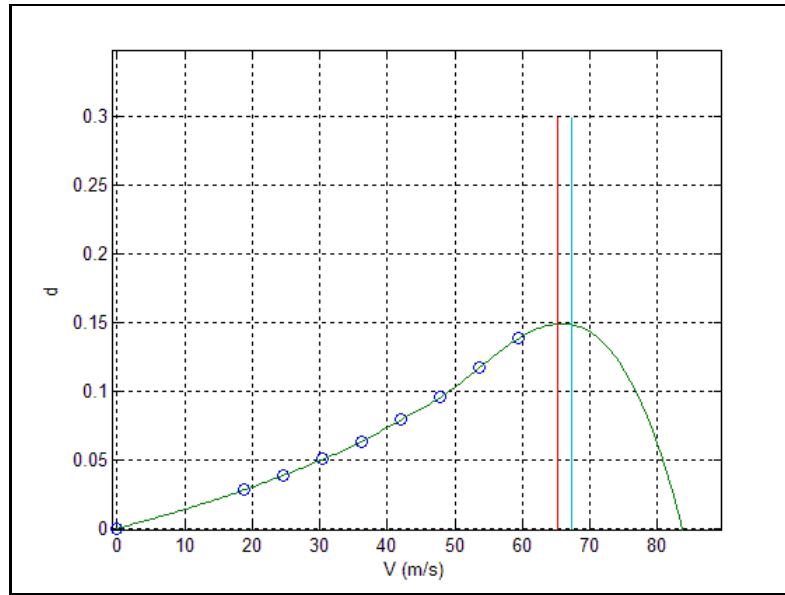
Figure 47. Extrapolated damping vs. speed curve for the first eight test points.

As can be seen from Figure 47, flutter speed is estimated as 83 m/s. The vertical red line indicates the next test point. The vertical blue line shows the 80% of the estimated flutter speed. Since 80% of the estimated flutter speed is higher than the next test point speed one can continue to the next test point which is 65.321 m/s.

The damping ratio is calculated as 0.1570 for the 9th test point and the extrapolated damping vs. speed curve is ploted for the first nine test points. The plot is given in Figure 48.
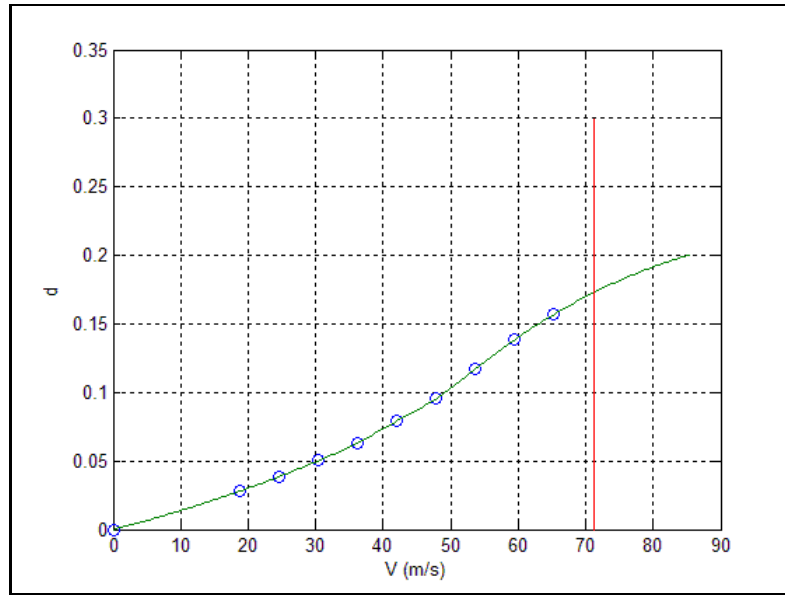
Figure 48. Extrapolated damping vs. speed curve for the first nine test points.

From Figure 48 for test point 10, for the 71.131 m/s speed the flutter clearance is ensured. So, test is continued. For test point 10 damping ratio is calculated as 0.0855.
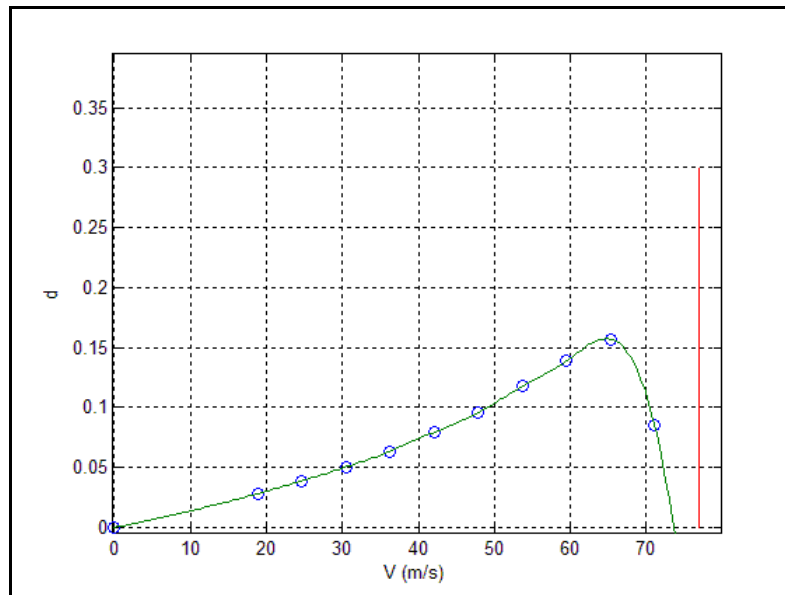

Figure 49. Extrapolated damping vs. speed curve for the first ten test points.

From Figure 49 flutter speed is estimated as 74 m/s. The vertical red line indicates the next test point. Since the next test point 76.941 m/s is greater than the estimated flutter speed test is ended. The final estimation for flutter speed for bending mode by simulated flutter test for the case study is determined as

$$U_f = 74 \text{ m/s} \tag{167}$$

One should notice that in earlier test steps, higher flutter speed estimations were made. Relying on those estimations and skipping the presteps may cause dangerous situations in real flight flutter testing. This case shows how crucial incremental approach is in flight flutter testing.

Torsion mode simulated flutter test results are analyzed following the same test steps. The simulated flutter test results for the first eight test points are given in Figure 50. At test point eight, stability check for the next test point fails and test is ended. Test results for the test point nine is given in Figure 51. The final estimation for the flutter speed for torsion mode by simulated flutter test for the case study is determined as

$$U_f = 80 \text{ m/s} \tag{168}$$

It should be noted that using the p-k method, the flutter occurance is expected in torsional mode at a speed of 83 m/s. Analyzing the responses both in bending and torsional modes one can see flutter is induced in both modes at close speeds.
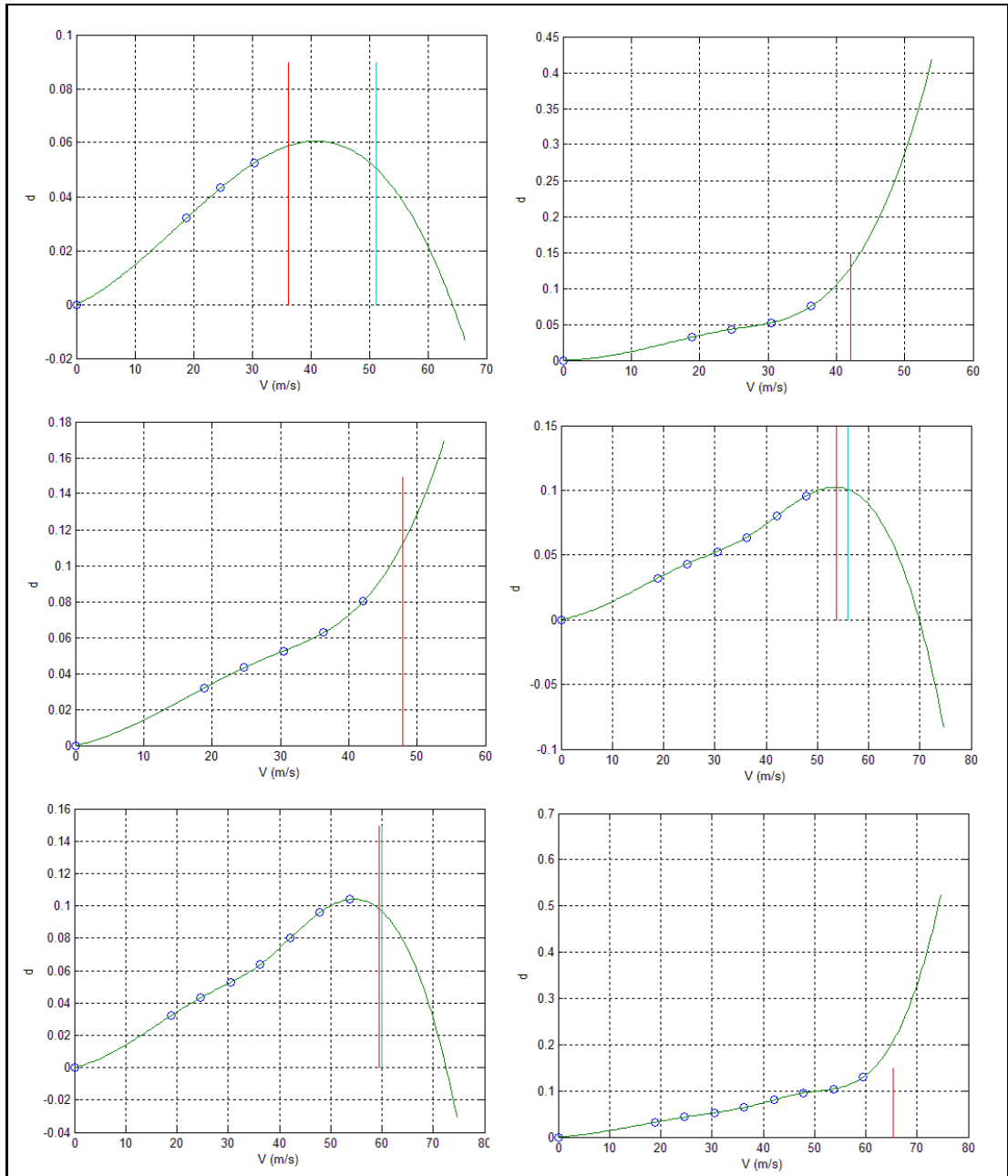
Figure 50. Extrapolated damping vs. speed curve for the first eight test points.
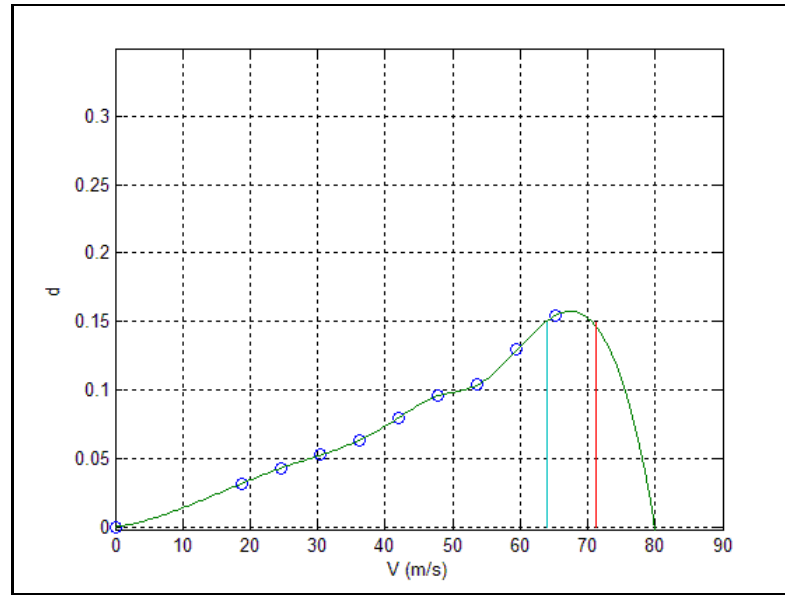
Figure 51. Extrapolated damping vs. speed curve for the first nine test points

4.7.   Damping vs. Speed Curves For Sinusoidal Excitation

Simulated flutter test is described in detail in the previous section. Time domain solutions are used in simulated flutter test at various air speeds. To simulate real flutter tests, the solutions are made for conservative subcritical airspeeds. However one can notice that using the equations in time domain, it is possible to estimate dampings for critical speeds as well. In this section, the 2D typical section on which the simulated flutter test is performed is subjected to a sinusoidal excitation and the results are obtained following the same procedure that has been used in performing simulated flutter tests. The main difference is that the stability check for the next test point is excluded in this section to see how the damping changes while getting close to the flutter speed.

For the sinusoidal excitation, the transient load which changes with respect to the reduced time is given by Equation (169)

$$F(\tau) = 20 \sin\left(32.5 \frac{b\tau}{U\infty}\right)[H(\tau) - H(\tau - 85.5)] \tag{169}$$

where, H is the unit step function. In Figure 52, the excitation is shown as force vs. dimensionless time plot.
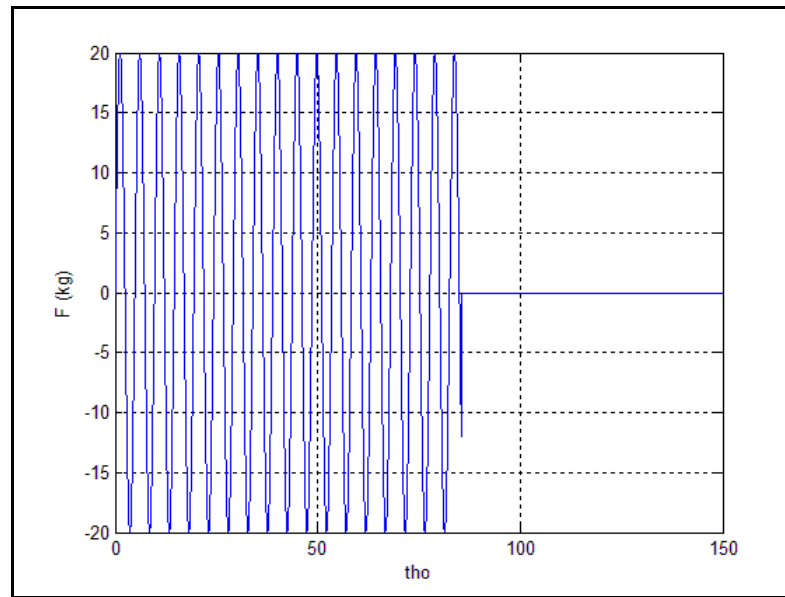

Figure 52. Sinusoidal excitation

One can notice that the excitation is applied between 0-83.5 nondimensionless time value which corresponds to an interval of 0-3.4 seconds for the speed 18.841m/s which is 22.7% of the predicted flutter speed by the p-k method using the expression for the reduced time given in Equation (115). It should also be noted that this period gets shorter when the speed is increased.

Response plots for pitch and plunge motions are plotted for 22.7%, 29.7%, 36.9%, 43.7%, 71.7% and from 90% to 100% by 1% increments of the predicted flutter speed by the p-k method. Damping estimations are obtained using the logarithmic

decrement method at each speed. Cubic piecewise polynomial interpolation is used to generate curve fit through the discrete data points, as shown in Figure 53 and 54 . Figures 51 and 52 give the damping versus airspeed plots for the plunging (bending) and pitching (torsion) modes, respectively.
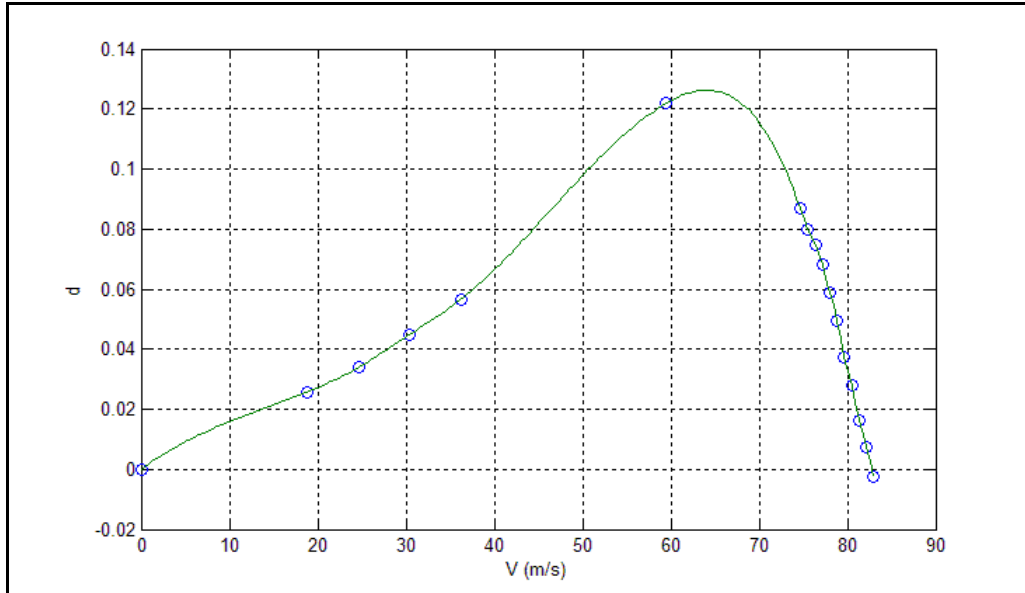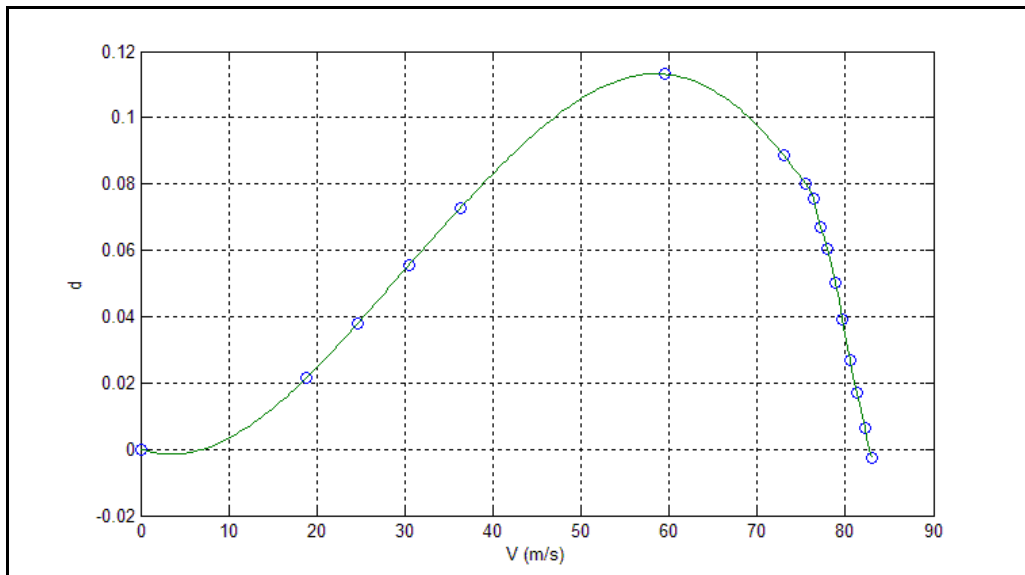

Figure 53. Damping vs. speed curve for bending mode.

Figure 54. Damping vs. speed curve for torsion mode.

100

From Figure 53 and 54, one can notice that the estimated flutter speeds for both modes using time domain solution are between 99% and 100% of the predicted flutter speed by the p-k method. Namely, for bending mode estimated flutter speed is 82.805 m/s, and for the torsion mode estimated flutter speed is 82.718 m/s.

Response vs. time plots for the bending and the torsional modes are given in Figure 55 for 99% of the predicted flutter speed by the p-k method, and the response vs. time plots for the bending and the torsional modes are given in Figure 56 for the 100% of the predicted flutter speed the by p-k method.
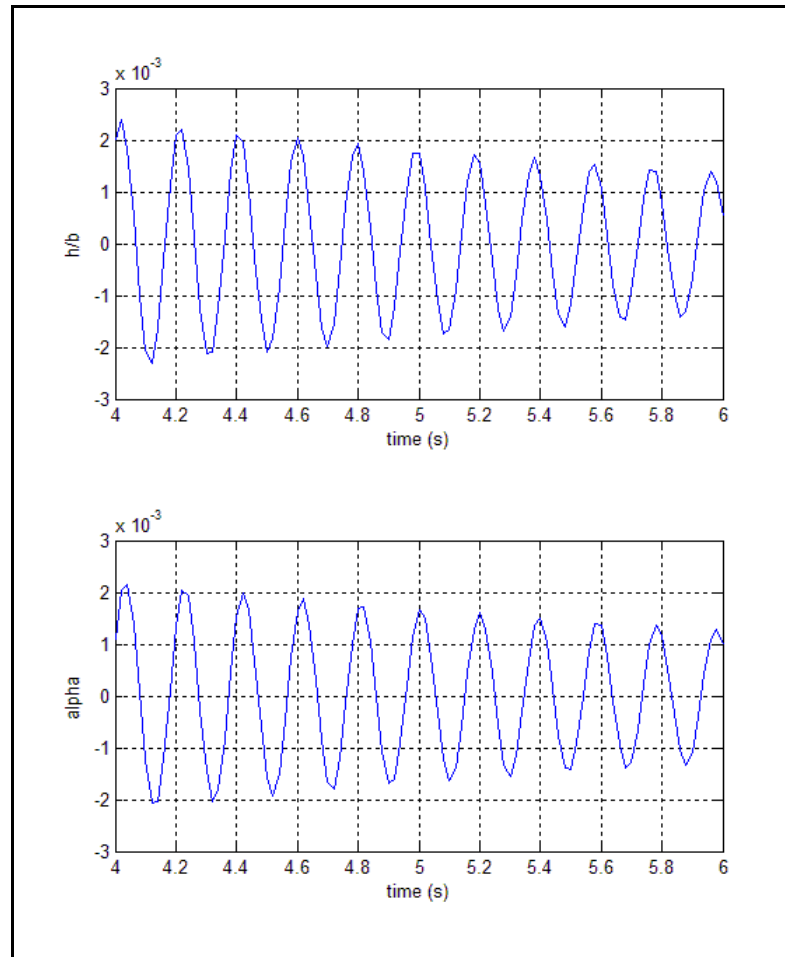

Figure 55. Response vs. time plots for bending and torsional mode for 99% of the predicted flutter speed by p-k method
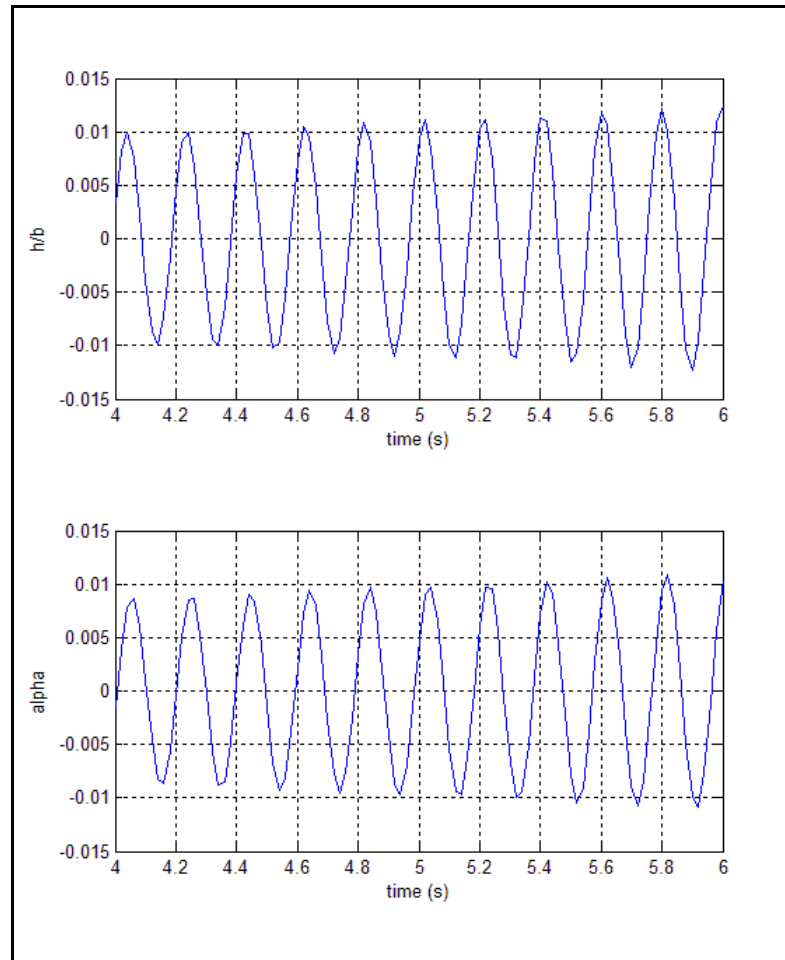
Figure 56. Response vs. time plots for bending and torsional mode for 100% of the predicted flutter speed by p-k method

One can notice that the plunge and pitch responses shown in Figure 55 are lightly damped, while the responses given in Figure 56 clearly show diverging behaviour.

As seen from the results obtained using the time domain solution and the p-k method solution very close results are obtained for flutter speed. However in time domain solution, flutter occurrence is predicted in both modes but flutter is predicted in torsional mode by the p-k method.

CHAPTER 5

CONCLUSION

The flutter analysis and preliminary work before performing flight flutter tests are the most critical certification processes. Accurate estimation of flutter speeds by means of analysis is required to plan the flutter test activities accordingly. Various fidelity models can be developed to perform flutter analysis. High fidelity approaches require numerical simulation involving finite element based structural models and computational aerodynamics based aerodynamics models. However, these high fidelity models require exceptionally long preprocessing and solution times.

The aim of this study is to provide a theoretical background on the estimation of flutter speed from the flutter flight test point of view. The study mainly focuses on the flutter prediction methods using low fidelity models such as 2D typical wing section model. With the 2D typical section models, one can gain more insight about the physics of the flutter phenomenon since all equations are analytically driven and parametric. The effect of parameter changes, such as stiffness, inertia, location of shear center etc. on the flutter speeds can be investigated much faster. In this respect, most commonly used methods of flutter analysis are investigated in detail. The mathematical theory behind these methods are investigated and implemented on

computer. In addition the effectiveness of the flutter analysis methods are also studied.

Flutter analysis of 3D wing rectangular and tapered wings are performed using NASTRAN's aeroelasticity module. The results of the 3D flutter analysis of wings with a variety of aspect ratios are compared with results of 2D typical section analysis.

A simulated flight test method is introduced and applied to a 2D typical section model. Damping values are obtained for incremental flight speeds using logarithmic decrement method, and the stability of the next test point is checked before continuing to the simulated flutter test. An estimation for flutter speed is made at the point that the stability control failed for the next test point.

It is concluded that typical wing section model is a sufficient tool to understand the mechanism of flutter. One can also get insight about the mechanism of flutter by working on typical section model and performing aeroelastic flutter analyses. In the flutter test, one of the most critical issue is to decide whether the flutter occurrence is explosive or mild. Explosive flutter occurs when the damping drops sharply above a certain speed, whereas in case of mild flutter damping reduces gradually until flutter occurs at zero damping. With the 2D typical section models, damping trend can be estimated, and flutter type can be identified.

Among the flutter analysis methods, k-method is a computationally efficient, straightforward, and robust method for predicting flutter by solving complex eigenvalue problem. Although the damping values found by k-method do not have physical meaning, except near the flutter boundary, mild flutter and explosive flutter character can be detected using the U vs g plots. However k method is not capable to predict the divergence instability.

p-k method is an approximation method to calculate more accurate damping values. However p-k method may produce discontinuities in U vs g and U vs ω plots which generally occurs as jumps between modes due to aerodynamic lag roots. Using the p-k method divergence can also be predicted. However, the solution takes more

computational time in p-k method compared to k-method. The solutions of both k-method and p-k method shows an excellent agreement at the flutter boundary.

Based on the comparisons of the flutter speed determined by the 3D flutter analysis of Nastran and typical section analyses, it is observed that there is approximately 10% difference between the flutter speeds calculated using 2D typical wing section and the 3D Nastran solution. For 2D typical section models, flutter speed is found to be higher. Since 2D typical section solutions are obtained much faster, they may be used in preliminary design phases or simulations by engineers before getting into the detailed design processes to have an idea about the approximate flutter speed. For tapered wings, it is shown that the wing section at about ¾ of the wing span from root represents the total wing properly for 2D typical section analysis. Flutter speeds obtained by the 3D Nastran analysis and the 2D typical section analysis matched closely when the typical section properties are extracted from the ¾ span location from the root of the wing.

Simulated flutter test method is an appropriate method to gain insight about the real flight flutter testing. One can get the simulated test data after complex time domain analysis which is similar to the test data of a real flight flutter test. The major difference of the simulated test data, from the real flight flutter test data collected by accelerometers is that it does not contain noise due to experimental deficiencies. Simulated flutter test may be very helpful to determine the test points which will be used in the flight flutter tests since the damping trend is traced just like every time a new test point is added to the damping versus airspeed curve.

Damping vs. speed curves are obtained using time domain solutions. It is shown that flutter speed obtained by the time domain solutions is in excellent agreement with the flutter speed predicted by the p-k method. However, in time domain solutions flutter is predicted in both modes whereas p-k method predicts flutter only in one mode.

It should be noted that in this study only incompressible flow is investigated. In further studies compressible flow and supersonic flow may be covered. In the simulated flutter test section only damping extrapolation method is used to estimate

flutter speed. In the future, other methods such as flutter margin, envelope function and Autoregressive Moving Average-Based (ARMA) methods may be used to analyze the simulated flutter test data.

REFERENCES

[1]. Wright, J. R., Cooper, J. E., Introduction to Aeroelasticity and Loads, Wiley Publications, England, 2007.

[2]. Bisplinghoff, R. L., Ashley, H., and Halfman, R. L., Aeroelasticity, Dover Publications, New York, 1996

[3]. Kehoe, M. W., A Historical Overview of Flight Flutter Testing, NASA Technical Memorandum 4720, October 1995.

[4]. Theodorsen, T., General Theory of Aerodynamic Instability and the Mechanism of Flutter. NACA Technical Report No: 496,1938.

[5]. Theodorsen, T., Garrick, I.E., Mechanism of Flutter- A Theoretical and Experimental Investigation of the Flutter Problem. NACA Technical Report No: 685, 1938.

[6]. Bisplinghoff, Raymond L., Ashley, H., Halfman, Robert L., Aeroelasticity. Addison-Wesley Publications, Massachusetts, 1957.

[7]. Fung, Y.C., An Introduction to the Theory of Aeroelasticity. Dover Publications, New York, 1993.

[8]. Hodges, Dewey H., Pierce, G. Alvin, Introduction to Structural Dynamics and Aeroelasticity. Cambridge University Press, Cambridge, 2002.

[9]. Scanlan, Robert H., Rosenbaum, Robert, Introduction to the Study of Aircraft Vibration and Flutter. The Macmillan Company, New York, 1951.

[10]. Dimitriadis, G., Cooper, J.E, Flutter Prediction from Flight Flutter Test Data, Journal of Aircraft, Vol. 38, No. 2, pp. 355-367, 2001.

[11]. Wright, J. R., Wong, J., Cooper, J. E., Dimitriadis, G, On the Use Of Control Surface Excitation in Flutter Testing, Journal of Aerospace Engineering 217, pp.317-332, 2003.

[12]. Seber, G., Ünlüsoy, L.,Sakarya, E., Flutter Characteristic of a Typical Section Model with a Trailing Edge Control Surface, 5th Ankara International Aerospace Conference, August 17-19, 2009, METU, Turkey.

[13]. Razak, N. A., Flutter Modeling and Simulation of Wing Section Using Bondgraph Technique, *M.S. Thesis*, University of Science, Pulau Pinang, Malaysia, 2005.

[14]. Bryson, A.E., Control of Spacecraft and Aircraft, Princeton University Press, 1994.

[15]. Edwards, J.W., Unsteady Aerodynamic Modeling and Active Aeroelastic Control, Ph.D. Thesis, Stanford University, Guidance and Control Laboratory, Department of Aeronautics and Astronautics, 1977.

[16]. Rodden, W.P., Taylor, P.F., McIntosh,S.C., Further Refinement of the Subsonic Doublet-Lattice Method, Journal of Aircraft, Vol. 35, No. 5, pp. 720-727, 1998.

[17]. Blair,M, A Compulation of the Mathematics Leading to the Doublet-Lattice Method, Final Report for Period June 1991-December 1991, Wright Patterson Air Force Base, Ohio, USA, 1992.

[18]. Castravete, S.C., Non-linear Flutter of a Cantilever Wing Including the Influence of Structure Uncertainties, Ph.D. Thesis, Wayne State University, Detroit, Michigan, USA, 2007.

[19]. Marzocca, P., Librescu, L., Chiocchia, G., Aeroelastic Response of 2-D Lifting Surfaces to Gust and Arbitrary Explosive Loading Signatures, International Journal of Impact Engineering 25, pp.41-65, 2001.

[20].   Benaroya, H., Nagurka, M.L., Mechanical Vibration: Analysis, Uncertainties, and Control, Third Edition, CRS Press, USA, 2010.

109